

UNIVERSITY OF CALIFORNIA

Los Angeles

High-Impedance Electromagnetic Surfaces

A dissertation submitted in partial satisfaction of the  
requirements for the degree of Doctor of Philosophy

in Electrical Engineering

by

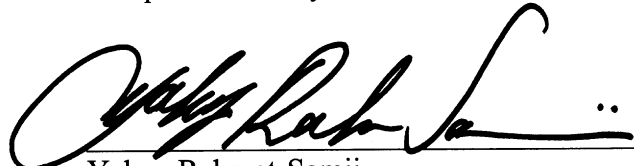
Daniel Frederic Sievenpiper

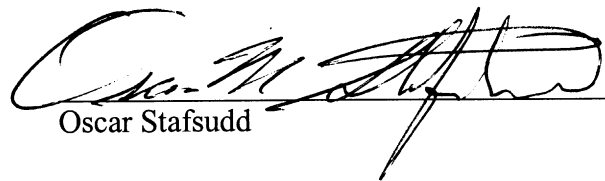
1999



The dissertation of Daniel Frederic Sievenpiper is approved.

  
Sudip Chakravarty

  
Yahya Rahmat-Samii

  
Oscar Stafsudd

  
Eli Yablonoitch, Committee Chair

University of California, Los Angeles

1999

## TABLE OF CONTENTS

1	Introduction .....	1
1.1	Electric Conductors .....	1
1.2	High Impedance Surfaces .....	5
2	Surface Waves .....	9
2.1	Dielectric Interfaces .....	9
2.2	Metal Surfaces.....	13
2.3	Impedance Surfaces.....	18
3	Textured Surfaces .....	23
3.1	Bumpy Surfaces .....	23
3.2	Corrugated Surfaces .....	25
3.3	High-Impedance Surfaces.....	28
4	Fabrication .....	31
4.1	Two-Layer Structure .....	31
4.2	Three-Layer Structure .....	33
5	Effective Medium Model .....	36
5.1	Circuit Parameters .....	36
5.2	Reflection Phase.....	45
5.3	Losses .....	47
5.4	Surface Waves.....	49
5.5	Radiation Bandwidth.....	55
5.6	Leaky Waves.....	59
5.7	Fundamental Limitations .....	61
6	Finite Element Model.....	64
6.1	Surface Waves.....	64
6.2	Leaky Waves.....	67
6.3	Vertical Connections .....	69
7	Measuring Surface Properties.....	71
7.1	TM Surface Waves.....	71
7.2	TE Surface Waves.....	75
7.3	Reflection Phase.....	77
7.4	Low-Frequency Structures .....	83
7.5	Other features.....	86
8	Alternative Structures.....	88
8.1	Frequency Selective Surfaces .....	88
8.2	Addition of a Ground Plane .....	90
8.3	Grounded Dielectric Slab .....	95
8.4	The Role of Conducting Vias .....	97

9	Antennas.....	100
9.1	The Vertical Monopole.....	101
9.2	The Patch Antenna.....	105
9.3	The Horizontal Wire.....	111
9.4	Circular Polarization.....	116
9.5	Large and Small Antennas.....	119
9.6	Portable Communications.....	125
10	Design.....	129
10.1	Frequency and Bandwidth.....	129
10.2	Geometry and Materials.....	135
10.3	Validation of the Model.....	140
11	Conclusion.....	143
11.1	Summary.....	143
11.2	Future Research.....	145

## LIST OF FIGURES

Figure 1.1.1 An antenna lying flat against a ground plane.....	2
Figure 1.1.2 An antenna separated by 1/4 wavelength from the ground plane .....	3
Figure 1.1.3 A TM surface wave propagating across a metal slab .....	4
Figure 1.1.4 Multipath interference due to surface waves on a ground plane.....	5
Figure 1.2.1 Cross-section of a high-impedance surface.....	5
Figure 1.2.2 Top view of the high-impedance surface.....	6
Figure 1.2.3 An equivalent circuit for the high-impedance surface.....	7
Figure 1.2.4 A TE surface wave propagating across a high-impedance surface .....	7
Figure 1.2.5 A flush-mounted dipole on a high-impedance ground plane .....	8
Figure 2.1.1 A surface wave on an interface between two dissimilar media. ....	9
Figure 2.2.1 Dispersion diagram for optical surface plasmons on metals.....	17
Figure 2.3.1 A rectangular area used for computing surface impedance .....	18
Figure 2.3.2 A surface wave propagating on an arbitrary impedance surface.....	19
Figure 3.1.1 A bumpy metal sheet with a narrow surface wave band gap.....	24
Figure 3.1.2 Evolution from a bumpy surface to a high impedance surface .....	25
Figure 3.2.1 A corrugated metal slab .....	26
Figure 3.2.2 A transmission line terminated at $X=0$ by an impedance, $Z$ .....	27
Figure 3.3.1 Origin of the equivalent circuit elements.....	29
Figure 3.3.2 Equivalent circuit model for the high-impedance surface .....	29
Figure 4.1.1 Copper clad dielectric circuit board material .....	32
Figure 4.1.2 Holes drilled to define the locations of the vertical connections .....	32
Figure 4.1.3 Plated copper forming vertical interconnections.....	32
Figure 4.1.4 Metal patches defined by etching .....	32
Figure 4.1.5 Perspective view of a two-layer printed circuit board.....	33
Figure 4.2.1 Materials for fabricating a three-layer printed circuit board.....	33
Figure 4.2.2 Inner layers patterned by etching.....	34
Figure 4.2.3 Two sheets bonded with an adhesive.....	34
Figure 4.2.4 Plated vias forming interconnects between all three layers .....	35
Figure 4.2.5 Top layer patterned by etching .....	35
Figure 4.2.6 Perspective view of a three-layer printed circuit board .....	35
Figure 5.1.1 Cross-section of a simple two-layer high-impedance surface.....	36
Figure 5.1.2 Origin of the capacitance and inductance in the effective circuit model.....	37
Figure 5.1.3 Effective circuit used to model the surface impedance .....	37
Figure 5.1.4 A pair of semi-infinite plates separated by a gap .....	38
Figure 5.1.5 Capacitor geometry in the two-layer high-impedance surface.....	38
Figure 5.1.6 A slab of dielectric divided into slices.....	40
Figure 5.1.7 Capacitor plates embedded in the dielectric slab .....	41
Figure 5.1.8 A solenoid of current used to calculate the sheet inductance.....	43
Figure 5.1.9 Impedance of a parallel resonant circuit .....	44
Figure 5.2.1 Reflection phase calculated using the effective circuit model .....	47
Figure 5.3.1 Surface impedance, including dielectric and conductive losses.....	48

Figure 5.3.2 Reflection magnitude, including dielectric and conductive losses.....	49
Figure 5.4.1 Dispersion diagram for bound surface waves, lying below the light line.....	53
Figure 5.5.1 A horizontal antenna above a ground plane.....	55
Figure 5.5.2 An antenna shunted by a textured surface .....	56
Figure 5.6.1 Circuit for modeling the radiation of leaky TE waves.....	60
Figure 5.6.2 Complete dispersion diagram, including leaky modes .....	61
Figure 5.7.1 Cross-section of one unit cell of a three-layer high-impedance surface.....	63
Figure 6.1.1 Geometry studied using the finite element method.....	65
Figure 6.1.2 Surface wave band structure for a two-layer, high-impedance surface.....	66
Figure 6.2.1 A bound surface wave, for which phase matching is impossible.....	68
Figure 6.2.2 Phase matching to a leaky wave.....	68
Figure 6.2.3 Calculation of leaky waves, illustrated by error bars .....	69
Figure 6.3.1 Surface wave band diagram in the absence of conducting vias .....	70
Figure 7.1.1 TM surface wave measurement using monopole probe antennas .....	72
Figure 7.1.2 TM surface wave measurement using flared parallel-plate waveguides .....	73
Figure 7.1.3 TM surface wave transmission data on a flat metal surface .....	73
Figure 7.1.4 TM surface wave transmission data on a textured surface .....	74
Figure 7.2.1 TE surface wave measurement using monopole probe antennas .....	75
Figure 7.2.2 TE surface wave measurement using small loop antennas .....	76
Figure 7.2.3 TE surface wave transmission data on a textured surface .....	77
Figure 7.3.1 Reflection phase measurement using a pair of horn antennas .....	78
Figure 7.3.2 Reflection phase of a textured surface.....	79
Figure 7.3.3 Waves impinging on, and reflected by a surface.....	80
Figure 7.3.4 Standing wave fields at a frequency far below resonance .....	81
Figure 7.3.5 Standing wave pattern just below resonance.....	82
Figure 7.3.6 Standing wave pattern at the resonance frequency.....	82
Figure 7.3.7 Standing wave pattern just above resonance.....	83
Figure 7.3.8 Standing wave pattern for a frequency far above resonance.....	83
Figure 7.4.1 Surface wave transmission across a three-layer high-impedance surface ....	84
Figure 7.4.2 Reflection phase of a three-layer high-impedance surface .....	85
Figure 7.5.1 A broad frequency sweep reveals other features of the band structure .....	87
Figure 7.5.2 Electric field lines for a possible mode in an upper band .....	87
Figure 8.1.1 A “capacitive” surface .....	89
Figure 8.1.2 An “inductive” surface.....	89
Figure 8.2.1 A capacitive sheet backed by a solid metal ground plane.....	90
Figure 8.2.2 Effective medium model for a capacitive sheet above a ground plane .....	91
Figure 8.2.3 A two-port network .....	91
Figure 8.2.4 Reflection phase of a capacitive sheet above a ground plane .....	93
Figure 8.3.1 Dispersion curves for surface waves on a grounded dielectric slab .....	96
Figure 8.3.2 Surface waves shifting toward the ground plane at higher frequencies .....	97
Figure 8.4.1 Metal corrugations preventing high frequency TM surface waves .....	98
Figure 8.4.2 Effective circuit in the absence of conducting vias .....	98
Figure 8.4.3 Vertical conducting vias linking the two surfaces together .....	99

Figure 9.1.1 Surface waves radiating at ground plane edges.....	101
Figure 9.1.2 Radiation pattern of a monopole antenna on a flat metal ground plane .....	102
Figure 9.1.3 Surface wave suppression on a high-impedance ground plane.....	103
Figure 9.1.4 Radiation pattern of a monopole on a high-impedance ground plane .....	103
Figure 9.1.5 Monopole radiation pattern below the TM surface wave band edge. ....	104
Figure 9.2.1 A patch antenna on a metal ground plane .....	105
Figure 9.2.2 A patch antenna embedded in a high-impedance ground plane.....	106
Figure 9.2.3 S11 measurements for patch antennas on two different ground planes.....	106
Figure 9.2.4 H-plane radiation patterns of two patch antennas. ....	107
Figure 9.2.5 E-plane radiation patterns of two patch antennas.....	108
Figure 9.2.6 Patch antenna.....	109
Figure 9.3.1 Horizontal wire antenna on a metal ground plane.....	111
Figure 9.3.2 Reflection loss of a horizontal wire antenna on a flat metal ground .....	111
Figure 9.3.3 A horizontal wire antenna on a high-impedance ground plane.....	112
Figure 9.3.4 Reflection loss of a horizontal wire on a high-impedance ground plane....	112
Figure 9.3.5 E-Plane radiation pattern of two horizontal wire antennas .....	113
Figure 9.3.6 H-plane radiation pattern of two horizontal wire antennas.....	114
Figure 9.3.7 A small kink placed near the feed point for impedance matching .....	115
Figure 9.4.1 A circular wire antenna on a high-impedance ground plane.....	116
Figure 9.4.2 A plus-shaped wire antenna .....	117
Figure 9.4.3 A figure-8-shaped wire antenna .....	118
Figure 9.5.1 Coupling between two antennas in TM configuration.....	120
Figure 9.5.2 Coupling between two antennas in TE configuration.....	121
Figure 9.5.3 Leaky TE waves radiate, and never reach the ground plane edge.....	122
Figure 9.5.4 Array design using stripes of metal and high-impedance material .....	123
Figure 9.6.1 Reference radiation pattern of a dipole antenna in free space.....	126
Figure 9.6.2 Experiment to measure effects of the user in portable communications ....	127
Figure 9.6.3 Radiation pattern of a dipole antenna near a jar of water .....	127
Figure 9.6.4 Wire antenna on high-impedance ground plane, near jar of water .....	128
Figure 10.1.1 Dimensions for calculating fringing-field capacitance .....	130
Figure 10.1.2 Dimensions for calculating sheet capacitance.....	132
Figure 10.2.1 Three common geometries used for 2-D periodic structures .....	136
Figure 10.2.2 Three-layer hexagonal structure .....	137
Figure 10.2.3 Three-layer triangular structure.....	138
Figure 10.2.4 Three-layer square structure with a hidden layer .....	139
Figure 10.2.5 Three-layer square structure with no hidden layer .....	139
Figure 10.2.6 Three-layer, lower-symmetry square structure .....	140
Figure 10.3.1 Graph of measured frequency versus calculated frequency.....	141
Figure 10.3.2 Measured versus calculated frequencies for three-layer structures.....	142

## LIST OF SYMBOLS

$a$	lattice constant
$c$	speed of light in vacuum
$d$	separation of capacitor plates, or depth of corrugations
$f$	frequency
$k$	wave vector
$l$	length
$m$	effective electron mass
$n$	refractive index, or electron number density
$q$	electron charge
$t$	thickness of circuit board
$w$	width
$A$	area
$B$	magnetic flux density
$C$	capacitance
$D$	electric displacement
$E$	electric field
$F$	geometrical correction factor
$H$	magnetic field
$I$	current
$J$	current density
$L$	inductance
$R$	resistance, or reflection coefficient
$T$	transmission coefficient
$V$	voltage
$Z$	surface impedance
$\alpha$	decay constant into free space
$\gamma$	decay constant into material
$\delta$	skin depth
$\epsilon$	electric permittivity
$\eta$	impedance
$\theta$	angle
$\lambda$	wavelength
$\mu$	magnetic permeability
$\sigma$	electrical conductivity
$\tau$	mean electron collision time
$\omega$	angular frequency
$\psi$	electric flux density
$\nabla$	vector differential operator
$\partial$	scalar differential operator

## VITA

October 15, 1972                      Born, Fort Leonard Wood, Missouri

1994                                      B.S. Electrical Engineering  
University of California, Los Angeles

1994-1999                              Graduate Student Researcher,  
Department of Electrical Engineering  
University of California, Los Angeles

## PUBLICATIONS AND PRESENTATIONS

- D. F. Sievenpiper, E. Yablonovitch; J.N. Winn, S. Fan, P.R. Villeneuve, J.D. Joannopoulos, "3D Metallo-Dielectric Photonic Crystals with Strong Capacitive Coupling Between Metallic Islands", *Phys. Rev. Lett.* 80, p2829 (1998)
- D. F. Sievenpiper, M. E. Sickmiller, E. Yablonovitch, "3D Wire Mesh Photonic Crystals", *Phys. Rev. Lett* 76, p2480 (1996)
- D. F. Sievenpiper, C. F. Lam, E. Yablonovitch, "Two-Dimensional Photonic Crystal Vertical-Cavity Array for Nonlinear Optical Image Processing", *Applied Optics* 37, p2074 (1998)
- C. F. Lam, R. B. Vrijen, P. P. L. Chang-Chien, D. F. Sievenpiper, E. Yablonovitch, "A Tunable Wavelength Demultiplexer Using Logarithmic Filter Chains", *J. Lightwave Tech.* 16, p1657 (1998)
- E. Yablonovitch, D. F. Sievenpiper, "Knitting a Finer Net for Photons", *Nature* 383, p665 (1996)
- C. F. Lam, R. B. Vrijen, P. Chang-Chien, D. Sievenpiper, E. Yablonovitch, "A Tunable Wavelength Demultiplexer Using Cascaded Photonic Crystal Filters", *Opt. Phot. News*, p48, January, 1998
- D. F. Sievenpiper, "High-Impedance Electromagnetic Crystal Ground Planes", Presented at the Workshop on Electromagnetic Crystal Structures, Design, Synthesis, and Applications, Laguna Beach, CA, USA, January 6-8, 1999

- D. F. Sievenpiper, E. Yablonovitch, "Eliminating Surface Currents with Metallodielectric Photonic Crystals", IEEE MTT-S International Microwave Symposium Digest, vol 2, p663, Baltimore, MD, USA, 7-12 June 1998
- D. F. Sievenpiper, E. Yablonovitch, "Controlling Surface Plasmons on Metallodielectric Photonic Crystals", CLEO '98. Summaries of Papers Presented at the Conference on Lasers and Electro-Optics. p186, San Francisco, CA, USA, May 3-8, 1998
- D. Sievenpiper, E. Yablonovitch, "Surface Plasmons on Metallodielectric Photonic Crystals", presented at the March Meeting of the American Physical Society, Los Angeles, CA, USA, 1998
- D. Sievenpiper, E. Yablonovitch, "Metallodielectric Photonic Crystals for Antenna Substrates", OSA Annual Meeting Conference Program, p142, Long Beach, CA, October 12-17, 1997
- D. F. Sievenpiper, M. E. Sickmiller, E. Yablonovitch, "3D Metallic Photonic Bandgap Structures", CLEO '96 Summaries of Papers Presented at the Conference on Lasers and Electro-Optics, p387, Anaheim, CA, USA, 2-7 June 1996
- D. F. Sievenpiper, M. E. Sickmiller, E. Yablonovitch, "3D Metallic Photonic Bandgap Structures", Proceedings of the NATO Advanced Study Institute on Photonic Band Gap Materials, p165 Elounda, Crete, Greece, June 18-30, 1995

## ABSTRACT OF THE DISSERTATION

High-Impedance Electromagnetic Surfaces

By

Daniel Frederic Sievenpiper

Doctor of Philosophy in Electrical Engineering

University of California, Los Angeles, 1999

Professor Eli Yablonovitch, Chair

A new type of metallic electromagnetic structure has been developed that is characterized by having high surface impedance. Although it is made of continuous metal, and conducts DC currents, it does not conduct AC currents within a forbidden frequency band. Unlike normal conductors, this new surface does not support propagating surface waves, and it reflects electromagnetic waves with no phase reversal. The geometry consists of a metal sheet, textured with a two-dimensional lattice of resonant elements, which act as a two-dimensional filter to prevent the propagation of electric currents. The surface can be described using a lumped parameter circuit model, which accurately predicts many of its electromagnetic properties. This unique material is applicable to a variety of electromagnetic problems, including new kinds of low-profile antennas.

# 1 Introduction

In some situations, the presence of electric conductors can have consequences that adversely affect the performance of electromagnetic devices, particularly those involving radio communication. Conductive surfaces are useful as reflectors, but they reverse the phase of reflected waves. They also support propagating surface waves, which can have deleterious effects on antenna performance. One can compensate for these properties, but this adds additional geometric constraints, often resulting in a design that is less than optimum.

By applying a special texture to a conducting surface, it is possible to alter its surface properties. [1] Made of solid metal, the structure conducts DC currents, but over a particular frequency range, it does not conduct AC currents. This new surface is characterized by having high electromagnetic surface impedance. It does not reverse the phase of reflected waves, and the image currents appear in-phase, rather than out-of-phase as they are on normal conductors. Furthermore, propagating surface waves are not supported. Instead, radio-frequency currents on the surface radiate efficiently into free space. This high-impedance surface provides a useful new ground plane for novel low-profile antennas, and other electromagnetic structures.

## 1.1 Electric Conductors

While a conductive surface is a good reflector, it has the unfortunate property of reversing the phase of reflected waves. Good conductors forbid internal electric fields, and continuity across the metal/air boundary forces the tangential electric field at the

surface to zero. When an electromagnetic wave impinges on a conductor, the reflected wave experiences a phase reversal to ensure that the electric field has a node at the surface. Likewise, the magnetic field has an antinode at the surface.

A flat metal sheet is used in many antennas as a reflector, or ground plane. [2] The presence of a ground plane redirects half of the radiation into the opposite direction, improving the antenna gain by 3dB, and partially shielding objects on the other side. Unfortunately, if the antenna is too close to the conductive surface, the phase of the impinging wave is reversed upon reflection, resulting in destructive interference with the wave emitted in the other direction. This is equivalent to saying that the image currents in the conductive sheet cancel the currents in the antenna, resulting in poor radiation efficiency. Figure 1.1.1 depicts an antenna in close proximity with a flat, conducting slab. The antenna is effectively shorted out by the metal surface, and negligible radiation is emitted.

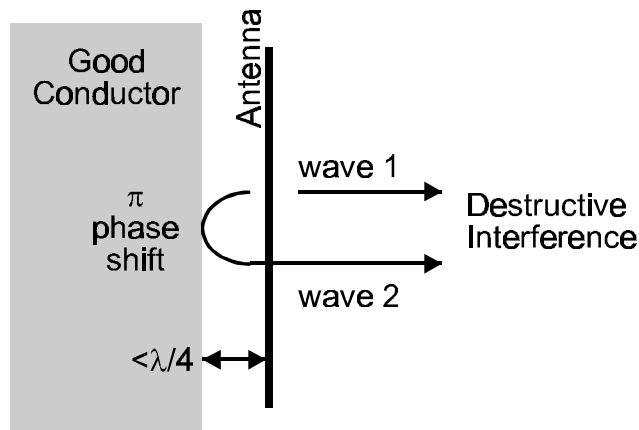


**Figure 1.1.1 An antenna lying flat against a ground plane**

This problem is solved by including a one-quarter wavelength space between the radiating element and the ground plane, as shown in Figure 1.1.2. The total round trip

phase shift from the antenna, to the surface, and back to the antenna, equals one complete cycle, and the waves add constructively. The antenna radiates efficiently, but the entire structure requires a minimum thickness of  $\lambda/4$ .

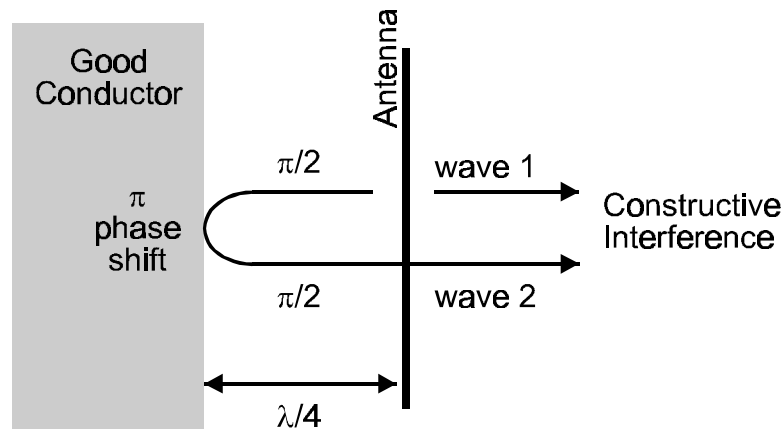


**Figure 1.1.2 An antenna separated by 1/4 wavelength from the ground plane**

Another property of metals is that they support surface waves.[3, 4] These are propagating electromagnetic waves that are bound to the interface between metal and free space. They are called surface plasmons at optical frequencies, [5] but at microwave frequencies, they are nothing more than the normal AC currents that occur on any electric conductor. If the conductor is smooth and flat, the surface waves will not couple to external plane waves. However, they will radiate if scattered by bends, discontinuities, or surface texture. Bound surface waves do not exist on an ideal “perfect electric conductor” since, in the limit of infinite conductivity, the fields associated with surface currents extend an infinite distance into space.

An example of a TM surface wave propagating across a metal slab is shown in Figure 1.1.3. The magnetic field is transverse to the direction of propagation, associated

with longitudinal currents flowing on the conductor. The electric field is linked to charge separation on the top of the conductor, and it jumps out of the surface in loops. The charges oscillate, and the wave propagates along the surface at nearly the speed of light. At optical frequencies, these surface plasmons are highly localized to the air/metal interface. At microwave or radio frequencies, the electromagnetic fields extend many thousands of wavelengths into the surrounding space, and these waves are described more appropriately as surface currents.

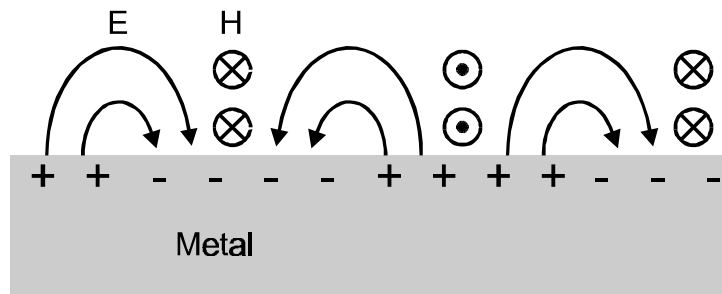


**Figure 1.1.3 A TM surface wave propagating across a metal slab**

Surface waves appear in many situations involving antennas. If an antenna is placed near a metal sheet, such as a reflector or ground plane, it will radiate plane waves into free space, but it will also generate currents that propagate along the sheet. On an infinitely large ground plane, the surface currents would be evident only as a slight reduction in radiation efficiency. In reality, the ground plane is always finite in size, and these currents propagate until they reach an edge or corner. Any break in the continuous translational symmetry of the smooth, flat surface allows the currents to radiate. The result is a kind of multipath interference or “speckle”, illustrated in Figure 1.1.4, which can be seen as ripples in the far field radiation pattern. Moreover, if multiple antennas

share the same ground plane, surface currents can cause unwanted mutual coupling between them.

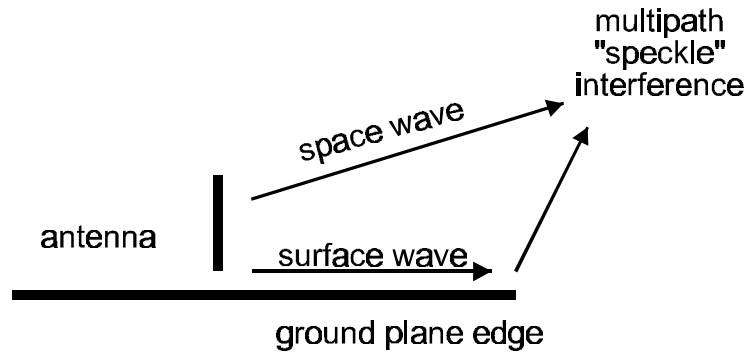


**Figure 1.1.4 Multipath interference due to surface waves on a ground plane**

## 1.2 High Impedance Surfaces

By incorporating a special texture on a conductor, it is possible to alter its radio-frequency surface properties. In the limit where the period of the surface texture is much smaller than the wavelength, the structure can be described using an effective medium model, and its qualities can be summarized into a single parameter, the surface impedance. This boundary condition defines the ratio of the tangential electric field to the tangential magnetic field at the surface. It is the same impedance given by Ohm's law: the ratio of the voltage to the current along the sheet, expressed in Ohms/square. A smooth conducting sheet has low surface impedance, while with a specially designed geometry, the textured surface can have high surface impedance.



**Figure 1.2.1 Cross-section of a high-impedance surface**

A high-impedance surface, shown in cross section in Figure 1.2.1, consists of an array of metal protrusions on a flat metal sheet. They are arranged in a two-dimensional lattice, and are usually formed as metal plates, connected to the continuous lower conductor by vertical posts. They can be visualized as mushrooms or thumbtacks protruding from the surface. An example of a top view is shown in Figure 1.2.2. The hexagonal metal patches are raised above the surface, and the dots in the center are vertical connecting posts.

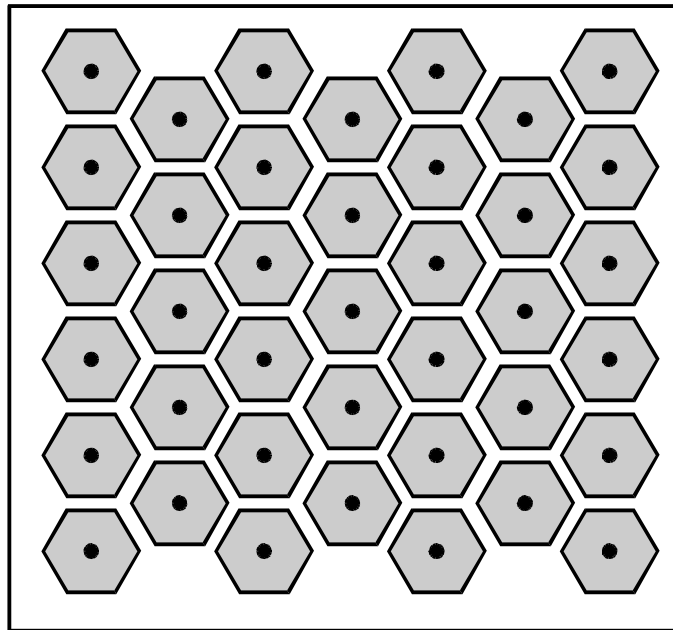


**Figure 1.2.2 Top view of the high-impedance surface**

If the protrusions are small compared to the wavelength, their electromagnetic properties can be described using lumped circuit elements – capacitors and inductors. The proximity of the neighboring metal elements provides the capacitance, and the long conducting path linking them together provides the inductance. They behave as parallel resonant LC circuits, which act as electric filters to block the flow of currents along the

sheet. An equivalent circuit is shown below in Figure 1.2.3. This is the origin of the high electromagnetic surface impedance.

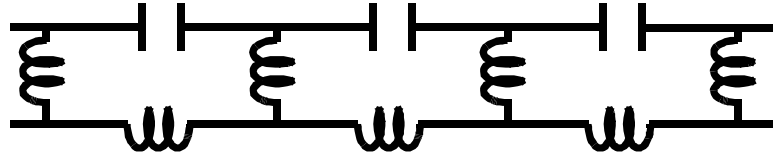


**Figure 1.2.3 An equivalent circuit for the high-impedance surface**

Because of its unusual impedance, the surface wave modes on this structure are very different from those on a smooth metal sheet. It can support tightly bound, radio frequency TM modes that propagate much more slowly than the speed of light. It can also support TE modes that are bound to the surface at some frequencies, but radiate readily at other frequencies. In TE surface waves, the electric field is tangential to the surface, and to the propagation direction, while the magnetic field extends out of the sheet in loops. They resemble the TM surface waves described earlier, but with the electric and magnetic fields exchanged, as shown in Figure 1.2.4.

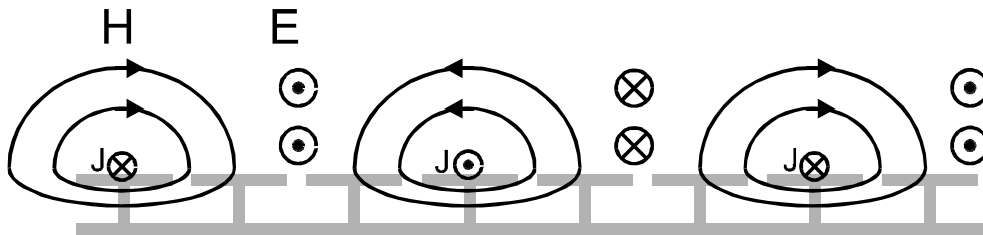


**Figure 1.2.4 A TE surface wave propagating across a high-impedance surface**

In the frequency range where the surface impedance is very high, the tangential magnetic field is small, even with a large electric field. Such a structure is sometimes described as a “magnetic conductor”. This is a mathematical idea that is used in certain

electromagnetics problems, but does not exist in reality. Having high impedance and being nearly lossless, this new surface can be regarded as a kind of magnetic conductor, over a certain frequency range.

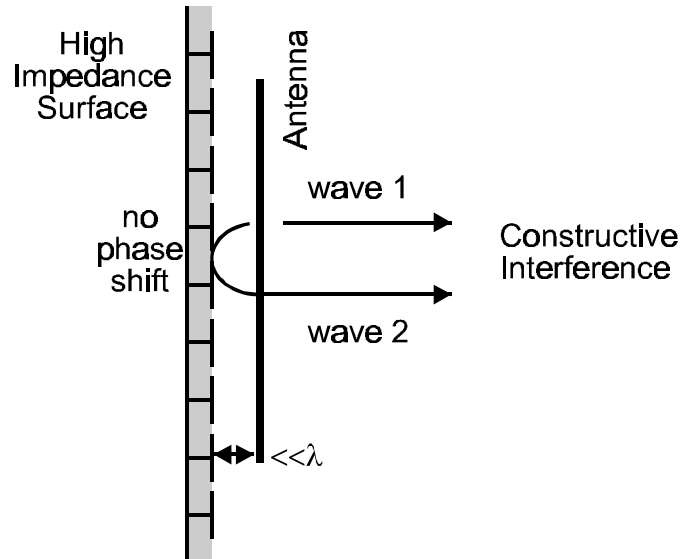


**Figure 1.2.5 A flush-mounted dipole on a high-impedance ground plane**

Because of this unusual boundary condition, the high-impedance surface can function as a unique new type of ground plane for low-profile antennas. For example, a simple dipole lying flat against a high-impedance ground plane, shown in Figure 1.2.5, is not shorted out as it would be on an ordinary metal ground plane. The high-impedance surface reflects all of the power just like a metal sheet, but it reflects in-phase, rather than out-of-phase, allowing the radiating element to be directly adjacent to the surface. In other words, the direction of the image currents results in constructive, rather than destructive interference, allowing the antenna to radiate efficiently. Furthermore, in a forbidden frequency band, the high-impedance ground plane does not support freely propagating surface currents, resulting in an improved radiation pattern.

## 2 Surface Waves

Surface waves can be illustrated in several different ways. In optics, they are called surface plasmons. They also exist at radio frequencies, where they are simply called surface currents. One way to derive their properties is to solve for waves that decay exponentially away from a dielectric interface. We find that such waves only exist on materials with a non-positive dielectric constant, such as metals. The same waves can be found by starting from the viewpoint that a material can be assigned an effective surface impedance. In the case of a metal, the surface impedance is determined by the skin depth. We find that the skin depth is equivalent to the surface wave penetration depth, and thus, surface waves are nothing more than ordinary surface currents, which are well understood at radio frequencies. MKSA units will be used throughout this discussion.

### 2.1 Dielectric Interfaces

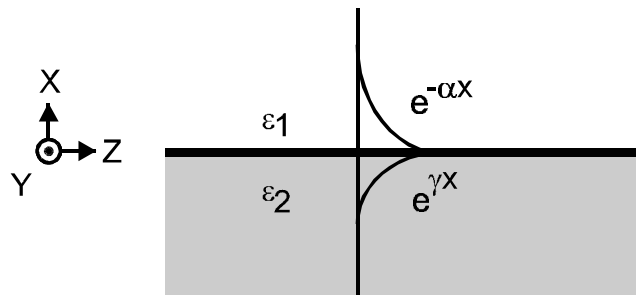


**Figure 2.1.1 A surface wave on an interface between two dissimilar media.**

Surface waves can occur on the interface between two dissimilar materials, such as metal and free space. To derive the properties of surface waves on a general interface, begin with two materials having different dielectric constants,  $\epsilon_1$  and  $\epsilon_2$ . [4, 6] The

surface is in the YZ plane, with material 1 extending in the +X direction, and material 2 in the -X direction, as shown in Figure 2.1.1.

For a wave to be bound to the surface, assume it decays in the +X direction with decay constant  $\alpha$ , and in the -X direction with decay constant  $\gamma$ . Consider first a TM surface wave, for which  $E_y=0$ . The electric field in material 1 has the following form, in which the factor  $e^{j\omega t}$  is implicit.

$$\begin{aligned} E_x &= A \cdot e^{-jkz-\alpha x} \\ E_y &= 0 \\ E_z &= B \cdot e^{-jkz-\alpha x} \end{aligned}$$

**Equation 2.1.1**

In material 2, the electric field has the same form, given below.

$$\begin{aligned} E_x &= C \cdot e^{-jkz+\gamma x} \\ E_y &= 0 \\ E_z &= D \cdot e^{-jkz+\gamma x} \end{aligned}$$

**Equation 2.1.2**

Here, A, B, C, and D are constants. Recall the following from Maxwell's equations.

$$\begin{aligned} \nabla \times \bar{\mathbf{B}} &= \frac{\epsilon_r}{c^2} \frac{\partial \bar{\mathbf{E}}}{\partial t} \\ \nabla \times \bar{\mathbf{E}} &= -\frac{\partial \bar{\mathbf{B}}}{\partial t} \end{aligned}$$

**Equation 2.1.3**

These can be combined to yield the equation below.

$$\nabla \times \nabla \times \bar{\mathbf{E}} = -\epsilon_r \frac{\omega^2}{c^2} \frac{\partial^2 \bar{\mathbf{E}}}{\partial t^2}$$

**Equation 2.1.4**

This can be expanded explicitly, bearing in mind that the Y derivative of the electric field on both sides is zero.

$$\hat{x} \left( \frac{-\partial^2 E_x}{\partial z^2} + \frac{\partial^2 E_z}{\partial x \partial z} \right) + \hat{z} \left( \frac{\partial^2 E_x}{\partial x \partial z} - \frac{\partial^2 E_z}{\partial x^2} \right) = \epsilon \frac{\omega^2}{c^2} (\hat{x} E_x + \hat{z} E_z)$$

**Equation 2.1.5**

By inserting Equation 2.1.1 into Equation 2.1.5, we obtain equations for the fields above the surface.

$$\begin{aligned} k^2 A + jk\alpha B &= \epsilon_1 \frac{\omega^2}{c^2} A \\ jk\alpha A - \alpha^2 B &= \epsilon_1 \frac{\omega^2}{c^2} B \end{aligned}$$

**Equation 2.1.6**

Similarly, by inserting Equation 2.1.2 into Equation 2.1.5, we obtain equations for the fields below the surface.

$$\begin{aligned} k^2 C - jk\gamma D &= \epsilon_2 \frac{\omega^2}{c^2} C \\ -jk\gamma C - \gamma^2 D &= \epsilon_2 \frac{\omega^2}{c^2} D \end{aligned}$$

**Equation 2.1.7**

Finally, the tangential electric field and the normal electric displacement must be continuous across the interface, as specified by the following boundary conditions.

$$A = C$$

$$\epsilon_1 \mathbf{B} = \epsilon_2 \mathbf{D}$$

**Equation 2.1.8**

We can combine Equation 2.1.6, Equation 2.1.7, and Equation 2.1.8 to solve for the wave vector,  $k$ , and the decay constants,  $\alpha$  and  $\gamma$ .

$$k = \sqrt{\frac{\epsilon_1 \epsilon_2}{\epsilon_1 + \epsilon_2}} \frac{\omega}{c}$$

**Equation 2.1.9**

$$\alpha = \sqrt{\frac{-\epsilon_1^2}{\epsilon_1 + \epsilon_2}} \frac{\omega}{c}$$

**Equation 2.1.10**

$$\gamma = \sqrt{\frac{-\epsilon_2^2}{\epsilon_1 + \epsilon_2}} \frac{\omega}{c}$$

**Equation 2.1.11**

These equations describe surface waves on a general interface between two dissimilar dielectric materials. For simplicity, assume that one of the materials is free space,  $\epsilon_1 = 1$ .

Dropping the subscript from  $\epsilon_2$ , we obtain the following results.

$$k = \sqrt{\frac{\epsilon}{1 + \epsilon}} \frac{\omega}{c}$$

**Equation 2.1.12**

$$\alpha = \sqrt{\frac{-1}{1 + \epsilon}} \frac{\omega}{c}$$

**Equation 2.1.13**

$$\gamma = \sqrt{\frac{-\epsilon^2}{1+\epsilon}} \frac{\omega}{c}$$

**Equation 2.1.14**

From these equations, it can be seen that TM surface waves do not exist on non-conductive, dielectric materials. If  $\epsilon$  is positive, then  $\alpha$  and  $\gamma$  are imaginary, and the waves do not decay with distance from the surface; they are simply plane waves propagating through the dielectric interface. On the other hand, if  $\epsilon$  is less than  $-1$ , or if it is imaginary, the solution describes a wave that is bound to the surface. These TM surface waves can occur on metals, or other materials with non-positive dielectric constants. The properties of surface waves under various conditions will be explored in the following sections.

The solution for TE surface waves can be obtained from the foregoing analysis by the principle of duality. [2] If the electric and magnetic fields are exchanged, and  $\mu$  is substituted for  $\epsilon$ , the solution above can be applied to the TE case.

## 2.2 Metal Surfaces

The effective, relative dielectric constant of a metal can be expressed in the following form. [6]

$$\epsilon = 1 - \frac{j\sigma}{\omega\epsilon_0}$$

**Equation 2.2.1**

$\sigma$  is the conductivity, which is given by the equation below.

$$\sigma = \frac{nq^2\tau/m}{1 + j\omega\tau}$$

**Equation 2.2.2**

$\tau$  is the mean electron collision time,  $q$  is the electron charge, and  $m$  and  $n$  are the effective mass and the density, respectively, of the conduction electrons.

For frequencies much lower than  $1/\tau$ , which includes the microwave spectrum, the conductivity is primarily real, and much greater than unity, so the dielectric constant is a large, imaginary number. Inserting Equation 2.2.1 into Equation 2.1.12 leads to a simple dispersion relation for surface waves at radio frequencies.

$$k \approx \frac{\omega}{c}$$

**Equation 2.2.3**

Thus, surface waves propagate at nearly the speed of light in vacuum, and they travel for many wavelengths along the metal surface with little attenuation. By inserting Equation 2.2.1 into Equation 2.1.13, we can find an expression for  $\alpha$ , the decay constant of the fields into the surrounding medium.

$$\alpha = \frac{\omega}{c} \sqrt{\frac{-1}{2 - \frac{j\sigma}{\omega\epsilon_0}}}$$

$$\alpha \approx \frac{\omega}{c} \sqrt{\frac{\omega\epsilon_0}{2\sigma}} (1 - j)$$

**Equation 2.2.4**

For good conductors at microwave frequencies, the surface waves extend a great distance into the surrounding space. For example, on a copper surface, the electromagnetic fields

associated with a 10 GHz surface wave extend about 70 meters, or 2300 wavelengths into free space. Hence, at microwave frequencies they are often described simply as surface currents, rather than surface waves. These surface currents are nothing more than the normal AC currents that occur on conductors in any electromagnetics problem.

We can also determine  $\gamma$ , the surface wave penetration depth into the metal. By inserting Equation 2.2.1 into Equation 2.1.14, we obtain the following equation.

$$\gamma = \frac{\omega}{c} \sqrt{\frac{-\epsilon^2}{1+\epsilon}} \approx \frac{\omega}{c} \sqrt{-\epsilon} = \frac{\omega}{c} \sqrt{\frac{j\sigma}{\omega\epsilon_0}}$$

$$\gamma \approx (1+j) \sqrt{\frac{\omega\mu_0\sigma}{2}} = \frac{(1+j)}{\delta}$$

**Equation 2.2.5**

The skin depth,  $\delta$ , is defined by the expression below. [3]

$$\delta = \sqrt{\frac{2}{\omega\mu_0\sigma}}$$

**Equation 2.2.6**

Thus, the surface currents penetrate only a very small distance into the metal. For example, at 10 GHz, the skin depth of copper is less than one micron.

From the skin depth, we can derive the surface impedance of a flat metal sheet. The current and the electric field decay exponentially into the metal with a decay constant of  $\gamma$ . From Equation 2.2.5, we can write an equation for the current in terms of the skin depth, in which  $E_0$  is the electric field at the surface.

$$J_z(x) = \sigma E_z(x) = \sigma E_0 e^{-x(1+j)/\delta}$$

**Equation 2.2.7**

The magnetic field at the surface is found by integrating around a path surrounding the thin surface layer of current, extending far into the metal beyond the skin depth.

$$H_0 = \int_0^{\infty} J_z(x) dx = \frac{\sigma \delta}{1+j} E_0$$

**Equation 2.2.8**

Thus, the surface impedance of a flat metal surface is derived.

$$Z_s = \frac{E_z}{H_y} = \frac{1+j}{\sigma \delta}$$

**Equation 2.2.9**

The surface impedance has equal positive real and positive imaginary parts, so the resistance of a metal surface is accompanied by an equal amount of inductance.

At higher frequencies, the dielectric constant of a metal takes a different form. When the frequency is much greater than  $1/\tau$ , the inverse collision time, the dielectric constant given in Equation 2.2.1 may be approximated as follows.

$$\epsilon \approx 1 - \frac{\omega_p^2}{\omega^2}$$

**Equation 2.2.10**

The plasma frequency,  $\omega_p$ , is the highest frequency to which the conduction electrons are able to respond, and it is given by the expression below.

$$\omega_p = \sqrt{\frac{nq^2}{\epsilon_0 m}}$$

**Equation 2.2.11**

Above  $\omega_p$ , which is usually in the ultraviolet range, the electrons cannot follow applied electric fields, so the metal is transparent to electromagnetic waves.

At optical frequencies, the dielectric constant is a negative real number. Surface waves, often called surface plasmons, propagate just below the speed of light. Inserting Equation 2.2.10 into Equation 2.1.12, we find that surface waves are cut off for frequencies above  $\omega_p / \sqrt{2}$ . The dispersion curve bends over flat, as shown in Figure 2.2.1, and the surface plasmons have a very high density of states.

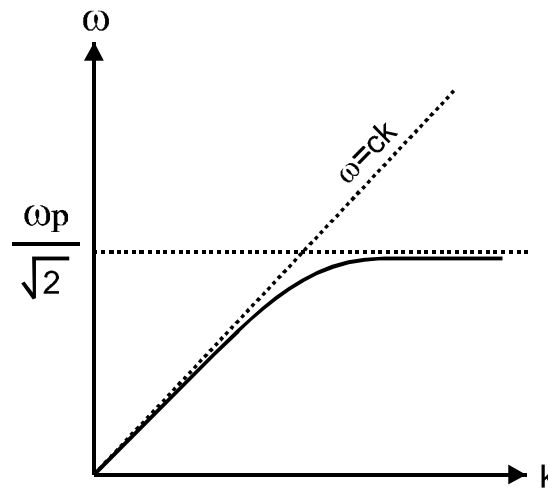


**Figure 2.2.1 Dispersion diagram for optical surface plasmons on metals**

Optical-frequency surface plasmons can be detected in several ways. For example, high-energy electrons launched through a thin metal film lose energy in multiples of the surface plasmon frequency. They can also be seen as a narrow-band dip in the optical reflectivity of metals. Although plasmons on a smooth surface cannot

couple to plane waves in free space, a small amount of roughness can facilitate phase matching between external plane waves and surface waves.

### 2.3 Impedance Surfaces

Figure 2.3.1 shows the geometry used for computing surface impedance. For an electromagnetic field above a surface of width  $w$  and length  $\ell$ , the current in the surface is equal to the magnetic field integrated around the surface.

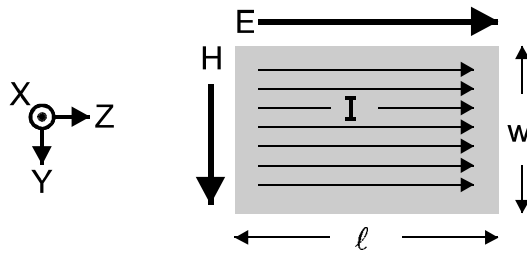


**Figure 2.3.1** A rectangular area used for computing surface impedance

$$I = H_y \cdot w \quad \text{Equation 2.3.1}$$

The voltage across length  $\ell$  is given by the electric field at the surface.

$$V = E_z \cdot \ell \quad \text{Equation 2.3.2}$$

The surface impedance can be defined as the ratio of the electric field over the magnetic field at the surface.

$$Z_s = \frac{E_z}{H_y} = \frac{V}{I} \left( \frac{w}{\ell} \right) \quad \text{Equation 2.3.3}$$

The factor of  $w/\ell$  is taken as unity, and the surface impedance defined this way is the same as that given by Ohm's law, expressed in Ohms/square.

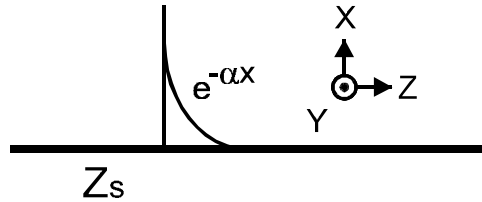


**Figure 2.3.2 A surface wave propagating on an arbitrary impedance surface**

The surface wave behavior can be derived for a general impedance surface. [3, 4] Assume a surface in the YZ plane with impedance  $Z_s$ . A surface wave propagates in the +Z direction, with fields decaying in the +X direction. The geometry of the problem is shown in Figure 2.3.2.

For TM surface waves,  $H_x = H_z = E_y = 0$ . Assume that the fields diminish in the X direction with decay constant  $\alpha$ , and travel along the Z direction with propagation constant  $k$ . Start with the Z component of the electric field.

$$E_z = C e^{-jkz - \alpha x} \tag{Equation 2.3.4}$$

$H_y$  can be derived from the Ampere's law.

$$\nabla \times \vec{H} = \epsilon \frac{\partial \vec{E}}{\partial t} \tag{Equation 2.3.5}$$

Writing out the derivatives explicitly, and taking into account the three field components that are known to be zero, we obtain the following expression.

$$j\omega\epsilon E_z = \frac{\partial H_y}{\partial x}$$

**Equation 2.3.6**

Equation 2.3.6 is solved with Equation 2.3.4.

$$H_y = \frac{-j\omega\epsilon}{\alpha} C e^{-jkz - \alpha x}$$

**Equation 2.3.7**

The surface impedance in this coordinate system is equal to the following expression.

$$Z_s = \frac{E_z}{H_y}$$

**Equation 2.3.8**

Inserting Equation 2.3.4 and Equation 2.3.7 into Equation 2.3.8 gives the required surface impedance for TM surface waves.

$$Z_s(\text{TM}) = \frac{j\alpha}{\omega\epsilon}$$

**Equation 2.3.9**

It is clear that TM waves only occur on a surface with positive reactance – an inductive surface impedance.

We can also determine the impedance required for TE surface waves. We use the same geometry as shown in Figure 2.3.2, and assume that the electric field is entirely transverse, oriented along the Y direction. The magnetic field forms loops that emerge from the surface in the XZ plane. Complimentary to the TM waves, assume the following form for the magnetic field.

$$H_z = C e^{-jkz - \alpha x}$$

**Equation 2.3.10**

We can solve for  $E_y$  using Faraday's law.

$$\nabla \times \vec{E} = -\mu \frac{\partial \vec{H}}{\partial t}$$

**Equation 2.3.11**

Writing out the derivatives of the non-zero fields gives the equation below.

$$\frac{\partial E_y}{\partial x} = -j\omega\mu H_z$$

**Equation 2.3.12**

Equation 2.3.12 is solved with Equation 2.3.10.

$$E_y = \frac{j\omega\mu}{\alpha} C e^{-jkz - \alpha x}$$

**Equation 2.3.13**

To obtain the correct sign for the surface impedance, it is important to consider the right hand rule, and the vector nature of the fields. The impedance of a surface is taken to be the ratio of the electric and magnetic fields, with an orientation that is consistent with a wave impinging on the surface from the outside. This convention ensures that an absorbing surface will have positive resistance, while a surface with reflective gain will have negative resistance. Thus, the surface impedance seen by TE waves is given by the following expression.

$$Z_s = \frac{-E_y}{H_z}$$

**Equation 2.3.14**

The difference between the TM and the TE case can be understood by remembering that in both situations, the signs are such that an incident plane wave would be absorbed. The TE case has  $E_y$  polarization, and the TM case has  $E_z$  polarization. The presence of the negative sign can be understood by imagining a rotation of the coordinate system around the X axis:

$$\begin{aligned} Y &\rightarrow Z \\ Z &\rightarrow -Y \end{aligned}$$

**Equation 2.3.15**

Following this convention, the surface impedance for TE waves is given below.

$$Z_s(\text{TE}) = \frac{-j\omega\mu}{\alpha}$$

**Equation 2.3.16**

Thus, a negative reactance – a capacitive surface impedance, is necessary to support TE surface waves.

### 3 Textured Surfaces

As we have seen in the previous chapter, metals support surface waves over a broad range of frequencies, spanning from DC up to visible light. These surface waves can be eliminated over a finite frequency band by applying a periodic texture, such as a lattice of small bumps. As surface waves scatter from the rows of bumps, the resulting interference prevents them from propagating, producing a two-dimensional electromagnetic bandgap.

By engineering the geometry of the surface texture, the period can be made much smaller than the wavelength of the surface waves. Such a structure can be described using an effective medium model, in which the surface is assigned an impedance that can predict many of its electromagnetic properties. As an example, this method will be used to analyze the simple case of a one-dimensional corrugated metal surface.

The high-impedance surface is an abstraction of the corrugated surface, in which the corrugations have been folded up into lumped circuit elements, and distributed in two dimensions. The surface impedance is that of a parallel resonant circuit, which can be tuned to exhibit high impedance over a predetermined frequency band.

#### 3.1 Bumpy Surfaces

Consider the evolution from a flat metal sheet to a nearly flat conductor covered with a two-dimensional lattice of small bumps. [7, 8] Surface waves are allowed, as they are on normal metals. When the wavelength is much longer than the period of two-dimensional lattice, the surface waves hardly notice the small bumps. As the wavelength

is reduced, the waves begin to feel the effects of the surface texture. When one-half wavelength fits between the rows of bumps, this corresponds to the Brillouin zone boundary [9] of the two-dimensional lattice. At this wavelength, a standing wave on the surface can have two possible positions: with the wave crests centered on the bumps, or with the nulls centered on the bumps, as shown in Figure 3.1.1. These two modes have slightly different frequencies, separated by a small band gap within which surface waves cannot propagate.

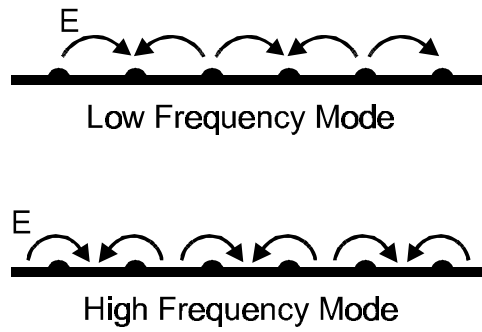


**Figure 3.1.1 A bumpy metal sheet with a narrow surface wave band gap**

This surface has been studied at optical frequencies by Barnes, Kitson, and others [7, 8] using a triangular lattice of bumps, patterned on a silver film. The period of the bumps was 300 nm, and the thickness of the film was 40 nm. The structure effectively suppressed surface plasmons within a 5% bandwidth, centered at 1.98 eV. The surface would have similar behavior at microwave frequencies, if it were scaled about 10,000 times larger.

Small bumps only provide a narrow bandwidth because they represent only a small perturbation of the flat metal surface. As the bumps are enlarged, the band gap

increases. The evolution from the bumpy surface to the high-impedance surface is shown in Figure 3.1.2.

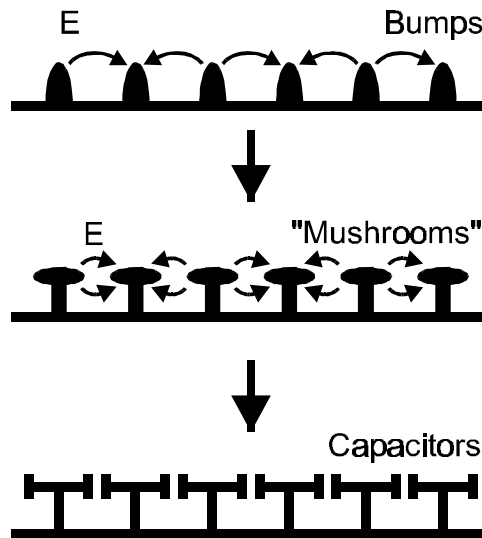


**Figure 3.1.2 Evolution from a bumpy surface to a high impedance surface**

As the bumps are stretched toward each other, like mushrooms or thumbtacks standing up on the surface, the electric field is localized to the narrow separation between them. As this separation becomes smaller, significant capacitance develops between neighboring protrusions. The currents traverse a long path as they slosh back and forth between the metal elements, providing inductance to the circuit. The structure acts as a kind of electric filter that prevents the propagation of currents on the surface.

### **3.2 Corrugated Surfaces**

The high-impedance surface can be understood by examining a similar structure, the corrugated surface, which is discussed in various textbooks, [3, 4] and review articles. [10, 11] Numerous authors have also contributed general treatments of corrugated surfaces, [12, 13, 14] and specific studies of important structures. [15, 16, 17, 18] A

corrugated surface is a metal slab, into which a series of vertical slots have been cut, as depicted in Figure 3.2.1. The slots are narrow, so that many of them fit within one wavelength across the slab. Each slot can be regarded as a parallel-plate transmission line, running down into the slab, and shorted at the bottom.

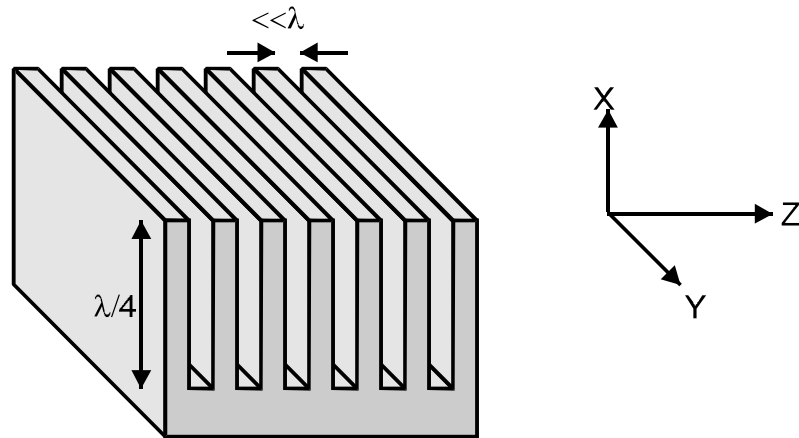


**Figure 3.2.1 A corrugated metal slab**

If the slots are one-quarter wavelength deep, then the short-circuit at the bottom end is transformed by the length of the slot into an open-circuit at the top end, and the impedance at the top surface is very high. This can be shown by assuming a sinusoidal wave traveling down a transmission line to a discontinuity positioned at  $x=0$ , as shown in Figure 3.2.2. Part of the wave is reflected by the discontinuity, forming a standing wave, consisting of forward,  $f$ , and backward,  $b$ , running waves.

$$E(x) = E_f e^{jkx} + E_b e^{-jkx}$$

$$H(x) = H_f e^{jkx} + H_b e^{-jkx}$$

**Equation 3.2.1**

The boundary condition at  $X=0$  is the impedance,  $Z$ .

$$\frac{E_{\text{total}}(x=0)}{H_{\text{total}}(x=0)} = Z$$

**Equation 3.2.2**

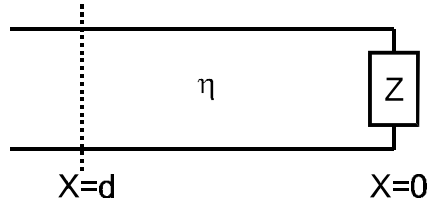


**Figure 3.2.2 A transmission line terminated at X=0 by an impedance, Z**

The negative sign is present in the denominator because of the direction of the field vectors for waves propagating in each direction. The fields in each running wave are related by the impedance of the waveguide,  $\eta$ .

$$\left| \frac{E_f(x)}{H_f(x)} \right| = \left| \frac{E_b(x)}{H_b(x)} \right| = \eta$$

**Equation 3.2.3**

If the discontinuity is a short, as in the case of the corrugated surface, then  $Z=0$ , and according to Equation 3.2.2 the electric field is reversed on reflection.

$$E_b(0) = -E_f(0)$$

**Equation 3.2.4**

The magnetic field is also reversed for the backward wave. Combining Equation 3.2.1, Equation 3.2.3 and Equation 3.2.4, yields the impedance as a function of distance from the short.

$$\frac{E_{\text{total}}(d)}{H_{\text{total}}(d)} = \frac{E_f e^{jkd} - E_f e^{-jkd}}{H_f e^{jkd} + H_f e^{-jkd}}$$

$$Z(x) = j\eta \tan(kd)$$

**Equation 3.2.5**

If there are many slots per wavelength, the top surface can be assigned an effective sheet impedance equal to the impedance of the slots. The behavior of the corrugations is reduced to a single parameter – the boundary condition at the top surface. We have already derived the surface wave properties of an impedance surface. If the depth of the slots,  $d$ , is greater than one-quarter wavelength, the tangent function is negative, and TM surface waves are cut off. Since TE surface waves are shorted by the continuous metal ridges, they only propagate along the Y-direction. Furthermore, a plane wave polarized with the electric field perpendicular to the ridges will appear to be reflected with no phase reversal, since the effective reflection plane is actually at the bottom of the slots, one-quarter wavelength away.

Corrugated surfaces have appeared in a variety of forms. Kildal [17, 18] identified the one-dimensional corrugated sheet as a soft surface, by analogy to acoustic boundary conditions. Lee and Jones [15] analyzed a two-dimensional corrugated surface resembling a lattice of rectangular metal pipes, and derived the surface wave dispersion relation for such a structure.

### 3.3 High-Impedance Surfaces

The properties of the new high-impedance surface are similar to those of the corrugated slab. The quarter-wavelength slots have simply been folded up into lumped

elements – capacitors and inductors – and distributed in two dimensions. Periodic two or three-dimensional dielectric, [19, 20, 21, 22, 23,] metallic, [24, 25, 26, 27] or metallodielectric [28, 29, 30, 31, 32] structures that prevent the propagation of electromagnetic waves are known as photonic crystals. [33, 34, 35] The high-impedance surface can be considered as a kind of two-dimensional photonic crystal that prevents the propagation of radio-frequency surface currents.

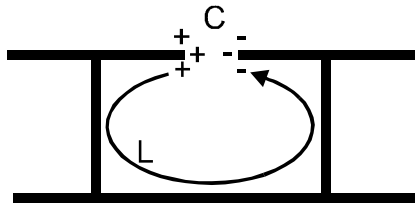


**Figure 3.3.1 Origin of the equivalent circuit elements**

The two-dimensional array of resonant elements can be viewed as a kind of electric filter, and many of its properties can be explained using a simple circuit model. The capacitance is due to the proximity of the top metal patches, while the inductance originates from current loops within the structure, as shown in Figure 3.3.1. The electromagnetic properties of the surface can be reduced to an equivalent LC circuit, shown in Figure 3.3.2.

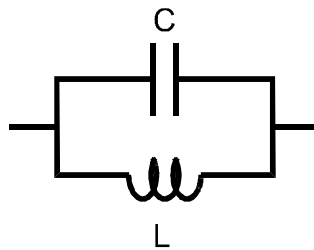


**Figure 3.3.2 Equivalent circuit model for the high-impedance surface**

$$Z = \frac{j\omega L}{1 - \omega^2 LC}$$

**Equation 3.3.1**

The impedance of a parallel resonant LC circuit, given in Equation 3.3.1, is qualitatively similar to the tangent function that describes the impedance of the corrugated surface. It is inductive at low frequencies, and thus supports TM surface waves. It is capacitive at high frequencies, and supports TE surface waves. In a narrow band around the LC resonance, the impedance is very high. In this frequency range, currents on the surface radiate very efficiently, and the structure suppresses the propagation of both types of surface waves. Having high surface impedance, it also reflects external electromagnetic waves without the phase reversal that occurs on a flat conductor. By using lumped elements, we retain the reflection phase and surface wave properties of the quarter-wave corrugated slab, while reducing the overall thickness to a small fraction of a wavelength.

## 4 Fabrication

The high-impedance surface can be easily fabricated using printed circuit board technology. The simplest design is a two-layer structure, consisting of a double-sided circuit board with metal patches on one side, connected by metal vias to a solid conducting sheet on the other side. The capacitance comes from the fringing electric fields between adjacent patches, while the inductance depends on the thickness of the board. The resonance frequency is determined by  $1/\sqrt{LC}$ , so it can be reduced for a given size structure by capacitive loading. [24] This is accomplished in a three-layer design, in which the capacitors are formed by overlapping metal plates on two different layers.

Other construction techniques may provide even higher capacitance. However, as we will see in Chapter 5, the bandwidth is related to  $\sqrt{L/C}$ , so increasing the capacitance also reduces the bandwidth. The techniques described below can provide bandwidths ranging from a few percent to nearly a full octave, with center frequencies ranging from hundreds of megahertz to tens of gigahertz.

### 4.1 Two-Layer Structure

Fabrication of a two-layer structure begins with a flat plastic sheet, usually a few millimeters thick, with several hundred microns of electrodeposited copper on each side, as shown in Figure 4.1.1. In this design, the capacitors use fringing electric fields, which extend into the surrounding dielectric. For this reason, the plastic is often a low-loss, teflon-based material such as Duroid, available from Rogers Corporation.

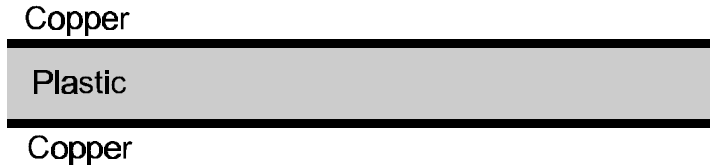


**Figure 4.1.1 Copper clad dielectric circuit board material**

The first step in the fabrication is to drill the vias, which form the vertical connections between the two layers, as shown in Figure 4.1.2.



**Figure 4.1.2 Holes drilled to define the locations of the vertical connections**

An electroless process is used to apply a thin metal coating to the inside of the vias. The entire structure is then electroplated with copper to thicken the metal coating.



**Figure 4.1.3 Plated copper forming vertical interconnections**

The copper is covered with photoresist, and one side of the circuit board is patterned and etched. The other side is left as continuous metal.

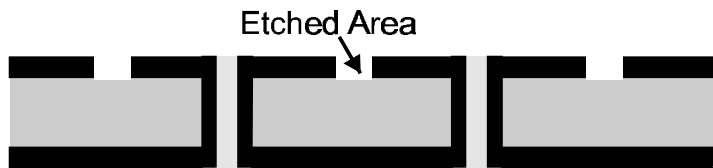


**Figure 4.1.4 Metal patches defined by etching**

Thus, in the final structure, the top layer is covered with metal patches, which are shorted to the bottom layer, consisting of a solid metal sheet. A perspective view of the metal regions, without the dielectric, is shown for a typical structure in Figure 4.1.5.

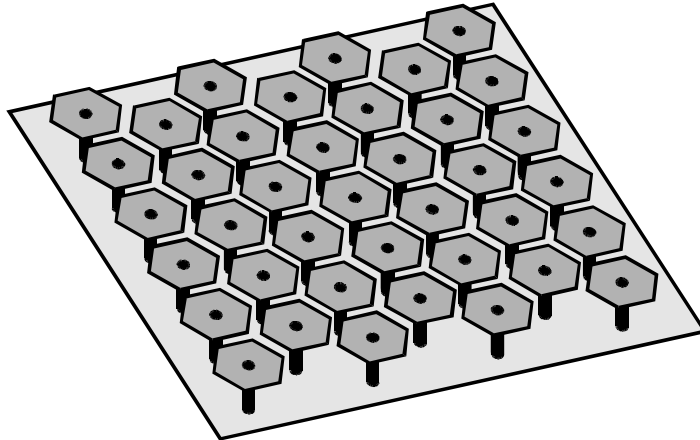


**Figure 4.1.5 Perspective view of a two-layer printed circuit board**

## 4.2 Three-Layer Structure

The two-layer circuit boards described above rely on the capacitance of fringing fields between neighboring metal patches. Higher capacitance can be achieved by using a three-layer design, in which two metal layers are separated by a very thin insulator. The fabrication begins with two separate plastic sheets, each covered on both sides with electrodeposited copper as shown in Figure 4.2.1.

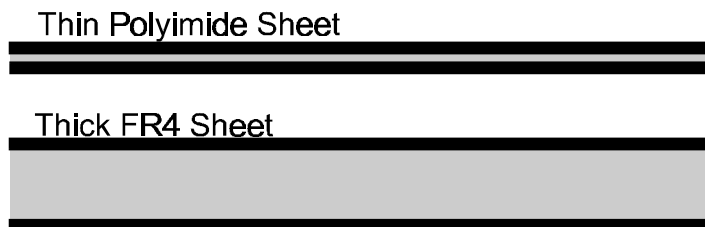


**Figure 4.2.1 Materials for fabricating a three-layer printed circuit board**

The thin layer is often Kapton polyimide film, available from DuPont, which is a standard material for making flexible printed circuits. It is currently available as thin as 50 microns, and has low loss, making it suitable for capacitors. Since the electric field is primarily concentrated in the polyimide capacitors, the thick, lower layer can be made of a lossier material such as FR4, a standard thermoset laminate used for printed circuit boards. The lower layer is typically several millimeters thick, depending on the frequency and bandwidth desired.

In the fabrication of multilayer circuit boards, the standard practice is to pattern the inner metal layers first, and then bond them together before drilling. In this design, the metal is completely etched away from the top of the thick, lower sheet, while the bottom of the thin, upper layer is patterned and etched as shown in Figure 4.2.2.



**Figure 4.2.2 Inner layers patterned by etching**

The two sheets are bonded together with an adhesive under heat and pressure, forming a single circuit board with an inner layer of patterned copper.



**Figure 4.2.3 Two sheets bonded with an adhesive**

The structure is then drilled and plated with copper, as was done on the two-layer circuit board.

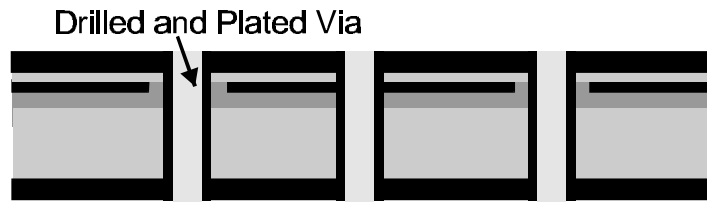


**Figure 4.2.4 Plated vias forming interconnects between all three layers**

Finally, the top layer is patterned with metal patches and etched, while the bottom layer is left as continuous metal.

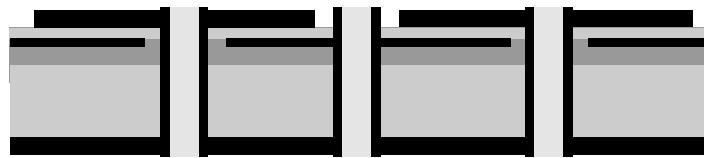


**Figure 4.2.5 Top layer patterned by etching**

In one example, the metal elements are arranged in a hexagonal array, shown in perspective view in Figure 4.2.6.

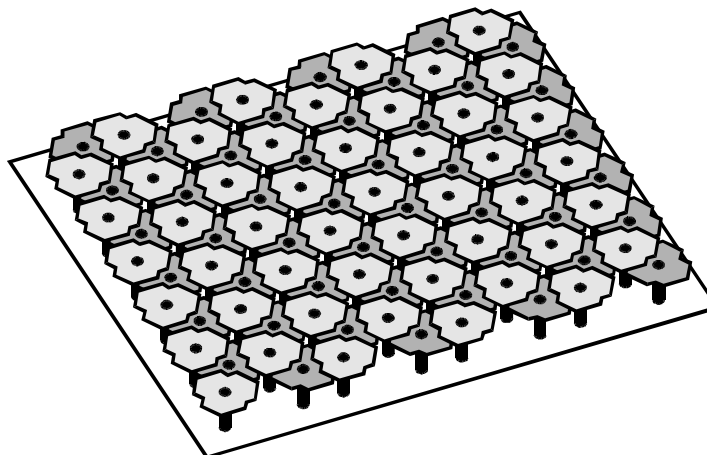


**Figure 4.2.6 Perspective view of a three-layer printed circuit board**

## 5 Effective Medium Model

Many properties of the high-impedance surface can be explained using an effective medium model. The structure is assigned a surface impedance equal to the impedance of a parallel resonant LC circuit, whose properties are derived from geometry. The use of lumped parameters to describe electromagnetic structures is valid as long as the wavelength is much longer than the size of the individual features. This is also the range of applicability of effective medium theory.

The capacitance in this model comes from the fringing electric field between adjacent metal plates in the two-layer design, or from the overlapping plates in the three-layer design. The inductance comes from the currents in the ground plane, and in the top capacitive layer. This effective circuit model is able to accurately predict the reflection phase, as well as some of the surface wave properties.

### 5.1 Circuit Parameters



**Figure 5.1.1 Cross-section of a simple two-layer high-impedance surface**

A cross-section of the structure is shown in Figure 5.1.1 above. As the structure interacts with electromagnetic waves, currents are induced in the top metal plates. A voltage applied parallel to the surface causes charge buildup on the ends of the plates, which can be described as a capacitance. As the charges slosh back and forth, they flow around a long path through the vias and the bottom plate. Associated with these currents

is a magnetic field, and thus an inductance. The origin of the capacitance and inductance are illustrated in Figure 5.1.2.

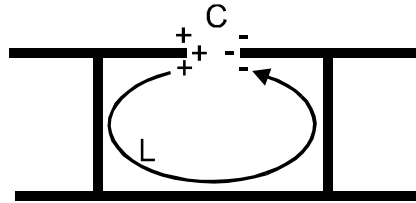


**Figure 5.1.2 Origin of the capacitance and inductance in the effective circuit model**

The behavior of the structure can be reduced to a parallel resonant circuit, shown in Figure 5.1.3. The appropriate values to use for the model are not the capacitance and inductance of the individual elements, but rather the sheet capacitance and sheet inductance. These depend on the value of each element, as well as their arrangement.

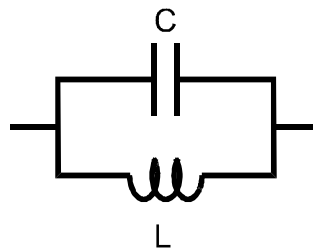


**Figure 5.1.3 Effective circuit used to model the surface impedance**

For the two-layer structures, the value of each capacitor is given by the fringing capacitance between neighboring co-planar metal plates. This can be derived using conformal mapping, a common technique for solving two-dimensional electrostatic field distributions. [3] A solution can be found for a pair of semi-infinite plates separated by a gap,  $g$ , with an applied voltage,  $V$ , as shown in Figure 5.1.4.

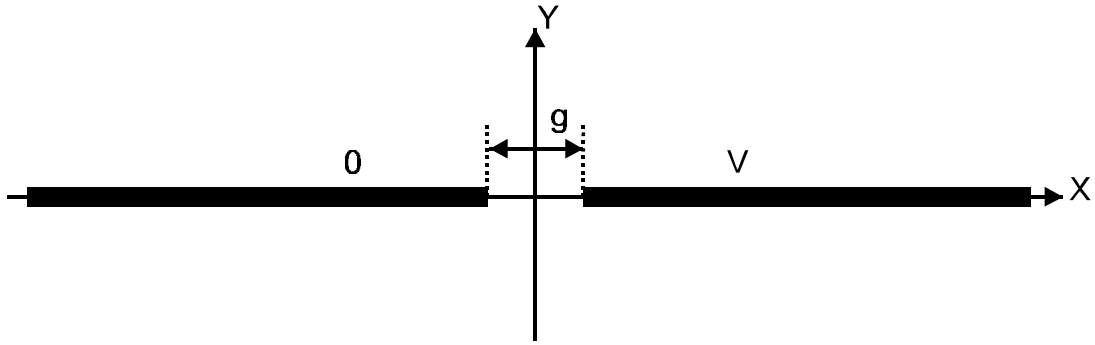


**Figure 5.1.4 A pair of semi-infinite plates separated by a gap**

From the theory of conformal mapping, the electric flux function for this geometry is described by the following function.

$$\psi = \text{Im} \left[ \frac{\epsilon V}{\pi} \text{Cos}^{-1} \left( \frac{x + jy}{g/2} \right) \right]$$

**Equation 5.1.1**

The capacitance is actually infinite, and the field decays nearly logarithmically with distance away from the gap. In our geometry, the plates end at point  $a/2$ , as in Figure 5.1.5.

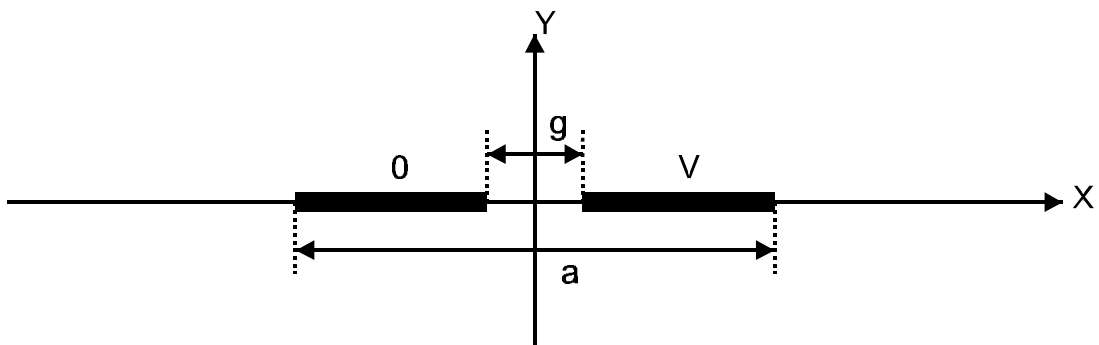


**Figure 5.1.5 Capacitor geometry in the two-layer high-impedance surface**

If  $a \gg g$ , we can estimate the capacitance by simply terminating  $\psi$  in Equation 5.1.1 at the ends of the plates. The flux ending on one plate is approximated by the expression below.

$$\psi \approx \text{Im} \left[ \frac{2\varepsilon V}{\pi} \text{Cos}^{-1} \left( \frac{a}{g} \right) \right] = \frac{2\varepsilon V}{\pi} \text{Cosh}^{-1} \left( \frac{a}{g} \right)$$

**Equation 5.1.2**

Assume the plates have width,  $w$ , and the structure is surrounded by  $\varepsilon_1$  on one side, and  $\varepsilon_2$  on the other. The flux ending on one plate is equal to the charge on that plate, which is equal to the product of the capacitance and the voltage across the plates. The edge capacitance between the two plates is therefore given the following expression.

$$C = \frac{w(\varepsilon_1 + \varepsilon_2)}{\pi} \text{Cosh}^{-1} \left( \frac{a}{g} \right)$$

**Equation 5.1.3**

For the three-layer circuit board, the capacitance is given by the well-known formula for a parallel plate capacitor.  $A$  is the overlap area of the plates, and they are separated by a distance,  $d$ , of dielectric constant,  $\varepsilon$ .

$$C = \frac{\varepsilon A}{d}$$

**Equation 5.1.4**

The sheet capacitance is the product of the individual capacitance and a geometrical factor. The sheet capacitance can be determined by considering a thin slab of dielectric, as shown in Figure 5.1.6. An electric field is applied tangentially along the slab, and we wish to find the effective sheet capacitance. The slab can be divided into narrow slices of

thickness,  $x$ . The slab itself has thickness,  $d$ , and we consider the total capacitance in an arbitrary region of length,  $\ell$ , and width,  $w$ .

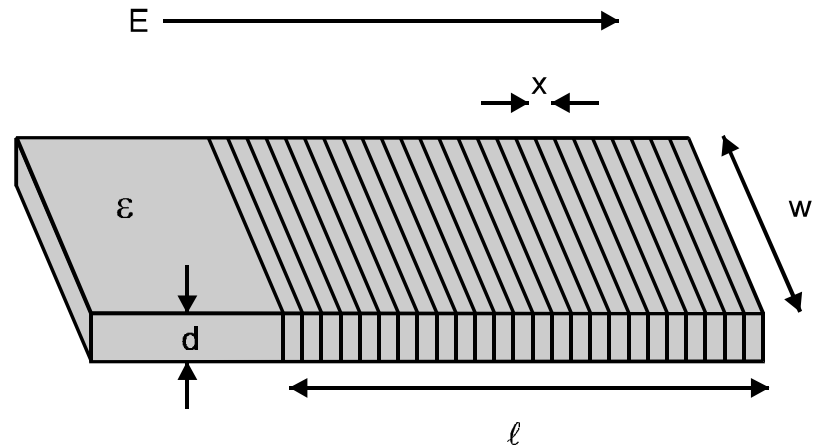


**Figure 5.1.6** A slab of dielectric divided into slices

Considering that the electric field is applied in the direction perpendicular to the slices, the capacitance of a single slice is as follows.

$$C = \frac{\epsilon d w}{x}$$

**Equation 5.1.5**

There are  $\ell/x$  slices in series contained in length  $\ell$ , so the total capacitance is equal to the expression below.

$$C_{\text{total}} = \epsilon d \left( \frac{w}{\ell} \right)$$

**Equation 5.1.6**

The factor of  $w/\ell$  can be normalized out, and we are left with the sheet capacitance in units of Farads-square.

$$C_{\text{sheet}} = \epsilon d$$

**Equation 5.1.7**

Next, insert metal plates to form discrete, vertical capacitors. The period of the plates is designated as  $a$ .

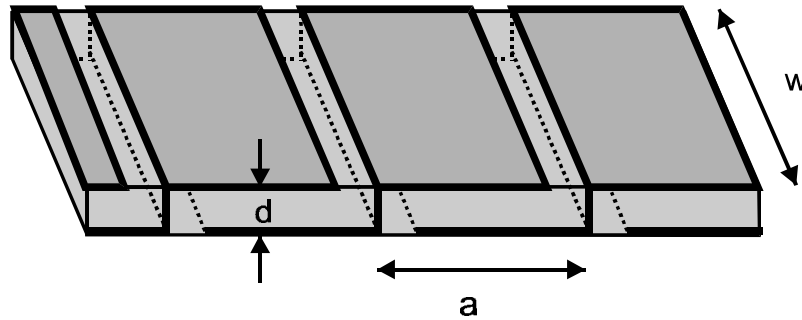


**Figure 5.1.7 Capacitor plates embedded in the dielectric slab**

The value of each capacitor is given by the following expression.

$$C = \frac{\epsilon a w}{d}$$

**Equation 5.1.8**

There are  $\ell/a$  series capacitors in length  $\ell$ , so the total capacitance is now given by the equation below.

$$C_{\text{total}} = \frac{\epsilon a^2}{d} \left( \frac{w}{\ell} \right)$$

**Equation 5.1.9**

Finally, we obtain the sheet capacitance in Farads-square.

$$C_{\text{sheet}} = \frac{\epsilon a^2}{d}$$

**Equation 5.1.10**

In effect, the dielectric constant of the thin sheet has been enhanced by the insertion of the metal regions.

$$\epsilon_{\text{eff}} = \epsilon \cdot \frac{a^2}{d^2}$$

**Equation 5.1.11**

The sheet capacitance given in Equation 5.1.10 includes only the length,  $a$ , of the individual capacitor plates and the thickness,  $d$ , of the dielectric insulator. Each plate could be divided into smaller widths without affecting the normalized capacitance-square of an area, so the width is not important. Conversely, the length of the plates is very important, since it affects the number of capacitors in series per unit distance. It is desirable to use all of the area in the two-dimensional lattice in order to get a large capacitance, but this area can be divided in various ways. The sheet capacitance is greatest if long, thin capacitors are used instead of short, wide capacitors. This point will be illustrated further in Chapter 10.

The inductance of a single, flat, conductive surface is extremely small. In fact, we have seen in Chapter 2 that the reactance of a metal surface is equal to its resistance, which is usually much less than one ohm per square. In the high-impedance surface, the inductance is much greater because of the conductive loops below the top layer, consisting of the vias, and both metal sheets. Figure 5.1.8 shows a solenoid of current with area  $t \cdot \ell$ , and width,  $w$ . The current around the outside is  $I$ , and the magnetic field through the solenoid is  $H$ . This geometry is equivalent to the current path in the high-impedance surface, consisting of rows of vias and metal plates.

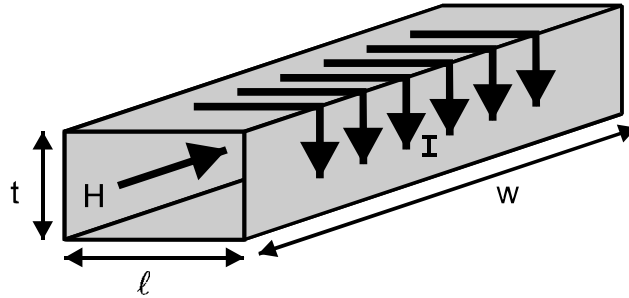


**Figure 5.1.8** A solenoid of current used to calculate the sheet inductance

The magnetic field through the solenoid is determined by the current flowing around the outside.

$$H = \frac{I}{w}$$

**Equation 5.1.12**

The energy stored in an inductor is equal to the energy stored in its magnetic field.

$$I^2 L = \int_{\text{vol}} (\mu H \cdot H) dv$$

**Equation 5.1.13**

This yields the inductance in the solenoid.

$$L = \mu t \left( \frac{\ell}{w} \right)$$

**Equation 5.1.14**

For the sheet inductance in Henrys/square, the factor of  $\ell/w$  can be taken as unity. Thus, the sheet inductance depends only on the thickness of the structure and the permeability.

$$L_{\text{sheet}} = \mu t$$

**Equation 5.1.15**

We assign to the surface a sheet impedance equal to the impedance of a parallel resonant circuit, consisting of the sheet capacitance and sheet inductance.

$$Z = \frac{j\omega L}{1 - \omega^2 LC}$$

**Equation 5.1.16**

The impedance of a parallel resonant circuit is shown in Figure 5.1.9. It is inductive at low frequencies, and capacitive at high frequencies. The impedance crosses through infinity at the resonance frequency, given by the expression below.

$$\omega_0 = \frac{1}{\sqrt{LC}}$$

**Equation 5.1.17**

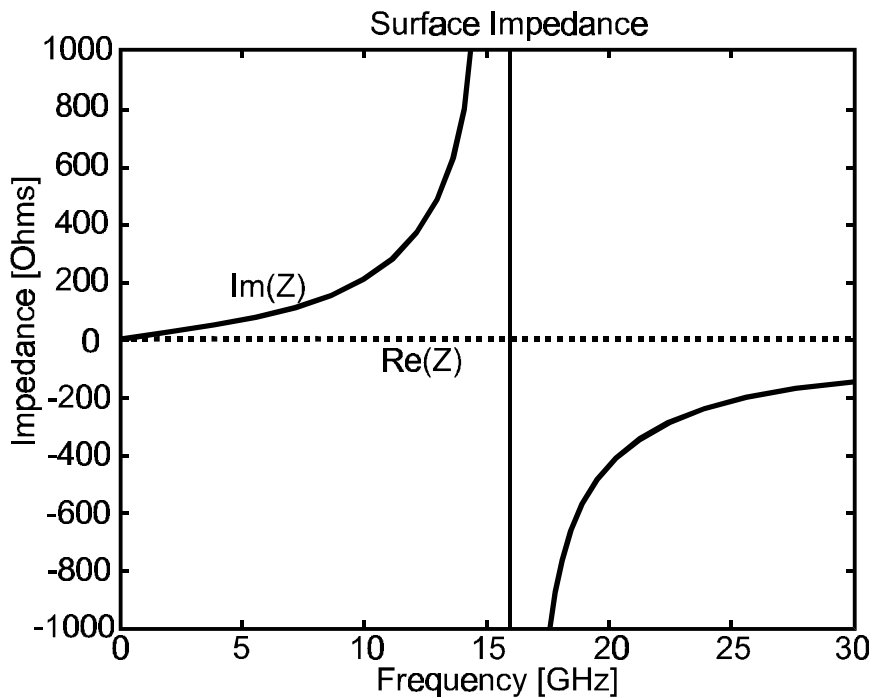


**Figure 5.1.9 Impedance of a parallel resonant circuit**

## 5.2 Reflection Phase

The surface impedance determines the boundary condition at the surface for a standing wave formed by the incident and reflected waves. For a surface in the YZ plane, the surface impedance seen by waves impinging on the surface from the X direction is equal to the following expression.

$$Z_s = \frac{E_z}{H_y}$$

**Equation 5.2.1**

As shown earlier, this is equivalent to Ohm's law. If the surface has very low impedance, such as in the case of a good conductor, the ratio of electric field to magnetic field is very small. The electric field has a node at the surface, and the magnetic field has an antinode. For a high impedance surface, the ratio in Equation 5.2.1 is very high, so the electric field has an antinode at the surface, while the magnetic field has a node. Another term for such a surface is a "magnetic conductor", because the tangential magnetic field at the surface is zero.

We can determine the reflection phase from an arbitrary impedance surface by considering the standing wave formed by a forward running wave impinging on the surface, and a backward running wave reflected from it. The fields of the standing wave have the following form.

$$\begin{aligned} E(x) &= E_f e^{-jkx} + E_b e^{jkx} \\ H(x) &= H_f e^{-jkx} + H_b e^{jkx} \end{aligned}$$

**Equation 5.2.2**

The boundary condition at the surface,  $x=0$ , is given by the surface impedance.

$$\frac{E_{\text{total}}(x=0)}{H_{\text{total}}(x=0)} = Z_s$$

**Equation 5.2.3**

The electric and magnetic fields of each running wave are related by the impedance of free space.

$$\left| \frac{E_f(x)}{H_f(x)} \right| = \left| \frac{E_b(x)}{H_b(x)} \right| = \sqrt{\frac{\mu_0}{\epsilon_0}} = \eta$$

**Equation 5.2.4**

The reflection phase is the phase difference between the backward and forward running waves.

$$\Phi = \text{Im} \left\{ \ln \left( \frac{E_b}{E_f} \right) \right\}$$

**Equation 5.2.5**

Combining this with Equation 5.2.3 and Equation 5.2.4 gives the reflection phase of a surface with impedance  $Z_s$ .

$$\Phi = \text{Im} \left\{ \ln \left( \frac{Z_s - \eta}{Z_s + \eta} \right) \right\}$$

**Equation 5.2.6**

When  $Z_s$  is low, the reflection phase is  $\pm \pi$ . When  $Z_s$  is very high, the reflection phase is zero. The phase crosses through  $\pm \pi/2$  when  $Z_s$  is equal in magnitude to the impedance of free space. Inserting Equation 5.1.16, we can plot the reflection phase of the high impedance surface. Typical parameters for a two-layer ground plane are 2 nH/square of

inductance, and 0.05 pF-square of capacitance. For these values, the reflection phase is plotted in Figure 5.2.1. The results are very similar to the measured reflection phase for a two-layer high-impedance surface with these circuit parameters.

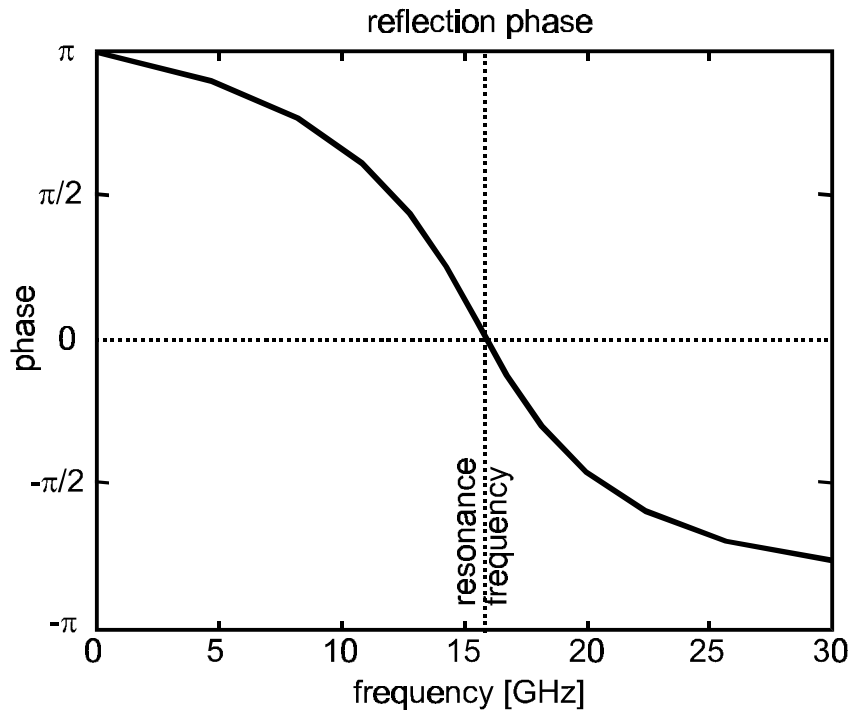


**Figure 5.2.1 Reflection phase calculated using the effective circuit model**

### 5.3 Losses

Although this surface has high impedance, it should not be confused with a lossy surface. The impedance is almost entirely reactive, with only a very small resistive part due to dielectric and conduction losses. Appropriate material losses can be included in the model to simulate real metals and real dielectrics. The dielectric loss is added as an imaginary component in the capacitance, obtained from the loss tangent supplied by the manufacturer. For Kapton polyimide film, the loss tangent is  $3 \times 10^{-3}$ . The conduction

losses in the upper and lower sheets of metal are added as a resistor in series with the inductor. For copper at 15 GHz, with a skin depth of 0.5  $\mu\text{m}$  the sheet resistance is  $3.2 \times 10^{-2} \Omega/\text{square}$ . This number is doubled because two copper surfaces contribute to the resistance. Inserting this resistance and the dielectric loss tangent into the circuit model gives the actual surface impedance, including the real part, which is plotted below.

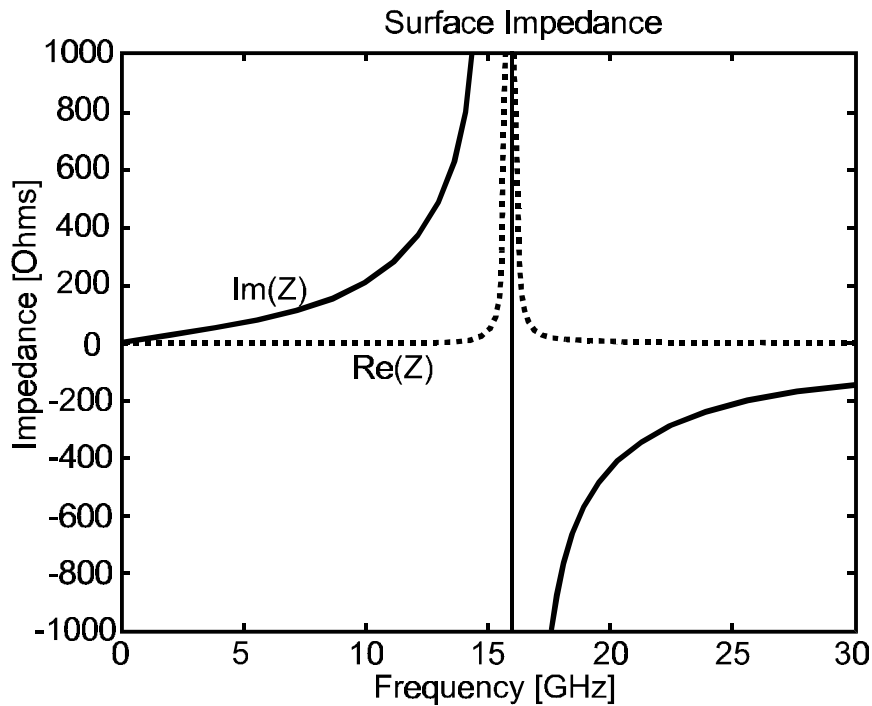


**Figure 5.3.1 Surface impedance, including dielectric and conductive losses**

Notice that the impedance is almost entirely imaginary, except in a narrow region near resonance. The reflection magnitude from a surface with this impedance is shown in Figure 5.3.2. It is clear that the total absorption is very small – the surface reflects nearly 100% of the incident power. For antenna applications, the performance is more than adequate.

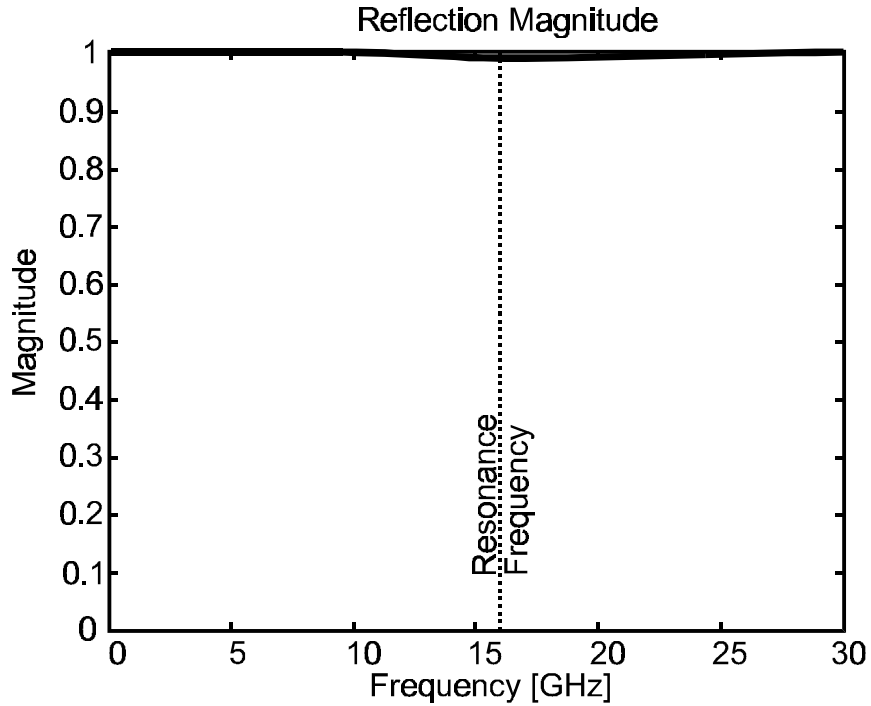


**Figure 5.3.2 Reflection magnitude, including dielectric and conductive losses**

Although the material loss is small, it is multiplied by the  $Q$  of the structure. If the bandwidth is greatly reduced, and lossier dielectric materials are used in the capacitive layer, then the absorption can be more significant. Furthermore, if an antenna is operated outside the surface wave band gap, they may cause additional losses. Surface waves spend much more time inside the materials that make up the structure as they propagate for long distances along the surface, so material losses are likely to be more significant for surface waves.

#### **5.4 Surface Waves**

We have previously derived the dispersion relation for surface waves on a flat metal surface. Now, we will derive the dispersion relation for surface waves on the high-

impedance ground plane, in the effective medium limit. Using the expressions for surface waves on an impedance surface, derived in Section 2.3, we can determine the dispersion relation for both TM and TE waves in the context of this effective medium model. Begin with the following Maxwell's equations.

$$\nabla \times \vec{E} = -\mu \frac{\partial \vec{H}}{\partial t}$$

**Equation 5.4.1**

$$\nabla \times \vec{H} = \epsilon \frac{\partial \vec{E}}{\partial t}$$

**Equation 5.4.2**

For TM surface waves, assume that the Z component of the magnetic field is as follows.

$$E_z = C e^{-jkz - \alpha x}$$

**Equation 5.4.3**

In the above equation, C is a constant. We write out the derivatives of Equation 5.4.1 and Equation 5.4.2 explicitly, taking into account the three field components that are known to be zero for TM waves. Assume that the surface is surrounded by free space with  $\epsilon = \epsilon_0$  and  $\mu = \mu_0$ .

$$j\omega\epsilon_0 E_z = \frac{\partial H_y}{\partial x}$$

**Equation 5.4.4**

$$j\omega\epsilon_0 E_x = \frac{-\partial H_y}{\partial z}$$

**Equation 5.4.5**

$$-j\omega\mu_0 H_y = \frac{\partial E_x}{\partial z} - \frac{\partial E_z}{\partial x}$$

**Equation 5.4.6**

Solving Equation 5.4.4 with Equation 5.4.3 gives

$$H_y = \frac{-j\omega\epsilon_0}{\alpha} C e^{-jkz - \alpha x}$$

**Equation 5.4.7**

Similarly, Equation 5.4.5 gives

$$E_x = \frac{-jk}{\alpha} C e^{-jkz - \alpha x}$$

**Equation 5.4.8**

Inserting the above results along with Equation 5.4.3 into Equation 5.4.6, we can find an expression relating  $k$ ,  $\alpha$ , and  $\omega$ .

$$k^2 = \mu_0\epsilon_0\omega^2 + \alpha^2$$

**Equation 5.4.9**

This represents the dispersion relation for TM surface waves, but the same expression applies to TE surface waves. It is equivalent to stating the total wave vector as a sum of its components, as shown below.

$$\mu_0\epsilon_0\omega^2 = k_x^2 + k_y^2 + k_z^2$$

**Equation 5.4.10**

Combine Equation 5.4.9 with the impedance that we derived for TM surface waves, which is restated here for convenience.

$$Z_s(\text{TM}) = \frac{j\alpha}{\omega\epsilon_0}$$

**Equation 5.4.11**

We can eliminate  $\alpha$  to find an equation for  $k$  as a function of  $\omega$ .

$$Z = \frac{j\alpha}{\omega\epsilon_0} = \frac{j}{\omega\epsilon_0} \sqrt{k^2 - \mu_0\epsilon_0\omega^2}$$

$$\omega^2\epsilon_0^2 Z^2 = \mu_0\epsilon_0\omega^2 - k^2$$

$$k_{\text{TM}} = \frac{\omega}{c} \sqrt{1 - \frac{Z^2}{\eta^2}}$$

**Equation 5.4.12**

In the above expression,  $\eta$  is the impedance of free space, and  $c$  is the speed of light in vacuum.

We can find a similar expression for TE waves by beginning with the equation we derived earlier for the TE surface impedance, which is restated here.

$$Z_s(\text{TE}) = \frac{-j\omega\mu_0}{\alpha}$$

**Equation 5.4.13**

Combining this with Equation 5.4.9 gives the dispersion equation for TE surface waves.

$$Z = \frac{-j\omega\mu_0}{\alpha} = \frac{-j\omega\mu_0}{\sqrt{k^2 - \mu_0\epsilon_0\omega^2}}$$

$$Z^2(k^2 - \mu_0\epsilon_0\omega^2) = -\omega^2\mu_0^2$$

$$k_{TE} = \frac{\omega}{c} \sqrt{1 - \frac{\eta^2}{Z^2}}$$

**Equation 5.4.14**

Using the effective circuit impedance, Equation 5.1.16, in Equation 5.4.12 and Equation 5.4.14, we can plot the dispersion diagram for surface waves. Typical values for the sheet capacitance and sheet inductance of a two-layer structure are 0.05 pF-square, and 2 nH/square, respectively. For this example, the dispersion diagram is plotted in Figure 5.4.1. The present analysis is limited to waves that are bound to the surface. Shortly, we will also consider leaky waves.

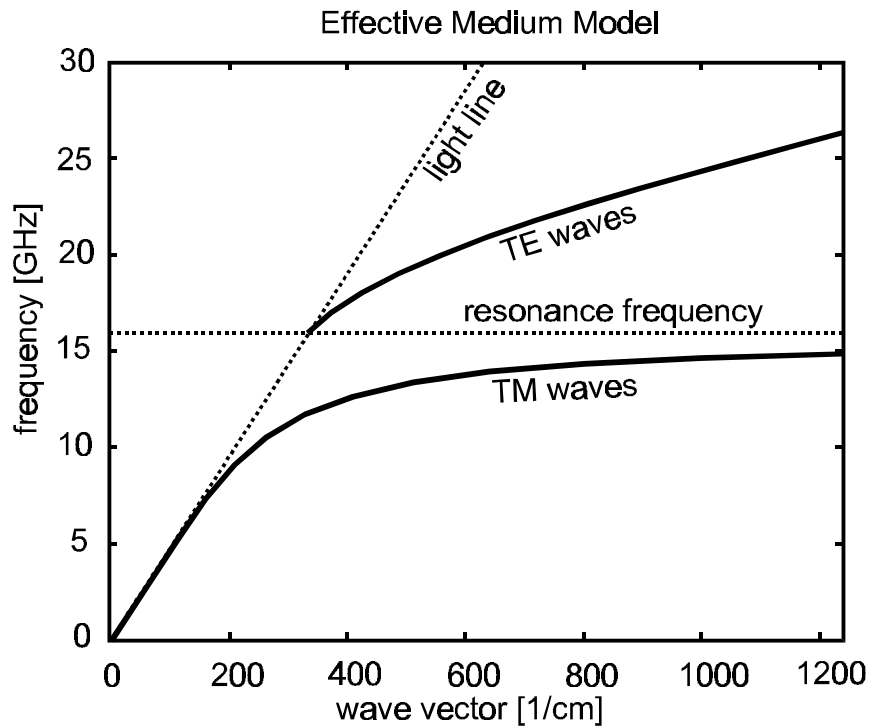


**Figure 5.4.1 Dispersion diagram for bound surface waves, lying below the light line**

Below resonance, TM surface waves are supported. At low frequencies, they lie very near the light line, and the fields extend many wavelengths beyond the surface, as

they do on ordinary metals. This can be seen mathematically in Equation 5.4.9. When  $k$  is very near  $\omega\sqrt{\epsilon_0\mu_0}$ , then  $\alpha$  is very small, so when the dispersion curve is near the light line, the surface waves extend far into space. Near the resonant frequency, the surface waves are tightly bound to the sheet, and have a very low group velocity, as seen by the fact that the dispersion curve is bent over, away from the light line. In the effective medium limit, the graph extends on to infinitely large wave vectors, and the TM dispersion curve approaches the resonance frequency asymptotically. The graph in Figure 5.4.1 has been terminated at the point where the Brillouin zone boundary would be for a structure with typical dimensions. No attempt has been made to include the periodicity in the effective medium limit, so the termination of the graph is artificial in this model.

Above the resonance frequency, the surface is capacitive, and TE waves are supported. The lower end of the dispersion curve is close to the light line, and the waves are weakly bound to the surface, extending far into the surrounding space. As the frequency is increased, the curve bends away from the light line, and the waves are more tightly bound to the surface. The slope of the dispersion curve indicates that the waves feel an effective index of refraction that is greater than unity. This is because a significant portion of the electric field is concentrated in the capacitors. As we have seen earlier in Equation 5.1.11, the effective dielectric constant of a material is enhanced if it is permeated with capacitor-like structures.

Notice that in the effective medium model, there is actually no band gap. The TM dispersion curve continues all the way up to the resonance frequency, while the TE curve begins at the resonance frequency. However, the structure does in fact have a band gap,

which has been seen in measurements, and in numerical calculations of the dispersion curves. Its absence here is one of the limitations of the effective medium model. The electromagnetic band gap becomes a frequency band of very high surface impedance in the effective medium limit, as will be illustrated shortly.

## 5.5 Radiation Bandwidth

An antenna lying parallel to the textured surface will see the impedance of free space on one side, and the impedance of the ground plane on the other side. Far from the resonance frequency, where the textured surface has low impedance, the antenna current is mirrored by an opposing current in the surface. The antenna is shorted out by the nearby conductor, and the radiation efficiency is very low. Near resonance, the textured surface has much higher impedance than free space, so the antenna is not shorted out. In this range of frequencies, the radiation efficiency is high.

Although the surface exhibits high impedance, it is not actually devoid of current. If there were no current, electromagnetic waves would be transmitted right through the ground plane. However, the resonant structure provides a phase shift, so the image currents in the surface reinforce the currents in the antenna, instead of canceling them.

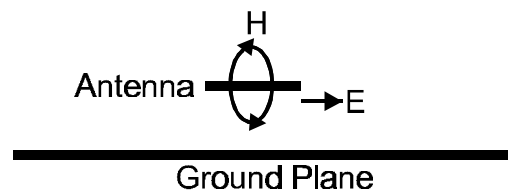


**Figure 5.5.1 A horizontal antenna above a ground plane**

Figure 5.5.1 shows a horizontal antenna above a ground plane. The electric field is parallel to the antenna, and to the ground plane, while the magnetic field encircles the antenna. Imagine a simpler problem in which the antenna is abstracted to a sheet of current just above the ground plane. [36] The electromagnetic radiation is due to the superposition of the antenna current and the image current.

$$I_{\text{antenna}} = I_{\text{image}} + H_{\text{radiation}}$$

**Equation 5.5.1**

The radiated magnetic field is linked to the electric field by the impedance of free space,  $H=E/\eta$ . The image current in the surface is given by  $I=E/Z$ . Substituting these expressions into Equation 5.5.1, the antenna can be described by an equivalent circuit, shown in Figure 5.5.2

$$I = \frac{E}{Z} + \frac{E}{\eta}$$

**Equation 5.5.2**

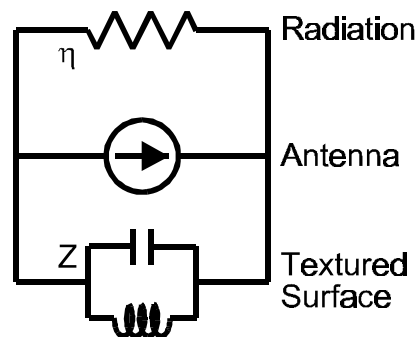


**Figure 5.5.2 An antenna shunted by a textured surface**

We can determine the frequency range over which the radiation efficiency is high by using a circuit model, in which the antenna is modeled as a current source. The

textured surface is modeled as an LC circuit in parallel with the antenna, and the radiation into free space is modeled as a resistor with a value of  $\sqrt{\mu_0/\epsilon_0} = 377\Omega$ . The amount of power dissipated in the resistor is a measure of the radiation efficiency of the antenna.

The maximum power dissipated in the resistor occurs at the LC resonance frequency of the ground plane, where the surface impedance crosses through infinity. At very low frequencies, or at very high frequencies, the current is shunted through the inductor or the capacitor, and the power flowing to the resistor is reduced. It can be shown from Equation 5.5.2 that the frequencies where the radiation drops to half of its maximum value occur when the magnitude of the surface impedance is equal to the impedance of free space.

$$|Z_s| = \left| \frac{j\omega L}{1 - \omega^2 LC} \right| = \eta = 377\Omega$$

$$\frac{\omega^2 L^2}{1 - 2\omega^2 LC + \omega^4 L^2 C^2} = \eta^2$$

$$\omega^4 L^2 C^2 \eta^2 - 2\omega^2 LC \eta^2 - \omega^2 L^2 + \eta^2 = 0$$

$$\omega^2 = \frac{1}{LC} + \frac{1}{2\eta^2 C^2} \pm \frac{1}{\eta C} \sqrt{\frac{1}{LC} + \frac{1}{4\eta^2 C^2}}$$

**Equation 5.5.3**

L is usually on the order of 1 nH, C is in the range of 0.05-10 pF, and  $\eta=377\Omega$ . With these values, the terms involving  $1/\eta^2 C^2$  are much smaller than the  $1/LC$  terms, so we

will eliminate them. This approximation yields the following expression for the edges of the operating band.

$$\omega^2 \approx \frac{1}{LC} \pm \frac{1}{\eta C} \sqrt{\frac{1}{LC}}$$

$$\omega = \frac{1}{\sqrt{LC}} \sqrt{1 \pm \frac{1}{\eta} \sqrt{\frac{L}{C}}}$$

$$\omega = \omega_0 \sqrt{1 \pm \frac{Z_0}{\eta}}$$

**Equation 5.5.4**

The resonance frequency is  $\omega_0 = 1/\sqrt{LC}$ , and  $Z_0 = \sqrt{L/C}$  is a kind of characteristic impedance of the surface. With the parameters for L, C, and  $\eta$  given above,  $Z_0$  is usually significantly smaller than  $\eta$ . Thus, the square root can be expanded in the following approximation.

$$\omega \approx \omega_0 \left( 1 \pm \frac{1}{2} \frac{Z_0}{\eta} \right)$$

**Equation 5.5.5**

The two frequencies designated by the +/- signs delimit the range over which an antenna would radiate efficiently on such a surface. Finally, the total bandwidth is roughly equal to the characteristic impedance of the surface divided by the impedance of free space.

$$\text{B.W.} = \frac{\Delta\omega}{\omega_0} = \frac{Z_0}{\eta}$$

**Equation 5.5.6**

This is also the bandwidth over which the reflection coefficient falls between  $+\pi/2$  and  $-\pi/2$ , and image currents are more in-phase than out-of-phase. It represents the maximum usable bandwidth of a flush-mounted antenna on a resonant surface of this type. We have found experimentally that the surface wave band edges occur where the reflection phase is equal to  $\pm \pi/2$ , so this also corresponds to the width of the surface wave band gap.

## 5.6 Leaky Waves

According to the effective medium model, the TM band begins at DC, and continues up to the resonance frequency for very large wave vectors. The TE band begins at the resonance frequency, and continues up with a slope that is less than the speed of light. However, the model described above only involves waves that are bound to the surface, and therefore lying below the light line. This gives the peculiar result that the TE band begins at a finite wave vector, branching out of the light line at the resonance frequency. The TE waves that lie to the left of the light line exist as radiative, leaky waves, and appear only when radiation is included in the model.

Following the method of the previous section, the radiation from these leaky TE modes is modeled as a resistor in parallel with the high-impedance surface. By definition of a normal mode, it must exist in the absence of an inhomogeneous driving current. Therefore, the driving current must disappear from Figure 5.5.2, and the equivalent circuit is shown in Figure 5.6.1. The circuit equations are satisfied at a frequency

$\omega = 1/\sqrt{LC}$ . Therefore, the leaky modes that exist to the left of the light line can be represented by a horizontal line at the resonance frequency, illustrated in Figure 5.6.2.

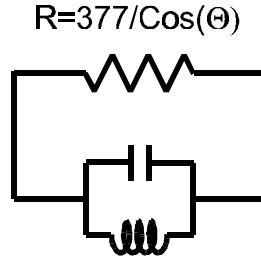


**Figure 5.6.1 Circuit for modeling the radiation of leaky TE waves**

The presence of radiation damping tends to blur the resonance frequency, so the leaky waves actually radiate within a finite bandwidth. The damping resistance is the impedance of free space, projected onto the surface according to the angle of radiation. Small wave vectors represent radiation perpendicular to the surface, while wave vectors near the light line represent radiation at glancing angles. For a TE polarized plane wave, the magnetic field,  $H$ , projected on the surface at angle,  $\theta$ , with respect to normal is  $H(\theta) = H_0 \text{Cos}(\theta)$ , while the electric field is just  $E(\theta) = E_0$ . The impedance of free space, as seen by the surface for radiation at an angle, is given by the following expression.

$$Z(\theta) = \frac{E(\theta)}{H(\theta)} = \frac{E_0}{H_0 \text{Cos}(\theta)} = \frac{\eta}{\text{Cos}(\theta)}$$

**Equation 5.6.1**

Thus, the radiation resistance is  $377\Omega$  for small wave vectors and normal radiation, but the damping resistance approaches infinity for wave vectors near the light line. Infinite resistance in a parallel circuit corresponds to no damping, so the radiative

band is reduced to zero width for grazing angles near the light line. This is shown in Figure 5.6.2, in which the high-impedance, radiative region is shown as a shaded area, representing the blurring of the leaky waves by radiation damping. In place of a band gap, the effective medium model produces a frequency band of high surface impedance.

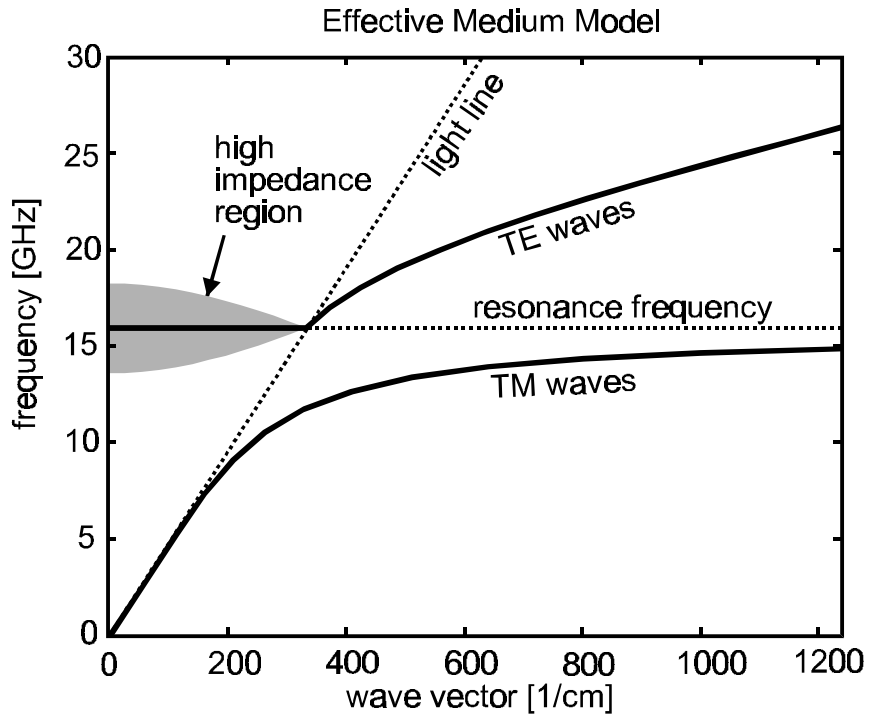


**Figure 5.6.2 Complete dispersion diagram, including leaky modes**

## 5.7 Fundamental Limitations

The resonance frequency is given by  $\omega = 1/\sqrt{LC}$ , so it can be lowered by increasing either the inductance or the capacitance. The sheet inductance,  $L=\mu t$ , depends on the thickness of the structure, as well as the permeability. Since low-loss, high-permeability materials do not currently exist at microwave frequencies, the inductance is

fixed by the thickness. Thus, the only way to lower the resonance frequency for a given thickness is to use capacitive loading.

The relative bandwidth,  $\Delta\omega/\omega$ , is proportional to  $\sqrt{L/C}$ , so if the capacitance is increased, the bandwidth suffers. Since the thickness is related to the inductance, the more the resonance frequency is reduced for a given thickness, the more the bandwidth is diminished. It would appear that a structure has a certain “natural frequency” that depends on the thickness, and that the bandwidth is related to the ratio of the actual resonance frequency to this natural frequency. This is suggested by the equation below.

$$\frac{\Delta\omega}{\omega_0} = \frac{\omega_0}{\omega_{\text{natural}}}$$

**Equation 5.7.1**

The natural frequency is easily calculated.

$$\frac{\sqrt{L/C}}{\sqrt{\mu_0/\epsilon_0}} = \frac{1/\sqrt{LC}}{\omega_{\text{natural}}}$$

$$\omega_{\text{natural}} = \frac{\sqrt{\mu_0/\epsilon_0}}{L} = \frac{\sqrt{\mu_0/\epsilon_0}}{\mu_0\mu_r t} = \frac{1/\sqrt{\mu_0\epsilon_0}}{\mu_r t}$$

$$\omega_{\text{natural}} = \frac{c}{\mu_r t}$$

**Equation 5.7.2**

In the above equation,  $c$  is the speed of light in vacuum, while  $\mu_r$  and  $t$  are the relative magnetic permeability and the thickness, respectively, of the material filling the lower, inductive part of the structure, as shown in Figure 5.7.1. Since the dielectric

constant does not appear in Equation 5.7.2, the bulk of a three-layer structure can be filled with a low-dielectric material without affecting frequency or bandwidth. In the two-layer structures, in which the capacitance is determined by the fringing electric fields, which extend into the lower dielectric material, Equation 5.7.1 is still satisfied, but the dielectric constant influences  $\omega_{\text{natural}}$ .

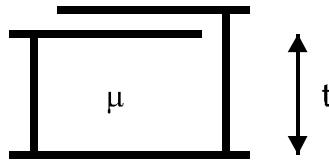


**Figure 5.7.1 Cross-section of one unit cell of a three-layer high-impedance surface**

## 6 Finite Element Model

The model described in the previous chapter is an effective medium approach, in which the properties of the surface are summarized into a single parameter, the surface impedance. This approach can be used when the periodicity of the structure is much less than the electromagnetic wavelength. The effective medium model correctly predicts the reflection properties of the high-impedance surface. However, it does not predict an actual band gap. Instead, it predicts a high-impedance, radiative region that corresponds roughly to the measured band gap.

Numerical methods exist that are more accurate for modeling structures of this type, in which the periodicity is not infinitesimally small. One such approach is the finite element method, employed by Zhang [37] in the UCLA Electrical Engineering department, to model a two-layer structure with a square lattice. This technique can give an accurate description of the surface wave bands by explicitly including the geometry of the metal and dielectric regions, as well as the periodicity.

### 6.1 Surface Waves

In the finite element method, the metal and dielectric regions of one unit cell are discretized on a grid. The electric field at all points on the grid can be reduced to an eigenvalue equation, which may be solved numerically. Bloch boundary conditions are used, in which the fields at one edge of the cell are related to the fields at the opposite edge by the wave vector. The calculation yields the allowed frequencies for a certain

wave vector, and the procedure is repeated for each wave vector to produce the dispersion diagram. The structure studied was a two-layer, high-impedance surface with square geometry, shown in Figure 6.1.1. The lattice constant was 2.4mm, the spacing between the plates was 0.15mm, and the width of the vias was 0.36mm. The volume below the square plates was filled with  $\epsilon=2.2$ , and the total thickness was 1.6mm.

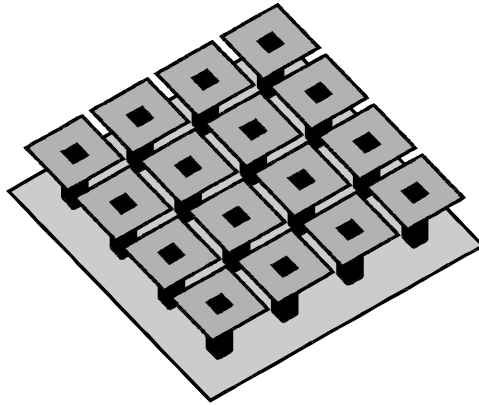


**Figure 6.1.1 Geometry studied using the finite element method.**

The results of the finite element calculation are shown in Figure 6.1.2. According to the finite element model, the TM band follows the light line up to a certain frequency, where it suddenly becomes very flat. The TE band begins at a higher frequency, and continues upward with a slope of less than the speed of light in vacuum, which is indicated by a dotted line. These results agree qualitatively with the effective medium model. The finite element method also predicts the higher-frequency bands that are seen in the measurements, but do not appear in the effective medium model. A second gap that was measured on the hexagonal structure appears on the square structure studied here, but only in the X-direction.

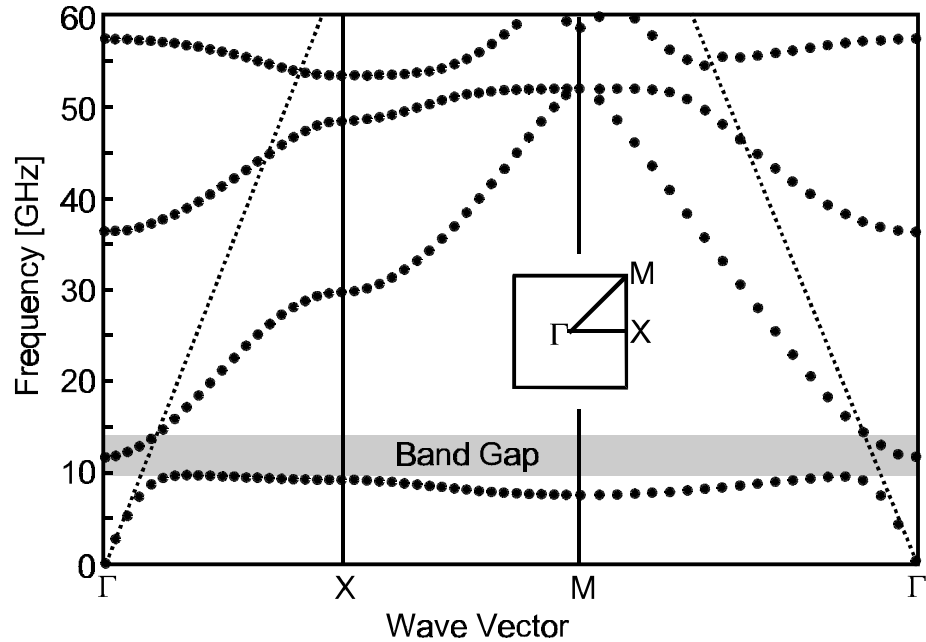


**Figure 6.1.2 Surface wave band structure for a two-layer, high-impedance surface**

According to the more accurate finite element model, the TM band does not reach the TE band edge as it does in the effective medium model, but stops slightly below it. Furthermore, the TE band slopes upward before crossing the light line, without the kink that appears in the effective medium model. Thus, the finite element model predicts a surface wave band gap that spans from the edge of the TM band, to the point where the TE band crosses the light line. If a resonance frequency is associated with the point where the TE band has zero wave vector, the width of the band gap is roughly equally distributed on either side of the resonance frequency.

In both the TM and TE bands, the  $k=0$  state represents a sheet of current that is continuous in space. The lowest TM mode, at zero frequency, is a sheet of DC current.

The highest TM mode, at the Brillouin zone edge, is a standing wave in which each row of metal protrusions has opposite charge.

The lowest TE mode is a sheet of current that is continuous in space, but oscillating at the LC resonance frequency. Since the wavelength along the surface is infinite, this mode occurs at the origin of k-space,  $k=0$ . The TE band slopes smoothly upward in frequency, crossing through the light line at some point. The slope is less than the speed of light, indicating that the TE waves interact significantly with the capacitors. At the highest TE mode, at the Brillouin zone boundary, transverse currents flow in opposite directions on each row of protrusions.

In the upper bands, the electric field is primarily concentrated in the region below the capacitor plates. The modes in these bands resemble the modes in a parallel plate waveguide, and begin at the frequency where one-half wavelength fits between the rows of metal vias.

## **6.2 Leaky Waves**

In order for a surface wave to couple to a plane wave in free space, phase matching must occur along the interface. For any surface wave lying below the light line, the wave vector along the surface exceeds that of an external plane wave of the same frequency, as shown in Figure 6.2.1. Since no plane wave can achieve phase matching, the surface wave is prevented from radiating, and is therefore stable.

Conversely, any surface wave that lies above the light line can radiate energy away by coupling to external plane waves, as shown in Figure 6.2.2. The short wave

vector along the surface is easily matched to a plane wave of the same frequency. Such modes are not strictly surface waves, but rather radiatively unstable, leaky waves. Thus, they have an imaginary frequency component.

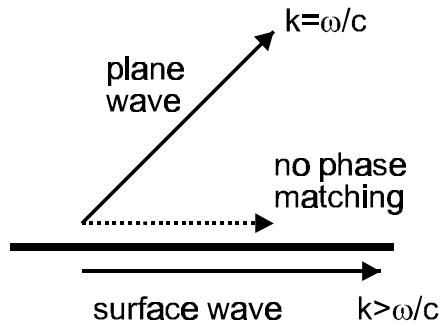


**Figure 6.2.1** A bound surface wave, for which phase matching is impossible

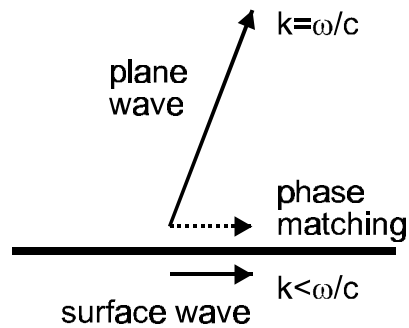


**Figure 6.2.2** Phase matching to a leaky wave

A small region of Figure 6.1.2 has been enlarged in Figure 6.2.3, in which the imaginary part of the frequency is plotted as an error bar on each data point of the TE band. The TE modes lying to the left of the light line are radiative, leaky modes, as indicated by the complex frequency. The TM band lies entirely below the light line, and therefore does not radiate. There are upper bands that exist above the light line, but their radiation properties are not known.

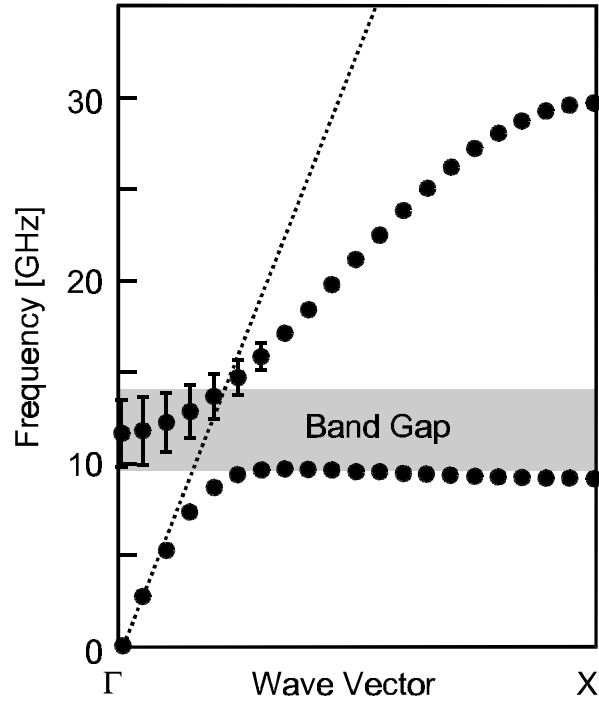


**Figure 6.2.3** Calculation of leaky waves, illustrated by error bars

### 6.3 Vertical Connections

Zhang has also calculated the same structure without the vertical conducting vias. The band diagram for this structure is shown in Figure 6.3.1. The TE surface waves are unaffected by the absence of the vias, and appear similar to the TE waves on the original structure. However, the TM waves are no longer terminated below the resonance frequency, as they were when the vias were present, and there is no band gap. The TM curve continues upward with a slope of slightly less than the speed of light. Therefore, the presence of the vertical connecting vias is critical for the suppression of TM surface waves, and the creation of a forbidden band.

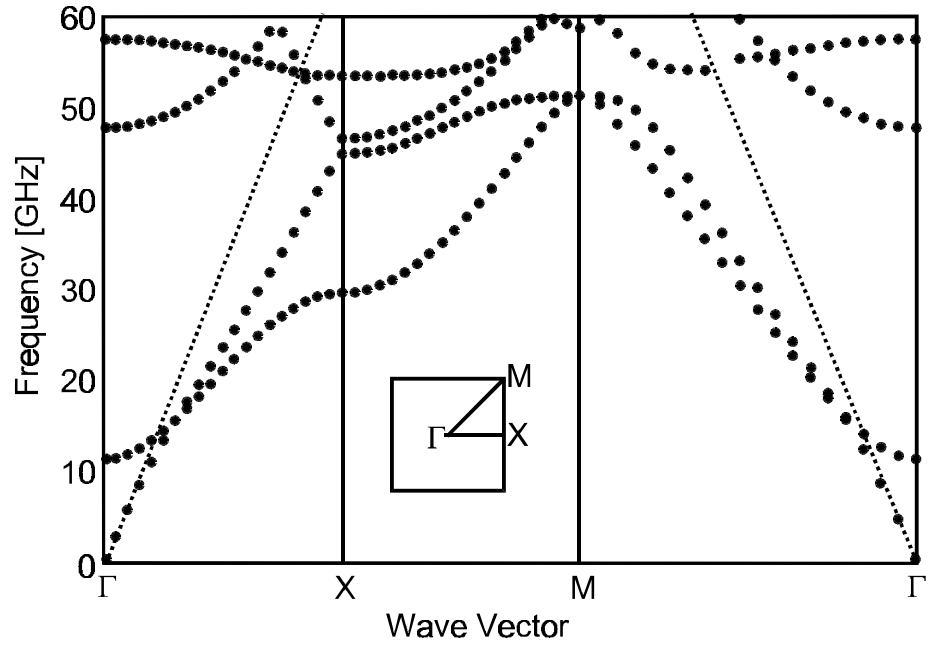


**Figure 6.3.1** Surface wave band diagram in the absence of conducting vias

## 7 Measuring Surface Properties

Techniques have been developed for measuring various properties of electromagnetic surfaces. The presence of surface wave modes is detected in the transmission between two antennas positioned near the surface. These antennas can be simple monopole probes, or they can be specifically designed to efficiently launch surface waves. By varying the polarization of the antennas, one can distinguish between TM and TE modes. The measurements on the textured surface indicate a frequency band in which there are no propagating surface waves.

The reflection phase can be measured using a pair of horn antennas directed toward the surface. The phase of the reflected wave is measured with respect to a surface with known reflection properties, such as a flat metallic surface. Within the surface wave band gap, the textured surface reflects in-phase, rather than out-of-phase.

### 7.1 TM Surface Waves

Since surface waves cannot generally couple to external plane waves, specialized methods must be used to measure them. At optical frequencies, surface plasmons are often studied using a technique called prism coupling. [7] A prism is placed next to the surface, and the refractive index of the prism is used to match the wave vector of a probe beam to that of a surface wave. Another method for coupling to surface waves, which is more practical at microwave frequencies, is to use a very small probe. A point source launches all wave vectors, so a small antenna brought near the surface is capable of

coupling to surface wave modes. Various types of antennas can be used for this purpose, and the antenna geometry can be tailored to distinguish surface wave polarization.

In TM surface waves, the electric field forms loops that extend vertically out of the surface. TM waves can be measured using a pair of small monopole antennas oriented normally with respect to the surface, as shown in Figure 7.1.1. The vertical electric field of the probe couples to the vertical electric field of the TM surface waves.

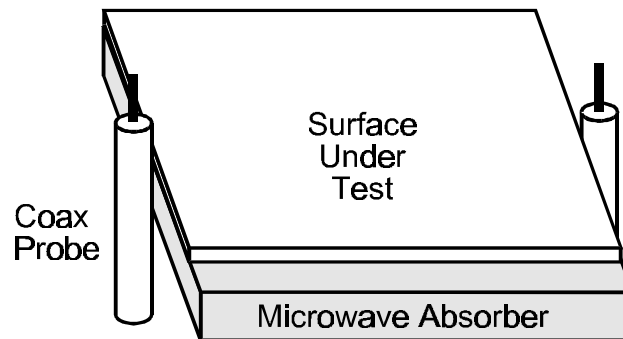


**Figure 7.1.1 TM surface wave measurement using monopole probe antennas**

For improved signal, a flared parallel-plate waveguide structure, pictured in Figure 7.1.2, functions as a more effective TM surface wave antenna. This type of antenna is built from a triangular piece of microwave circuit board material, with copper cladding on both sides. The upper and lower copper surfaces are soldered to the inner and outer conductors of a coaxial cable. The triangular part functions as a parallel-plate waveguide. A wave is launched between the plates from the coaxial cable at the narrow end, and spreads out to a flat wave front at the wide end. This structure provides a smooth transition between the mode in the coaxial cable and the surface wave mode, producing a stronger transmission signal than the small monopole.

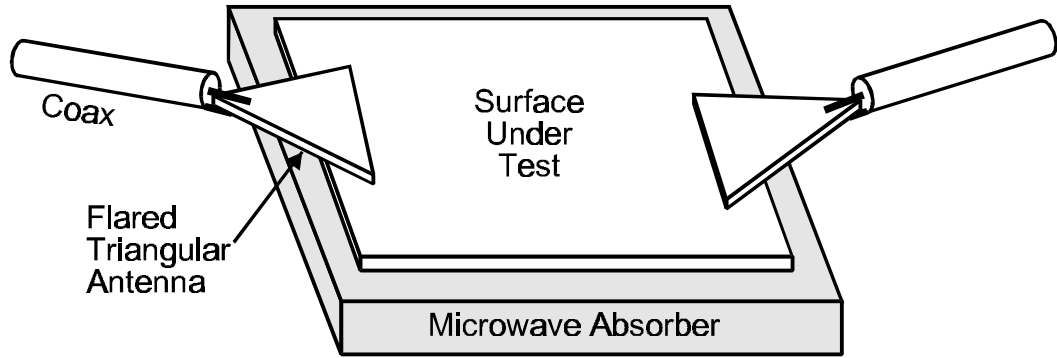


**Figure 7.1.2 TM surface wave measurement using flared parallel-plate waveguides**

On a flat metal sheet, a TM surface wave measurement produces the results shown in Figure 7.1.3. The surface under test was a 25 cm square sheet of flat metal. The measurement represents the transmission between a pair of monopole probes oriented vertically at the edges of the metal sheet.

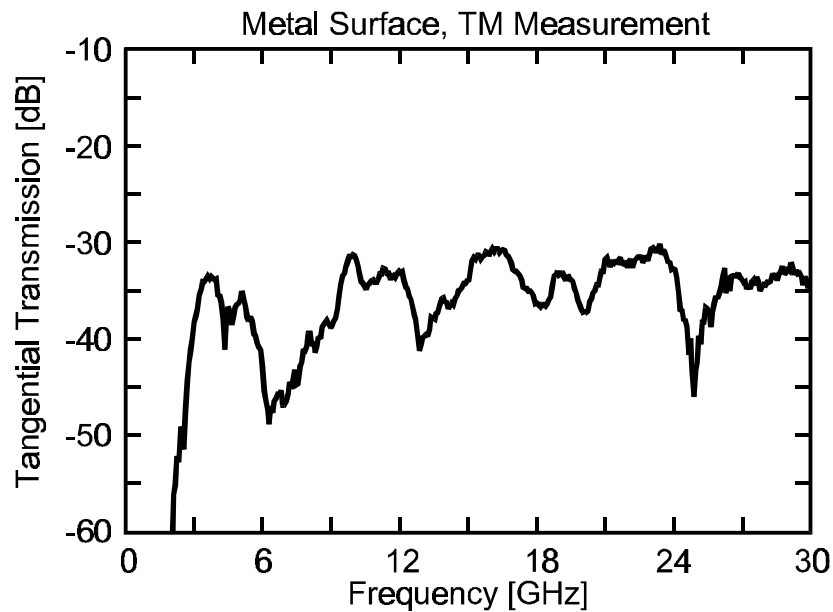


**Figure 7.1.3 TM surface wave transmission data on a flat metal surface**

The data has variations of 10-15 dB, but remains relatively flat over a broad spectrum. The variations are produced by multipath interference, or speckle, which

occurs in coherent measurements whenever multiple signal paths are present. Multipath interference can be distinguished from other effects because it is characterized by narrow-band fading, whose details depend on the exact antenna position. The transmission drops off at low frequencies because the small probes are inefficient at exciting long wavelengths.

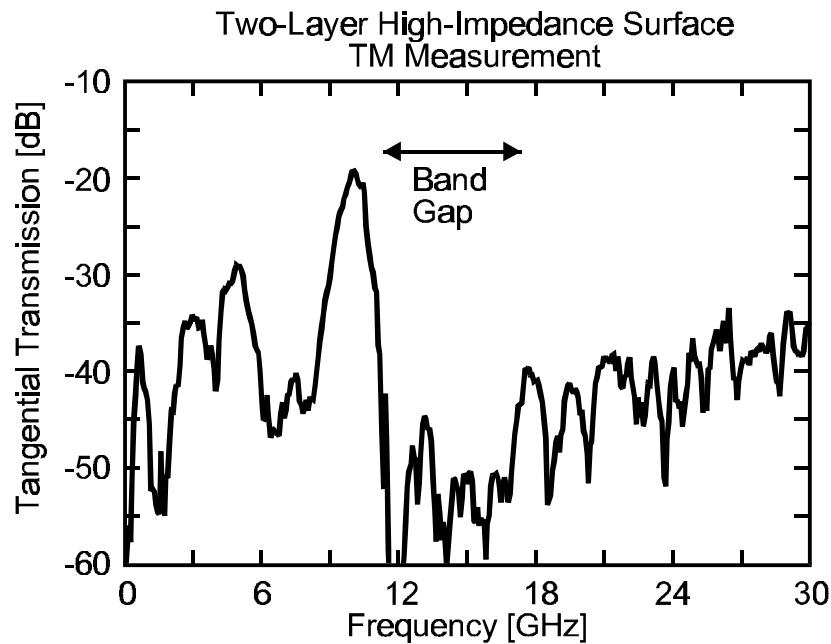


**Figure 7.1.4** TM surface wave transmission data on a textured surface

A typical TM surface wave measurement on a textured surface is shown in Figure 7.1.4. The size of the sheet and the measurement technique were the same as those used for the flat metal surface. The structure consisted of a triangular array of hexagonal patches, with a period of 2.54 mm and a gap between the patches of 0.15 mm. The thickness of the board was 1.55 mm, and the dielectric constant was 2.2.

The transmission is strong at low frequencies, and exhibits the same multipath interference seen on the metal surface. At 11 GHz, the transmission drops by about

30 dB, indicating the edge of the TM surface wave band. Beyond this frequency, the transmission level remains low and flat, eventually sloping upward at much higher frequencies because of weak coupling to TE surface waves. The TE band edge is not apparent in this measurement, but the region corresponding to the surface wave band gap is indicated on the graph with an arrow.

## 7.2 TE Surface Waves

In TE surface waves, the electric field is parallel to the surface, and the magnetic field forms vertical loops that arc out of the surface. They can be measured with a pair of small monopole probes oriented parallel to the sheet, as shown in Figure 7.2.1. The horizontal electric field of the antenna couples to the horizontal electric field of the TE waves. Since this configuration lacks the symmetry of the vertical monopole, there will be much greater cross-coupling to TM waves, that may complicate the measurement.

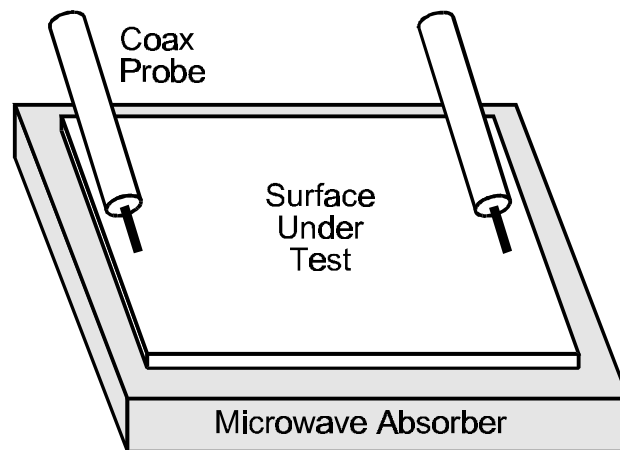


**Figure 7.2.1 TE surface wave measurement using monopole probe antennas**

Another antenna for measuring TE surface waves is a small loop, shown in Figure 7.2.2.. This type of probe can be constructed as a small wire loop connecting the two

conductors of a coaxial cable. The plane of the loop is parallel to the surface, creating a vertical magnetic field that couples to the magnetic field of TE surface waves.

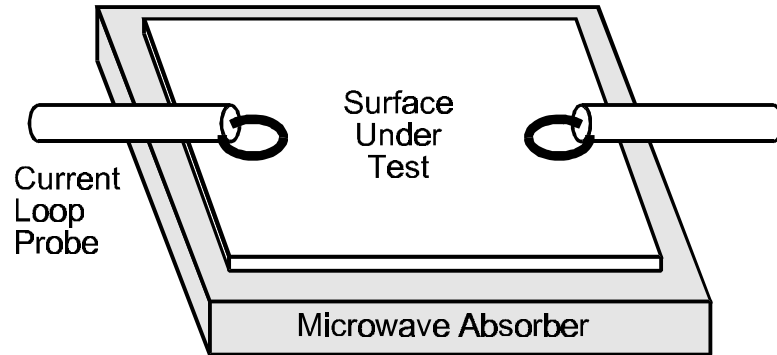


**Figure 7.2.2 TE surface wave measurement using small loop antennas**

On a flat metal surface, a TE surface wave measurement produces no significant signal, because any antenna that excites TE waves is shorted out on a conducting surface. It is only on the textured surface, with its unusual surface impedance, and tightly bound TE modes, that significant transmission signal levels can be obtained.

The measurement shown in Figure 7.2.3 was taken using a pair of small straight-wire coaxial probes, oriented parallel to the high-impedance surface. A similar profile is obtained if magnetic loop probes are used. The transmission is weak at low frequencies, and strong at high frequencies, the reverse of the TM data. A sharp jump of 30 dB occurs at 17 GHz, indicating the TE band edge. Beyond this frequency, the transmission is flat, with only small fluctuations due to speckle. The TE probes also couple slightly to TM surface waves, so there is an additional transmission peak at 11 GHz, at the TM band edge, where the density of TM states is high. Both TM and TE probes tend to couple slightly to both surface wave polarizations. However, the cross-coupling is weaker

between the TM probe and the TE surface waves because of the symmetry of the vertical monopole.

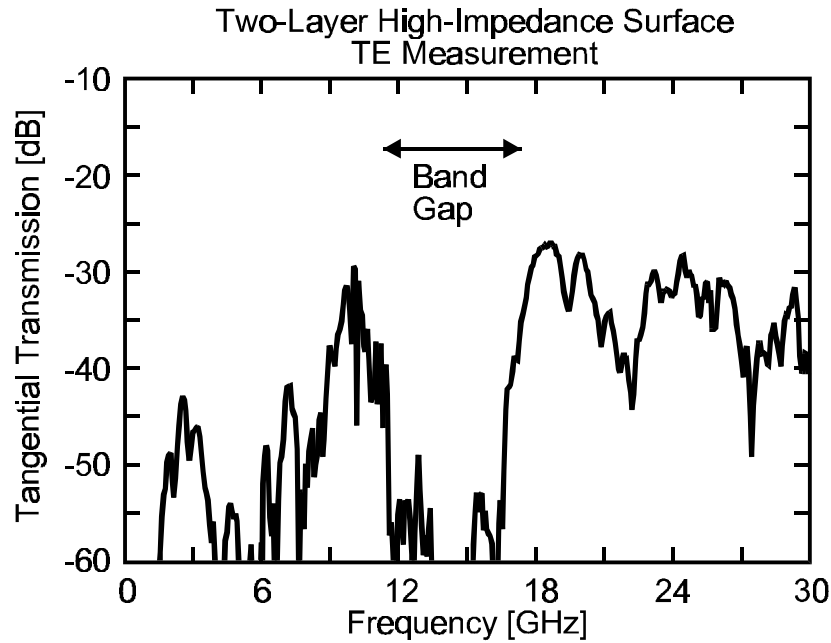


**Figure 7.2.3 TE surface wave transmission data on a textured surface**

A surface wave band gap exists between the TM band edge at 11 GHz and the TE band edge at 17 GHz. Within this range, neither type of measurement produces significant transmission. Currents cannot propagate across the surface, and any currents induced in the surface radiate rapidly into free space.

### 7.3 Reflection Phase

The reflection phase of the high-impedance surface can be measured using two microwave horn antennas, as shown in Figure 7.3.1. A single antenna can also be used, but the data contains much more interference because of radiation trapped between the horn and the ground plane. The measurement is done in an anechoic chamber lined with

microwave absorbing foam. The two horns are placed next to each other, aimed at the surface. Two windows are cut in the chamber, one for the antennas, and one for the surface under test.

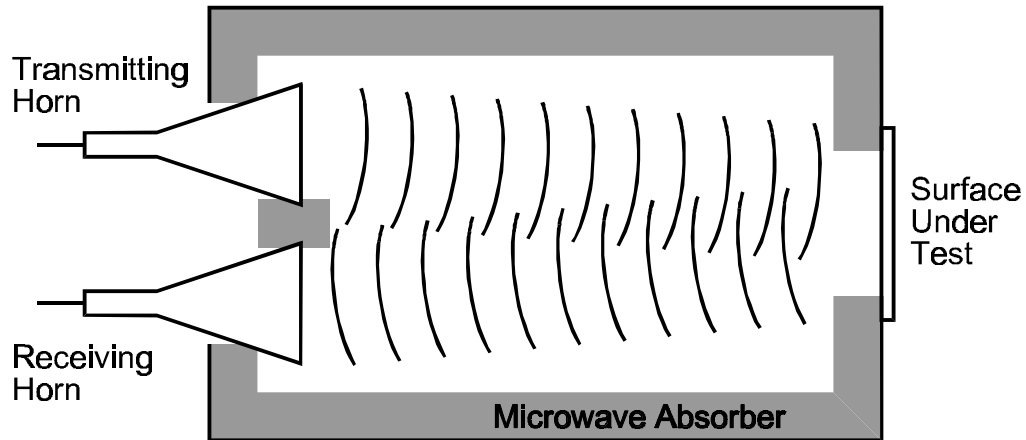


**Figure 7.3.1 Reflection phase measurement using a pair of horn antennas**

A reference measurement is taken of a surface with known reflection properties, such as a sheet of metal, and all subsequent measurements are divided by this reference. The metal surface is then removed from the chamber and replaced by the surface under test. When performing phase measurements, the surface under test must be placed in exactly the same location as the reference metal surface, because variations in path length would create an additional phase shift. A factor of  $\pi$  is added to the phase data to account for the reference scan of the metal sheet, which is known to have a reflection phase of  $\pi$ .

The reflection phase of the high impedance surface is shown in Figure 7.3.2. At low frequencies, it reflects with a  $\pi$  phase shift, just like a metal surface. As the frequency is increased, the phase slopes downward, and eventually crosses through zero at the resonance frequency of the structure. At higher frequencies, the phase continues to

slope downward, and eventually approaches  $-\pi$ . Within the region between  $+\pi/2$  and  $-\pi/2$ , indicated on the graph by arrows, plane waves are reflected in-phase, rather than out-of-phase as occurs on a smooth metal surface. This range also corresponds to the surface wave band gap, indicated on the graph by a shaded region, with the TM and TE band edges falling approximately at the points where the phase crosses through  $+\pi/2$  and  $-\pi/2$ , respectively.

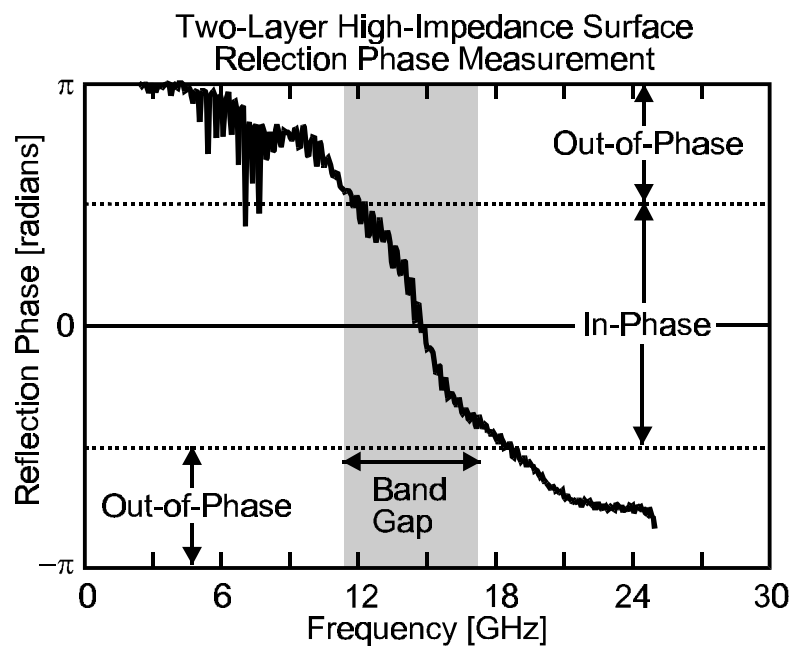


**Figure 7.3.2 Reflection phase of a textured surface**

The reflection phase is related to the surface impedance in the following way. Consider a forward-running wave impinging on the surface, with electric and magnetic fields given by the expressions below.

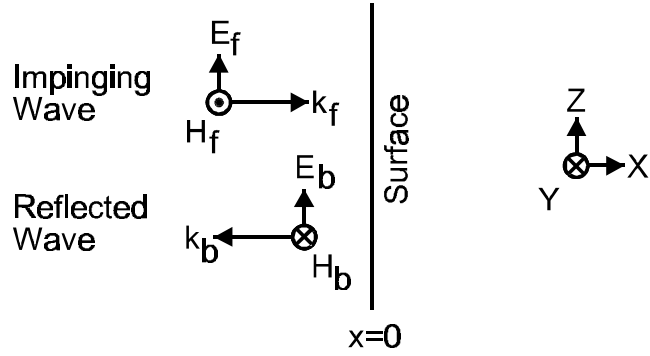


**Figure 7.3.3** Waves impinging on, and reflected by a surface

$$E_f = E_0 e^{-jkx}$$

$$H_f = H_0 e^{-jkx}$$

**Equation 7.3.1**

The wave is reflected from the surface, and the backward-running wave has a similar form, as indicated in Figure 7.3.3.

$$E_b = E_0 e^{jkx}$$

$$H_b = -H_0 e^{jkx}$$

**Equation 7.3.2**

The negative sign on the magnetic field is due to the convention of the right hand rule.

The field components of each wave are related by the impedance of free space,  $\eta$ .

$$\left| \frac{E_f}{H_f} \right| = \left| \frac{E_b}{H_b} \right| = \eta$$

**Equation 7.3.3**

The electric and magnetic fields of the standing waves, and thus the impedance, can be expressed in terms of the phase shift that occurs upon reflection from the surface,  $\phi$ .

$$\frac{E(x)}{H(x)} = \frac{E_f(x) + E_b(x)}{H_f(x) + H_b(x)} = \eta \frac{e^{-jkx} + e^{jkx+j\phi}}{e^{-jkx} - e^{jkx+j\phi}} = j\eta \cot\left(kx + \frac{\phi}{2}\right)$$

**Equation 7.3.4**

From the above equation, the apparent reflection point moves in the positive X-direction as the reflection phase,  $\phi$ , decreases. This point is illustrated below.

At frequencies that are far below resonance, the surface has low impedance, so the electric field has a node at the surface, and the magnetic field has an antinode, as shown in Figure 7.3.4. This also describes reflection from a flat metal surface. The figure shows the electric and magnetic fields of a standing wave, which are the vector sums of the two running wave fields. The position of the surface is indicated by the solid vertical line. It is assumed that the sign shown for each field is consistent with the field direction of an incoming wave. This convention ensures that an absorbing surface has positive, real impedance, while a radiating surface has negative, real impedance.

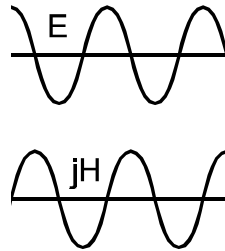


**Figure 7.3.4 Standing wave fields at a frequency far below resonance**

With increasing frequency, the phase in Figure 7.3.2 slopes downward, as if the effective reflection point of the surface were receding. The standing wave shifts forward, toward the surface, as indicated by the arrows in Figure 7.3.5. Actually, the surface just has higher impedance, so the electric field no longer has a node at the surface. The

standing wave shown in Figure 7.3.5 is for a frequency just below resonance, near the TM band edge. The apparent reflection point is indicated by the dotted vertical line.

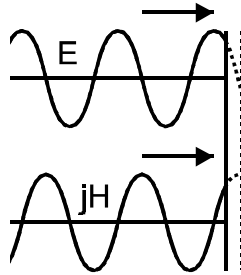


**Figure 7.3.5 Standing wave pattern just below resonance**

Just below resonance, the surface impedance is positive imaginary, or inductive, but its value is much higher than that of a smooth metal surface. At the resonance frequency, the reflection phase crosses through zero. The surface impedance is very large, so the electric field has an antinode at the surface, as shown in Figure 7.3.6.

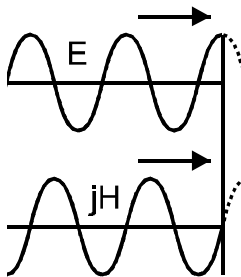


**Figure 7.3.6 Standing wave pattern at the resonance frequency**

With higher frequency, the standing wave continues to shift toward the surface and the phase slopes farther downward towards  $-\pi$ . The impedance has switched sign, and the surface is now capacitive. This is indicated in Figure 7.3.7, in which the magnetic field is now negative.

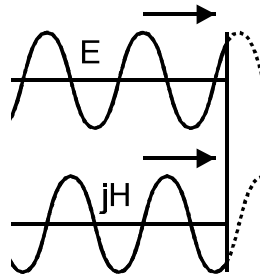


**Figure 7.3.7 Standing wave pattern just above resonance**

At frequencies much higher than resonance, the surface impedance has returned to near zero. The reflection phase has returned to the same point where it started, but it has gone through one complete cycle. The standing wave is shown in Figure 7.3.8. As the frequency is increased through the resonance, it is as if the effective reflection plane has slipped into the surface by one-half wavelength.

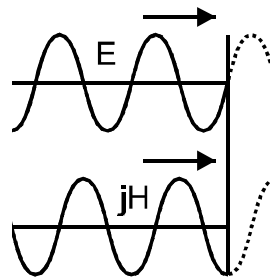


**Figure 7.3.8 Standing wave pattern for a frequency far above resonance**

#### **7.4 Low-Frequency Structures**

The measurements in the previous sections are representative of a typical two-layer, high-impedance surface. With two-layer construction, the capacitors are formed by the fringing capacitance between two metal plates lying edge-to-edge, usually separated by a few hundred microns. If the substrate has a dielectric constant between 2 and 10, and

the period is a few millimeters, the capacitance is generally on the order of a few tens of femtoFarads. With a thickness of a few millimeters, the inductance is a few nanoHenrys, so the resonance frequency is on generally the order of about 10 GHz.

If the desired resonance frequency is less than about 5 GHz, the thickness can be kept within reasonable limits by using three-layer construction. Since the capacitors are formed between overlapping metal plates, a capacitance of several picoFarads is easily achievable. With this method, resonance frequencies of less than 1 GHz can be produced, while maintaining the thickness and period on the order of a few millimeters. As we will see in Chapter 5, by forcing a thin structure to have a low resonance frequency, the bandwidth is also reduced.

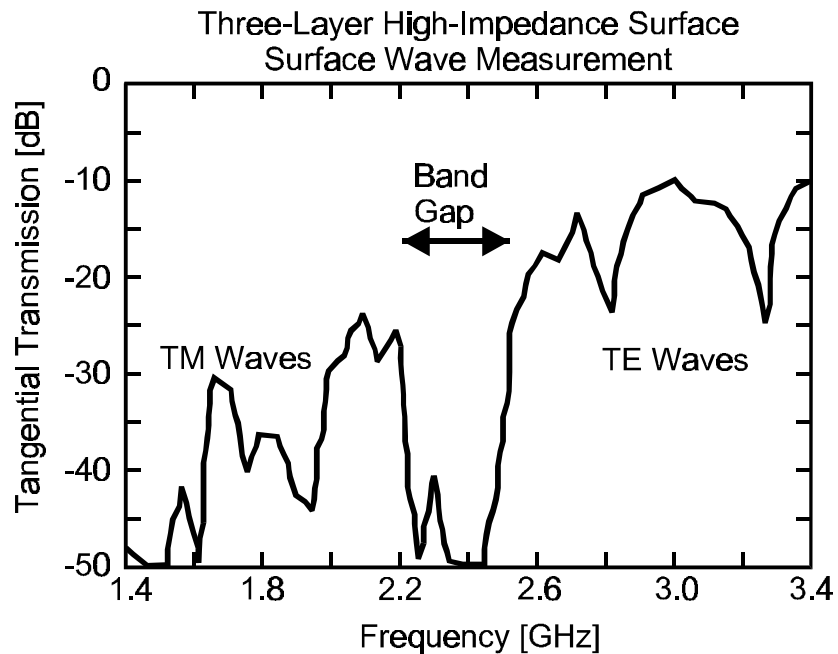


**Figure 7.4.1** Surface wave transmission across a three-layer high-impedance surface

The three-layer, high-impedance surface maintains the same general properties as the two-layer structure, with TM and TE surface wave bands separated by a gap, within

which there are no propagating surface wave modes. A surface wave measurement is shown in Figure 7.4.1 for a typical three-layer structure. The data shows the transmission between two straight coaxial probes lying parallel to the surface, in what is usually considered the TE configuration. The frequency is so low that the free-space wavelength is much greater than the probe length, which is only a few millimeters, so the antennas tend to couple equally well to TM and TE modes. Transmission can be seen in both the TM and TE bands, and a gap is visible between 2.2 and 2.5 GHz.

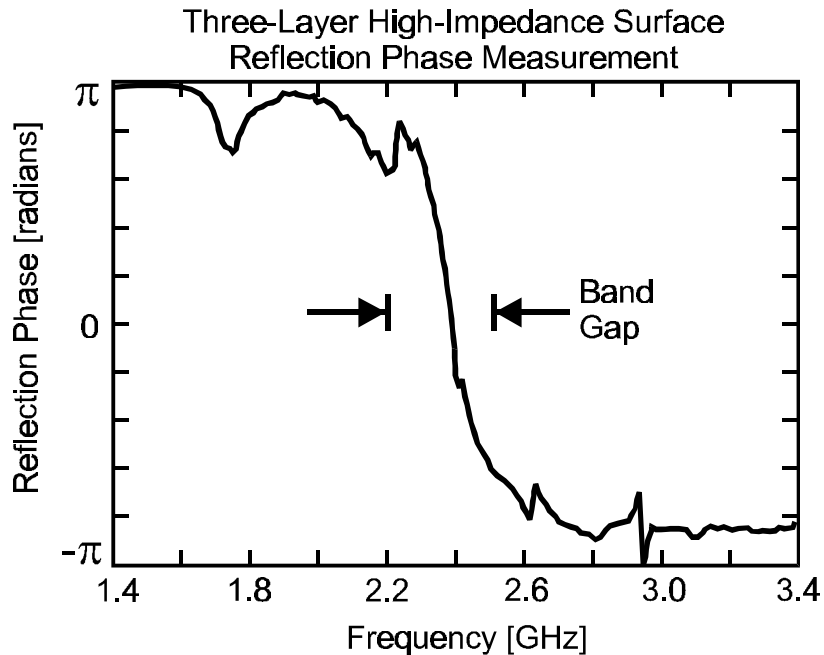


**Figure 7.4.2 Reflection phase of a three-layer high-impedance surface**

The reflection phase is shown in Figure 7.4.2. The region corresponding to the surface wave band gap is designated by arrows. Inside this gap, the reflection phase crosses through zero, and plane waves are reflected in-phase rather than out-of-phase. For this low-frequency structure, the data contains multipath interference from other sources

of reflection. The absorbing foam is less effective at lower frequencies, the horn antennas have lower gain, and the structure is smaller compared to the wavelength. Because of these factors, the edges and other surroundings introduce unwanted interference in the reflection measurement. Nevertheless, the data follows the same trends as for the two-layer structure.

## **7.5 Other features**

Until now, we have focused primarily on frequencies near the high-impedance condition, where the TM band ends, the reflection phase crosses through zero, and the TE band begins. There are numerous other interesting electromagnetic features at higher frequencies, which could be the subject of further study. Some of these features are illustrated in Figure 7.5.1, which shows the surface wave transmission across the three-layer structure studied in the previous section.

The TM band is visible up to 2.2 GHz, where the first gap begins. The TE band begins at 2.5 GHz, and continues up to about 5.5 GHz where a second, much wider gap begins. In this second gap, there are no detectable surface waves, but the structure does not exhibit the favorable surface impedance of the first gap. It is not known whether the second gap can be useful for electromagnetic devices.

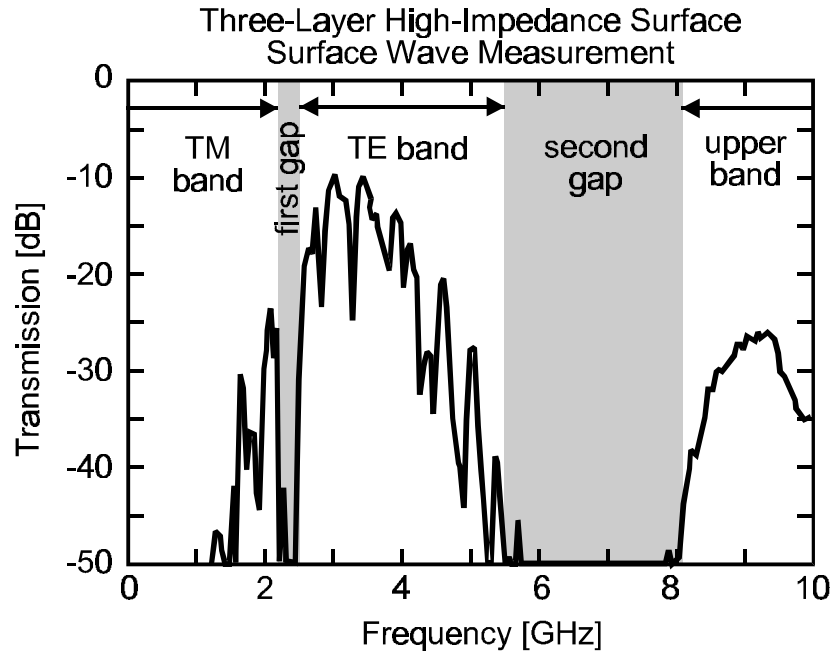


**Figure 7.5.1** A broad frequency sweep reveals other features of the band structure

At much higher frequencies, another band appears. The modes in this band probably occupy the space between the top capacitive layer and the lower ground plane, as shown in Figure 7.5.2. In one such possible mode, the electric field is vertically oriented, and the magnetic field runs parallel to the plates, similar to a mode in a parallel-plate waveguide. This upper band begins at the frequency where one-half wavelength fits between the metal vias.

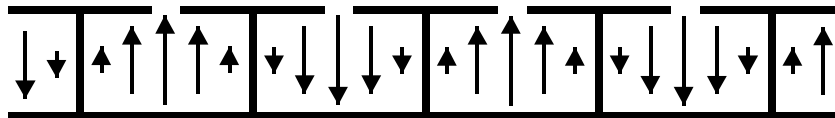


**Figure 7.5.2** Electric field lines for a possible mode in an upper band

## 8 Alternative Structures

The high-impedance surface can be related to several other approaches for controlling electromagnetic waves. However, these alternative structures fail to exhibit the unique properties of the high-impedance electromagnetic ground plane. An examination of these structures can illustrate the features of the high-impedance surface that are important for its electromagnetic properties. The simplest alternative is a thin sheet of metal islands, without the ground plane or the conducting vias. Such a structure will not support surface waves over a certain frequency range, but it is a poor reflector. If a ground plane is added, the structure is completely reflective, and it has the favorable reflection phase properties of the high-impedance surface, but it permits the propagation of surface waves. It is only when both the ground plane and the vias are included that the two important properties of the high-impedance surface are obtained: (a) in-phase, 100% reflection, and (b) suppression of surface current propagation

### 8.1 Frequency Selective Surfaces

Consider a structure consisting of only the top layer of the high-impedance surface – a sheet of metal islands, such as the one shown in Figure 8.1.1. This top layer alone can effectively suppress surface waves, because currents cannot travel across the breaks between the plates. It is only at very high frequencies, when the effective capacitors between neighboring plates behave as shorts, that surface waves can propagate. It would seem that a structure like this could be used in many of the same

applications as the high-impedance surface. However, over the frequency range where it prohibits surface waves, it is only partially reflective.

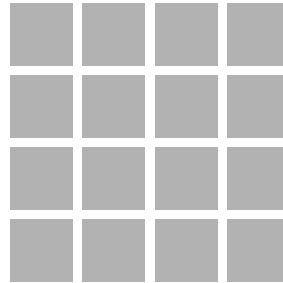


**Figure 8.1.1 A “capacitive” surface**

This structure is often called a frequency selective surface. [38, 39] If the metal plates are not connected, it is called a “capacitive” surface, and it transmits low frequencies while reflecting high frequencies. The inverse geometry, shown in Figure 8.1.2, is called an “inductive” surface, and it transmits high frequencies while reflecting low frequencies.

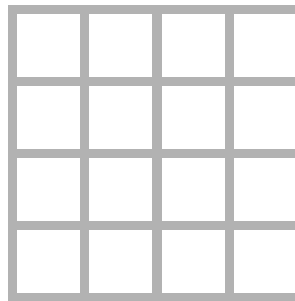


**Figure 8.1.2 An “inductive” surface**

The behavior of these two surfaces is easily understood from the following argument. For the inductive surface, waves that are short compared to the diameter of the holes will easily fit through the mesh, while longer waves see the sheet as continuous metal. Since each structure represents the Babinet complement of the other, [2] they have

complimentary transmission spectra. Therefore, the sheet of metal islands transmits long wavelengths, while reflecting short wavelengths. At low frequencies, where it can prevent the propagation of surface waves, the capacitive sheet is not completely reflective. Conversely, while the inductive sheet is reflective at low frequencies, surface waves can propagate easily along the continuous metal wires.

The high-impedance surface represents a new class of electromagnetic structures, distinct from frequency selective surfaces. Since it is backed by continuous, solid metal, it reflects at all frequencies. Nonetheless, the phase of the reflected waves can vary greatly with frequency. In addition, surface current propagation is controlled.

## 8.2 Addition of a Ground Plane

By augmenting the sheet of metal islands with a conducting ground plane, shown in Figure 8.2.1, it can be made completely reflective. In this example, the capacitance has been enhanced by overlapping the metal plates, but the same idea applies to any capacitive surface.

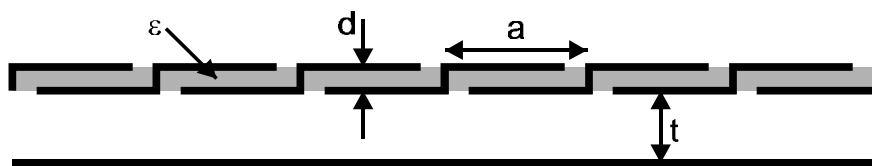


**Figure 8.2.1 A capacitive sheet backed by a solid metal ground plane**

We can calculate the reflection phase using an effective medium approach. We found earlier that a sheet of capacitors can be considered as an effective dielectric slab. The layer has thickness,  $d$ , the capacitors are arranged with lattice constant,  $a$ , and they

are filled with dielectric  $\epsilon$ . The effective dielectric constant of the slab, which is shown in Figure 8.2.2, is given by the following expression, derived in Chapter 5.

$$\epsilon_{\text{eff}} = \epsilon \frac{a^2}{d^2}$$

**Equation 8.2.1**

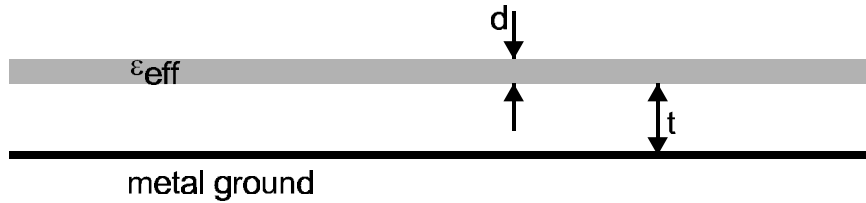


**Figure 8.2.2 Effective medium model for a capacitive sheet above a ground plane**

The reflection properties of a layered structure can be calculated using a transmission matrix approach. [40] Each layer or interface is described as a two-port network, shown in Figure 8.2.3.

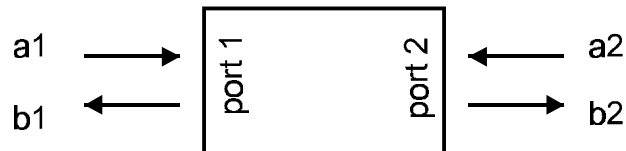


**Figure 8.2.3 A two-port network**

The network is expressed mathematically as a  $2 \times 2$  matrix. The incident, transmitted, and reflected wave amplitudes on either side of the network are related by the following matrix equation.

$$\begin{bmatrix} a_1 \\ b_1 \end{bmatrix} = \begin{bmatrix} M_{11} & M_{12} \\ M_{21} & M_{22} \end{bmatrix} \begin{bmatrix} a_2 \\ b_2 \end{bmatrix}$$

**Equation 8.2.2**

Stacking additional layers corresponds to cascading additional two-port networks, and the complete structure is described by the product of the individual matrices.

The transmission matrix across an interface from a material with impedance  $\eta_1$  to a material with impedance  $\eta_2$  can be shown to be equal to the expression below.

$$M_{\eta_1 \rightarrow \eta_2} = \begin{bmatrix} \frac{\eta_1 + \eta_2}{2\eta_1} & \frac{\eta_1 - \eta_2}{2\eta_1} \\ \frac{\eta_1 - \eta_2}{2\eta_1} & \frac{\eta_1 + \eta_2}{2\eta_1} \end{bmatrix}$$

**Equation 8.2.3**

The transmission matrix for a wave traveling through a material with index of refraction  $n$ , with thickness  $x$ , at frequency  $\omega$  is easily derived.

$$M_{n,x,\omega} = \begin{bmatrix} \exp\left(\frac{j\omega n x}{c}\right) & 0 \\ 0 & \exp\left(\frac{-j\omega n x}{c}\right) \end{bmatrix}$$

**Equation 8.2.4**

The matrices for each interface or thickness are multiplied in reverse order with respect to the direction of the impinging wave because of the convention chosen in Equation 8.2.2. Finally, the transmission coefficient of the entire stack is given by the following equation.

$$T = M_{11} - \frac{M_{12} \cdot M_{21}}{M_{22}}$$

**Equation 8.2.5**

The reflection coefficient is similarly obtained

$$R = -\frac{M_{21}}{M_{22}}$$

**Equation 8.2.6**

This method can be used to analyze structures containing dielectrics, magnetic materials, metals, and other lossy materials. One only needs the impedance and refractive index, or the dielectric constant and magnetic permeability, which can be complex.

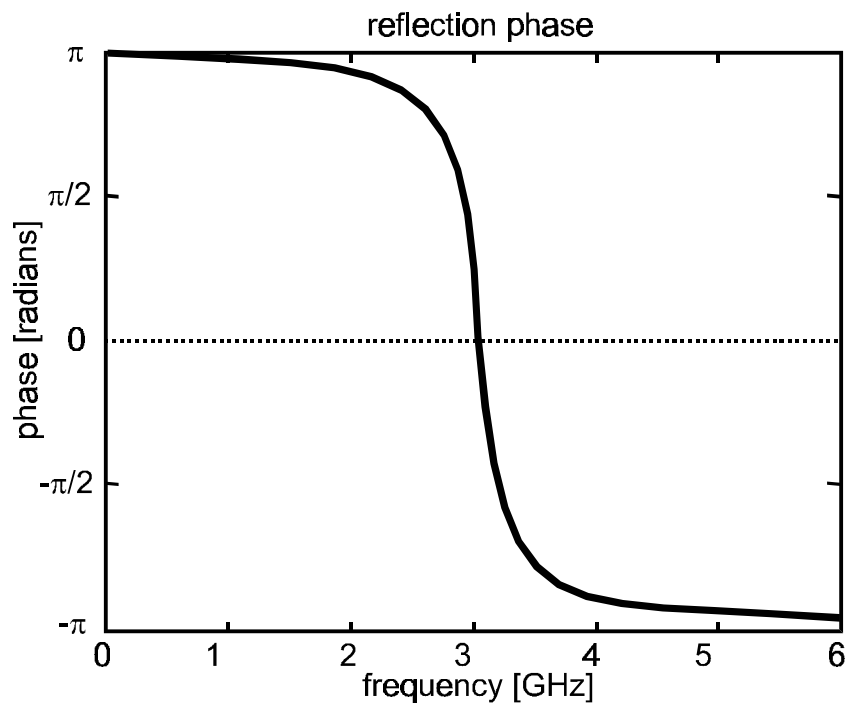


**Figure 8.2.4 Reflection phase of a capacitive sheet above a ground plane**

A typical structure might have a 50  $\mu\text{m}$  thick dielectric layer with  $\epsilon=4$ . If the embedded capacitor plates are 2 mm long, the effective dielectric constant, from Equation 8.2.1, is equal to  $4 \times (2/0.05)^2 = 6400$ . A typical thickness for the lower portion of the structure is 1.5 mm. For these parameters, the transmission matrix model gives the reflection phase shown in Figure 8.2.4. At low frequencies, the reflection phase begins at

$\pi$ . It crosses through zero at some resonance frequency, and continues toward  $-\pi$  at higher frequencies.

When the capacitive layer is very thin, with a very high effective dielectric constant, the resonance frequency appears to scale according to a simple set of rules. By simulating numerous structures, we can determine the dependence of the resonance frequency on various parameters. It appears to depend on the inverse square root of both the effective dielectric constant, and thickness of the capacitive sheet. It does not depend significantly on the dielectric constant of the thick lower layer, but it varies inversely with the square root of its thickness. If the lower layer is assigned a magnetic permeability other than unity, the resonance frequency also has an inverse square root dependence on that quantity. These observations are summarized by the following empirical formula.

$$\omega \approx \frac{c}{\sqrt{\epsilon_{\text{eff}} \cdot d \cdot \mu_r \cdot t}}$$

**Equation 8.2.7**

$\epsilon_{\text{eff}}$  and  $d$  are the effective dielectric constant and thickness of the capacitive layer,

while  $\mu_r$  and  $t$  are the relative permeability and thickness of the spacer layer.

Substituting the expression for the effective dielectric constant into the above equation yields the following simplification.

$$\omega \approx \frac{1}{\sqrt{\epsilon_0 \mu_0}} = \frac{1}{\sqrt{\epsilon_r \frac{a^2}{d^2} \cdot d \cdot \mu_r \cdot t}} = \frac{1}{\sqrt{\left(\epsilon_0 \epsilon_r \frac{a^2}{d}\right) \cdot (\mu_0 \mu_r t)}} = \frac{1}{\sqrt{LC}}$$

**Equation 8.2.8**

Thus, the empirical formula obtained from the simulations reduces to the same expression derived earlier from the effective circuit model. These calculations support the assumption that the thick lower region can be considered the inductive part of the structure, and its dielectric constant is immaterial.

### 8.3 Grounded Dielectric Slab

For plane waves impinging on a high-impedance ground plane at normal incidence, the electric field is parallel to the surface. The current through the vias is zero, so they do not influence the reflection phase. Furthermore, we have seen that a layered dielectric structure can have the same reflection phase behavior as what has been measured on the complicated metallic structure. It might appear that the vias and metal plates are unnecessary, and a simple dielectric slab on a ground plane can produce the same results. However, such a structure cannot prevent the propagation of surface waves.

The analysis of the grounded dielectric slab can be found in many electromagnetics textbooks. [3, 4] Its surface wave properties are summarized in the dispersion diagram shown in Figure 8.3.1. Unlike the high-impedance surface, the grounded dielectric slab supports TM waves at all frequencies, and TE waves above a cutoff frequency given by the expression below.

$$f = \frac{c}{4t\sqrt{\epsilon - 1}}$$

**Equation 8.3.1**

At this frequency, the thickness is slightly over one-quarter wavelength, and the surface impedance is capacitive. Higher order TM and TE surface waves also occur at multiples of the  $TE_1$  cutoff frequency.

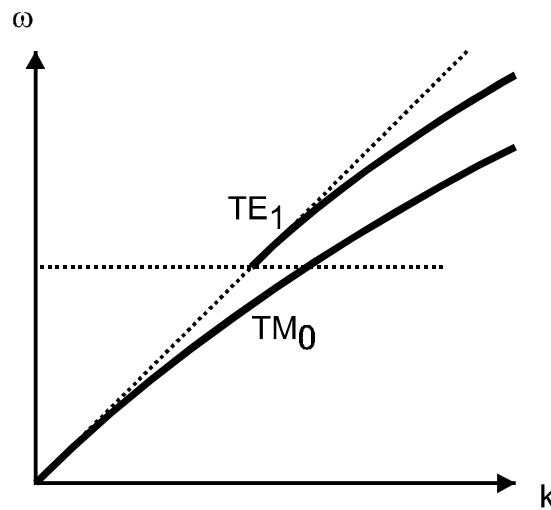


**Figure 8.3.1 Dispersion curves for surface waves on a grounded dielectric slab**

Although the surface impedance is capacitive when the dielectric layer is more than one-quarter wavelength thick, the TM dispersion curve has no upper limit. The wave simply adjusts its position toward the metal surface, as illustrated in Figure 8.3.2, so that the apparent surface impedance remains inductive, as required by TM surface waves.

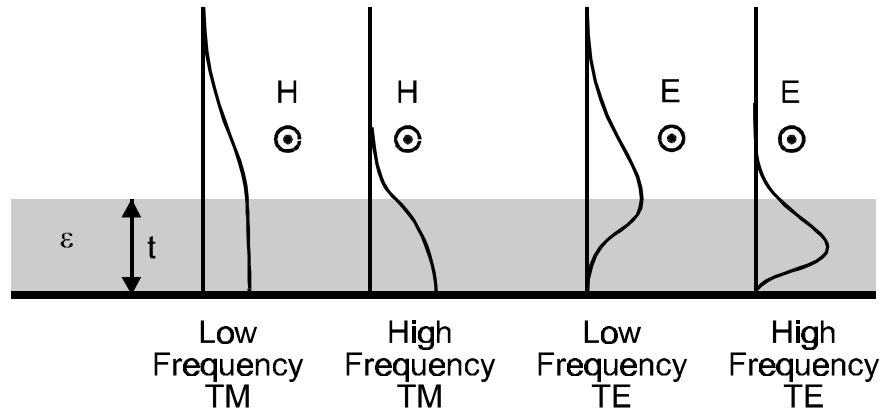


**Figure 8.3.2 Surface waves shifting toward the ground plane at higher frequencies**

The high-impedance surface behaves similarly if the vias are drilled out. A measurement of its TM surface wave properties without vias yields a similar result as an ordinary metal surface. The suspended sheet of capacitors acts as an additional dielectric layer, and is ineffective at preventing TM surface waves.

#### **8.4 The Role of Conducting Vias**

The importance of the conducting vias can be understood by adding metallic corrugations to the grounded dielectric slab. As the frequency increases, the wave attempts to move downward into the dielectric material. The more it interacts with the corrugations, the more it is slowed down. Eventually the wave fits entirely inside one of the corrugations, and ceases to propagate. This condition, illustrated in Figure 8.4.1, occurs when the structure is one-quarter wavelength thick. We saw in an earlier section that this condition is analogous to the resonance frequency of the high-impedance surface.

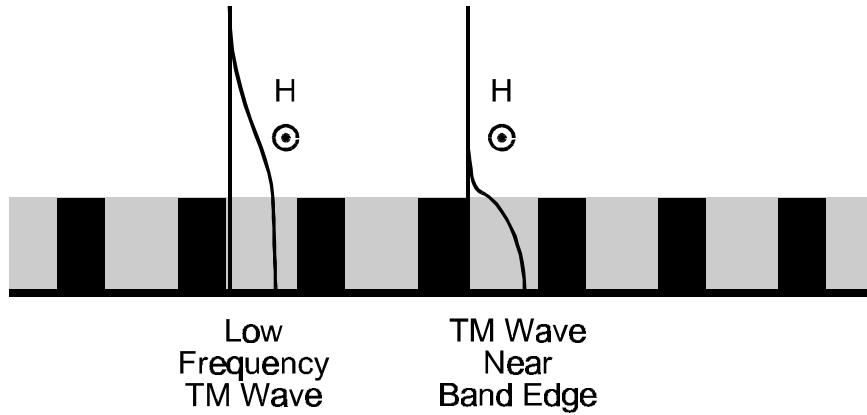


**Figure 8.4.1 Metal corrugations preventing high frequency TM surface waves**

TM waves are similarly suppressed on the high-impedance surface by the presence of vertical conducting vias. These necessary vertical connections occur naturally as the “bumpy surface” is extended into a circuit model, but their significance has not been adequately explored. A possible circuit for a structure without conducting vias is shown in Figure 8.4.2. Although the capacitive layer does not support propagating TM surface waves, the inductive metal surface below it does. The two are not electrically connected, and the capacitive sheet behaves as nothing more than a dielectric film suspended above the metal.

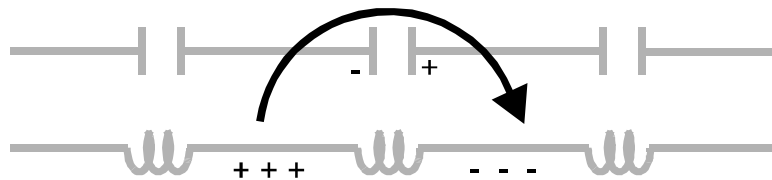


**Figure 8.4.2 Effective circuit in the absence of conducting vias**

When conducting vias are added, the nature of the structure is changed. The vertical electric field of a TM surface wave causes currents to flow through the vias, as shown in Figure 8.4.3. The two surfaces are linked together, and the combined structure

has the impedance of a parallel resonant circuit. Above the resonance frequency, the circuit is capacitive, and the structure does not support TM surface waves.

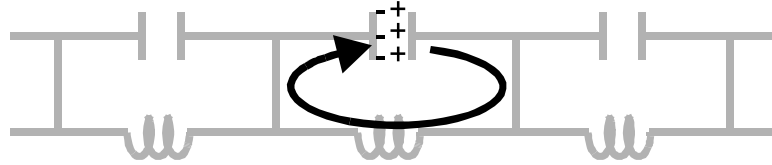


**Figure 8.4.3 Vertical conducting vias linking the two surfaces together**

Thus, one can conclude that the specific two-dimensional topology of the high-impedance surface is necessary for its full range of valuable properties.

## 9 Antennas

The high-impedance surface has proven useful as an antenna ground plane. Antennas have been demonstrated that take advantage of both the suppression of surface waves, and the unusual reflection phase. As a result of the suppression of surface waves, an antenna on a high-impedance ground plane produces a smoother radiation profile than a similar antenna on a conventional metal ground plane, with less power wasted in the backward direction. This can be applied to a variety of antenna designs, including patch antennas, which often suffer from the effects of surface waves. For phase-arrays, the suppression of surface waves can reduce inter-element coupling, and help to eliminate blind angles.

Various workers have studied antennas on photonic crystals, which are closely related to the high-impedance surface. [41, 42, 43, 44, 45] The unique reflection phase properties of the high-impedance surface can allow for new, low-profile antenna designs, with radiating elements lying flat against the ground plane. These antennas can take on a variety of forms, including straight wires to produce linear polarization, or various other shapes to generate circular polarization.

The high-impedance surface is particularly applicable to the field of portable hand-held communications, in which the interaction between the antenna and the user can have a significant impact on antenna performance. Using this new ground plane as a shield between the antenna and the user in portable communications equipment can lead to higher antenna efficiency, longer battery life, and lower weight.

## 9.1 The Vertical Monopole

One of the simplest antennas is a vertical monopole, shown in Figure 9.1.1. It can be fabricated by feeding a coaxial cable through a metal sheet, and extending the center conductor to form a radiating wire. The outer conductor is shorted to the metal surface, which acts as a ground plane. The wire is usually one-quarter wavelength long, and acts as one half of a dipole. The other half of the dipole is formed by the image currents that are driven in the ground plane.

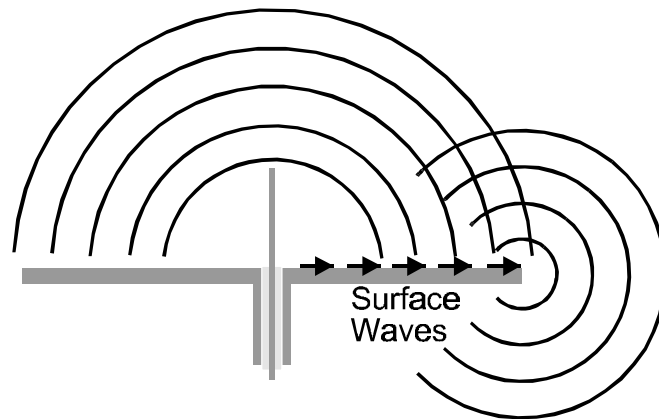


**Figure 9.1.1 Surface waves radiating at ground plane edges**

On an infinitely large ground plane, an antenna of this type would ideally have a smooth, half-doughnut shaped radiation pattern, with a null on the axis of the wire, and no radiation in the backward direction. In reality, the ground plane is always finite, and its edges contribute to the radiation pattern. In addition to space waves, the antenna generates surface waves in the ground plane, which then radiate from edges and corners. The combined radiation from the wire and the ground plane edges interfere to form a series of multipath lobes and nulls at various angles. The edges radiate backwards as well as forwards, causing a significant amount of wasted power in the backward hemisphere.

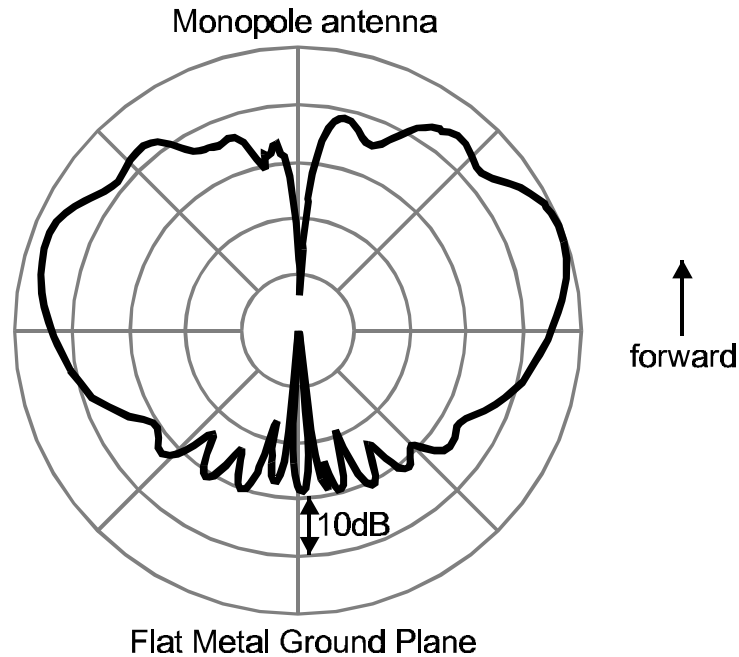


**Figure 9.1.2 Radiation pattern of a monopole antenna on a flat metal ground plane**

The radiation pattern of a monopole antenna on a metal ground plane is shown in Figure 9.1.2. The antenna is 3 mm long, and the ground plane is 5 cm square. The frequency of the measurement is 35 GHz. The important features of the antenna pattern are the ripples that appear in the forward direction, and the amount of wasted power in the backward direction. These features are both due to surface waves that propagate away from the antenna and radiate from the ground plane edges.

If the metal ground plane is replaced with a high-impedance ground plane, as shown in Figure 9.1.3, the surface waves are suppressed. While driven currents can exist on any reflective surface, they do not propagate on our high-impedance ground plane. Any induced currents are restricted to a localized region around the antenna, and never reach the edges of the ground plane. The absence of multipath interference results in a smoother radiation pattern, with less wasted power in the backward hemisphere.

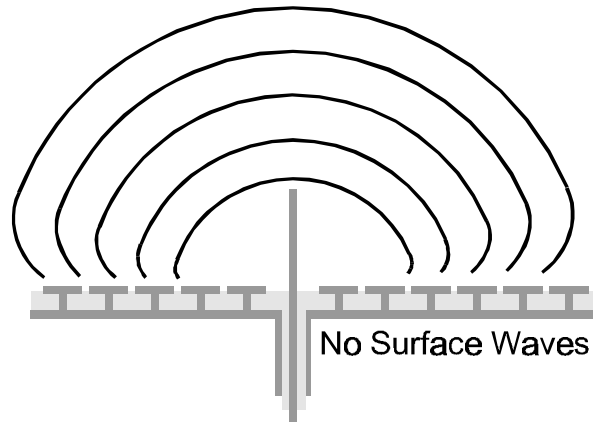


**Figure 9.1.3 Surface wave suppression on a high-impedance ground plane**

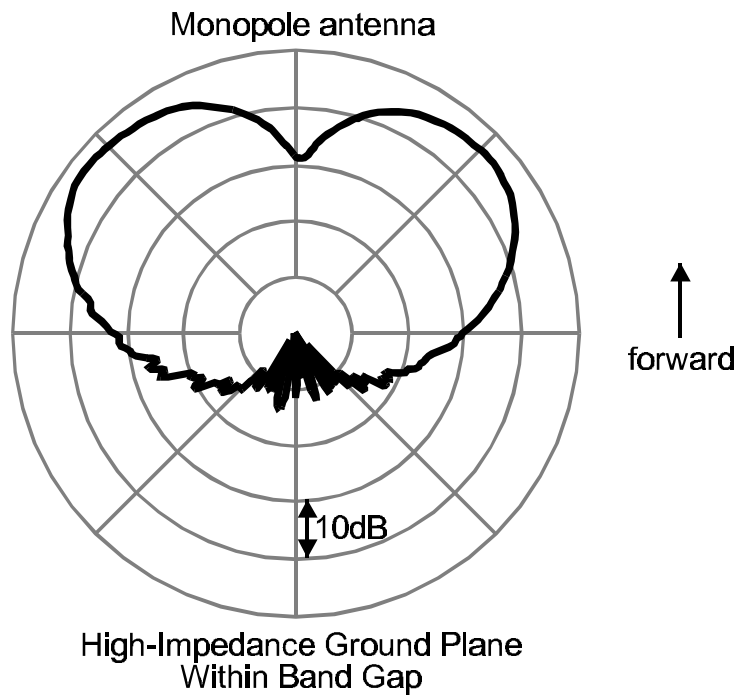


**Figure 9.1.4 Radiation pattern of a monopole on a high-impedance ground plane**

For the radiation pattern shown in Figure 9.1.4, the flat metal ground plane is replaced with a textured, high-impedance ground plane. The frequency and dimensions are the same as in the previous example. The radiation pattern in the forward direction is

smooth, showing only the two main lobes, and the power wasted in the backward direction is significantly reduced.

Two additional features are apparent in Figure 9.1.4. First, the center null is diminished because of asymmetry in the local geometry of the antenna wire and the surrounding metal patches. With more symmetrical construction, the null could be recovered. Second, the received power is lower with the high-impedance ground plane, especially at the horizon. This is because the image currents on the high-impedance ground plane are reversed with respect to their direction on a metal ground plane. For the vertical monopole, this tends to cancel the antenna current, particularly at the horizon.

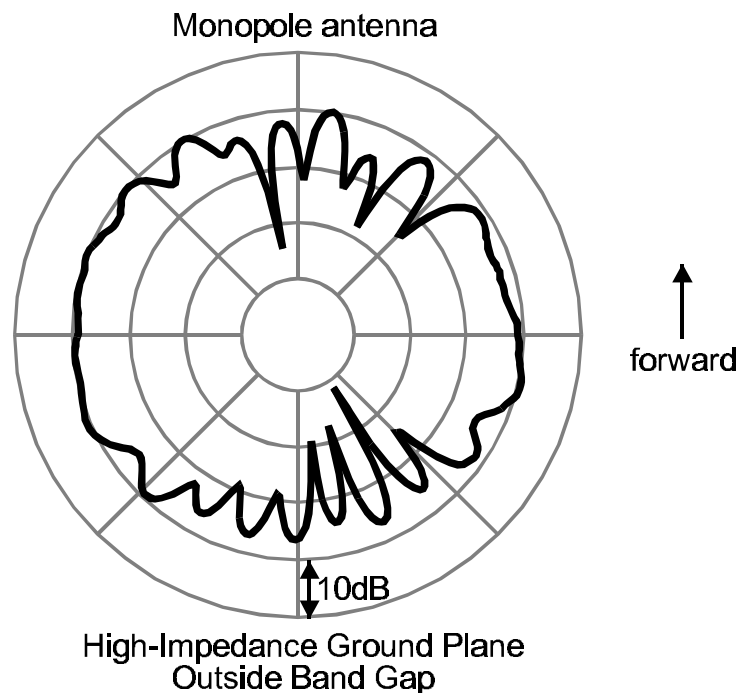


**Figure 9.1.5 Monopole radiation pattern below the TM surface wave band edge.**

If the antenna is operated outside the band gap, the ground plane behaves very much like an ordinary flat sheet of metal. Figure 9.1.5 shows the radiation pattern of the

monopole antenna on the high-impedance ground plane, operated within the TM surface wave band, at a frequency of 26 GHz. Because of the presence of surface waves, the pattern contains many lobes and nulls, and a significant amount of power is wasted in the backward hemisphere.

## 9.2 The Patch Antenna

The beneficial effects of surface wave suppression can also be applied to patch antennas. A patch antenna is a flat, metal shape printed on a dielectric substrate, which acts as a leaky cavity. The metal patch often takes the form of a circle or rectangle, but other shapes are possible. Antennas of this type are low profile, but because they are highly resonant, they also tend to have narrow bandwidth. A patch antenna can be fed by a microstrip line on the top surface, by a slot in the ground plane below the patch, or by a coaxial probe. An example of a patch antenna fed using the coaxial probe method is shown in Figure 9.2.1. The probe is placed off-center to excite an asymmetric mode, because the symmetric modes do not radiate efficiently.

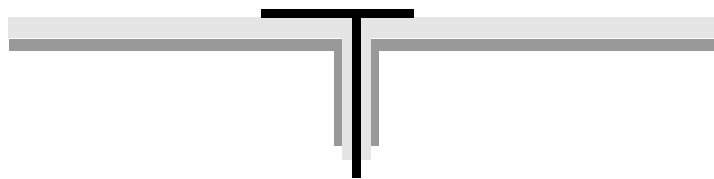


**Figure 9.2.1 A patch antenna on a metal ground plane**

The radiation pattern of the patch antenna is degraded by surface waves in the same way as the wire monopole. Surface waves radiate from the edges of the ground plane, causing ripples in the antenna pattern, and radiation in the backward direction. If

the substrate is thick, or it has a high dielectric constant, the surface wave problem is exacerbated.

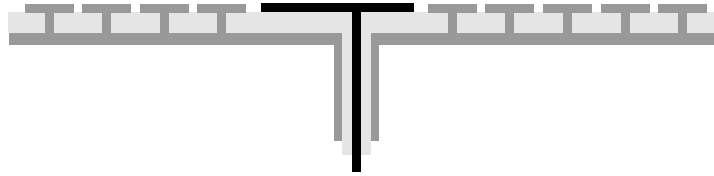


**Figure 9.2.2 A patch antenna embedded in a high-impedance ground plane**

Surface waves can be suppressed by embedding the patch in a high-impedance ground plane, as shown in Figure 9.2.2. The presence of the nearby metal protrusions tends to raise the resonance frequency of the patch, since the effective cavity volume is reduced. This can be corrected by leaving a small guard ring of bare substrate around the patch, or by increasing the size of the patch.

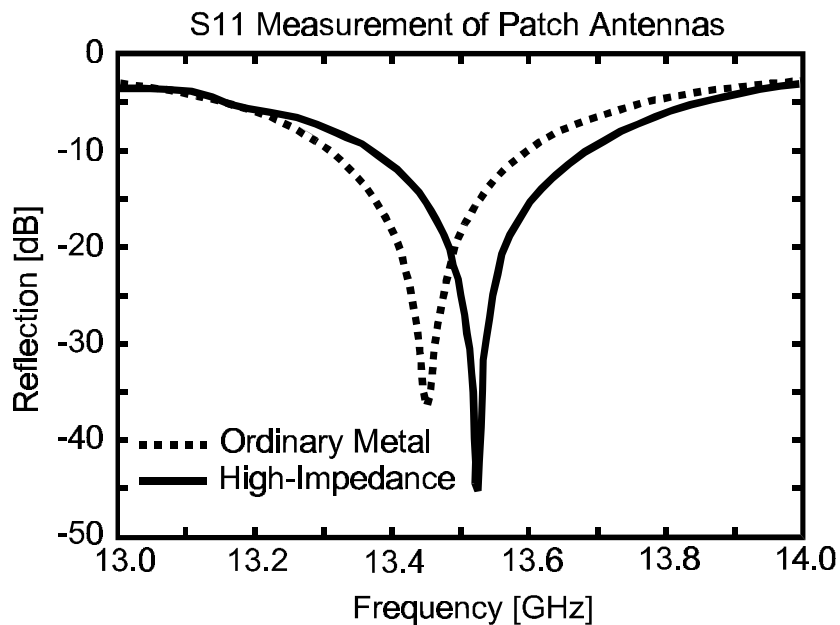


**Figure 9.2.3 S11 measurements for patch antennas on two different ground planes**

Figure 9.2.3 shows the S11 measurement of two patch antennas – one on an ordinary, metal ground plane, and one on a high-impedance ground plane. This measurement, also called the antenna return loss, is a measure of the amount of power reflected by the antenna toward the generator. A low return loss suggests that the antenna is radiating.

In both cases shown, the substrate has a dielectric constant of 10.2, a thickness of 0.625 mm, and a size of 5 cm square. Circular patches were used, with a diameter of 3.5 mm. A coaxial probe was used to feed the antennas. The patch on the high-impedance ground plane was surrounded by a guard ring consisting of 3 mm of bare dielectric. The presence of the surrounding metal protrusions tends to confine the electromagnetic fields, reducing the effective size of the cavity, and increasing the resonance frequency slightly.

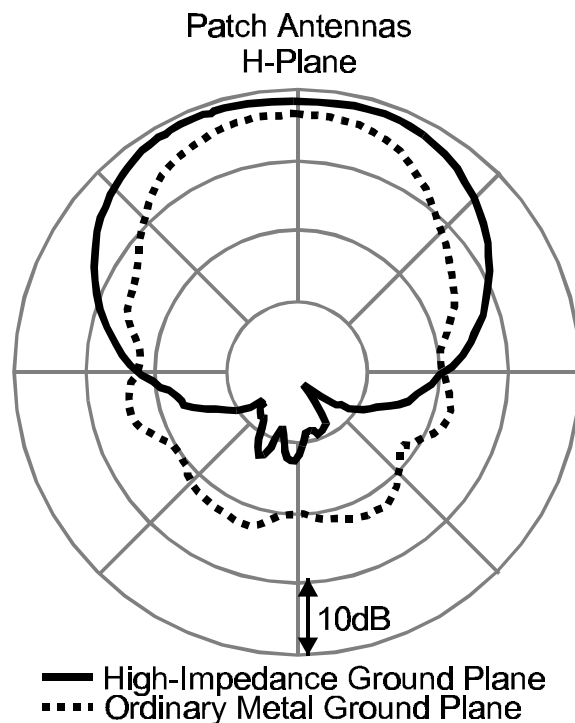


**Figure 9.2.4 H-plane radiation patterns of two patch antennas.**

The radiation patterns of the two antennas are shown in Figure 9.2.4 and Figure 9.2.5. The measurements are at a frequency of 13.5 GHz, where the two antennas have the same return loss. In both the H-plane and E-plane, the patch on the ordinary, metal ground plane shows significant radiation in the backward direction, and ripples in the forward direction. The pattern is not rotationally symmetric, and is much thinner in the H-plane than in the E-plane. Conversely, the patch on the high-impedance ground plane produces a smooth, symmetric pattern with little backward radiation.

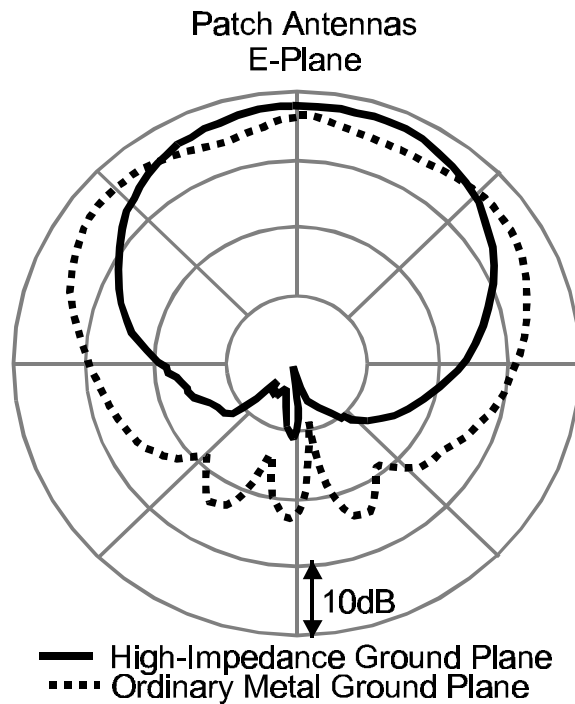


**Figure 9.2.5 E-plane radiation patterns of two patch antennas.**

The high-impedance ground plane is related to the patch antenna in that both are highly resonant, radiating structures. The frequency and bandwidth of the patch antenna can be expressed in the same form as we derived earlier for the high-impedance surface. Begin with the patch shown in Figure 9.2.6.

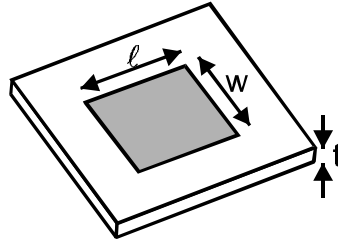


**Figure 9.2.6 Patch antenna**

Following the method of Chapter 5, the patch can be considered as a resonator with a particular capacitance and inductance. The capacitance is given by the following equation.

$$C = \epsilon \frac{w\ell}{t}$$

**Equation 9.2.1**

If the electric field of the patch is directed along  $\ell$ , then the inductance is given by the following expression.

$$L = \mu \frac{t\ell}{w}$$

**Equation 9.2.2**

If we assume that the resonance frequency is proportional to the inverse square root of the inductance and the capacitance, as it is in the high-impedance surface, we obtain the following.

$$\omega_0 \propto \frac{1}{\sqrt{LC}} = \frac{c}{n\ell}$$

**Equation 9.2.3**

In the above expression,  $c$  is the speed of light in vacuum, and  $n$  is the index of refraction of the substrate material. The resonance frequency is therefore inversely proportional to the length of the patch, and the index of refraction, which is known to be correct. [46]

The fractional bandwidth of the patch can be estimated using the same formula derived previously for the high-impedance surface.

$$\text{B.W.} \propto \frac{\sqrt{L/C}}{\sqrt{\mu_0/\epsilon_0}} = \sqrt{\frac{\mu_r}{\epsilon_r}} \cdot \frac{t}{w}$$

**Equation 9.2.4**

Therefore, the bandwidth is proportional to the substrate thickness, and inversely proportional to the width of the patch. This is reasonable, because thinner, wider patches confine the electromagnetic fields more, resulting in a higher  $Q$ .

Finally, we can determine the natural frequency of the patch, as was done in Section 5.7 for the high-impedance surface. The fractional bandwidth can be described in terms of the ratio of the resonance frequency to the natural frequency, which is then easily derived

$$\frac{\Delta\omega}{\omega_0} = \frac{\omega_0}{\omega_{\text{natural}}}$$

$$\omega_{\text{natural}} \propto \frac{cw}{\mu_r t \ell}$$

**Equation 9.2.5**

If the patch is roughly square,  $w/\ell \approx 1$ , then the natural frequency reduces to the same result obtained for the high-impedance surface. It only depends on the magnetic permeability and the thickness.

### 9.3 The Horizontal Wire

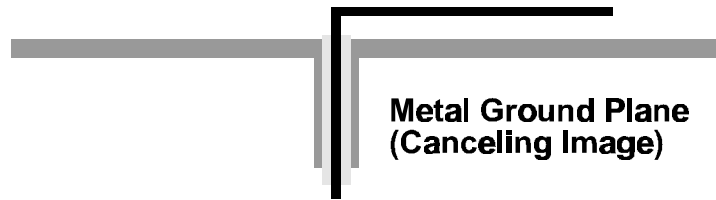


Figure 9.3.1 Horizontal wire antenna on a metal ground plane

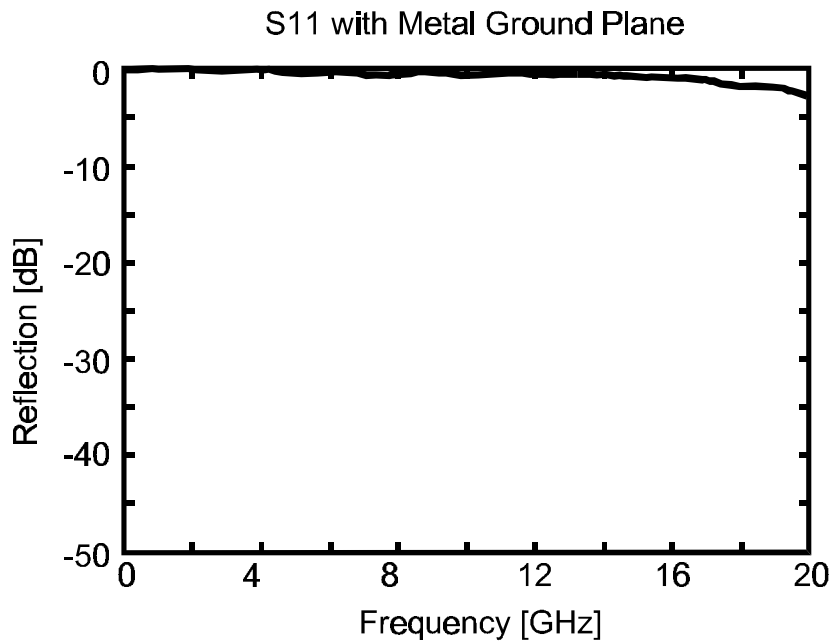
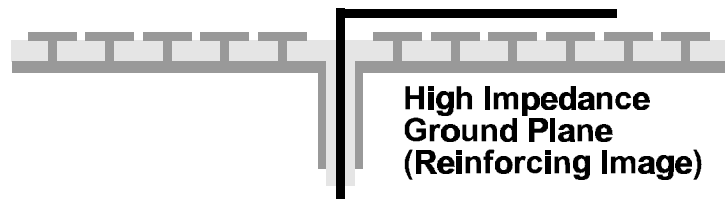


Figure 9.3.2 Reflection loss of a horizontal wire antenna on a flat metal ground

The benefits of surface wave suppression have been established through two examples: the vertical monopole, and the patch antenna. The other important property of the high-impedance surface is that it reflects in-phase, rather than out-of-phase. This is equivalent to a reversal of the direction of the image currents. This unusual property allows antennas to be constructed that are not possible on a flat, conducting ground plane.

An example, shown in Figure 9.3.1, is a wire antenna that has been bent over so that it lies parallel to a conducting surface.

A horizontal wire radiates very poorly on an ordinary, metal ground plane because the image currents cancel the currents in the antenna. The S11 measurement, or return loss of this antenna is shown in Figure 9.3.2. Most of the power is reflected back toward the generator, so the radiation efficiency is poor. In this example, the antenna was 1 cm long, and separated by a distance of 1 mm from a 3 cm square ground plane.



**Figure 9.3.3** A horizontal wire antenna on a high-impedance ground plane

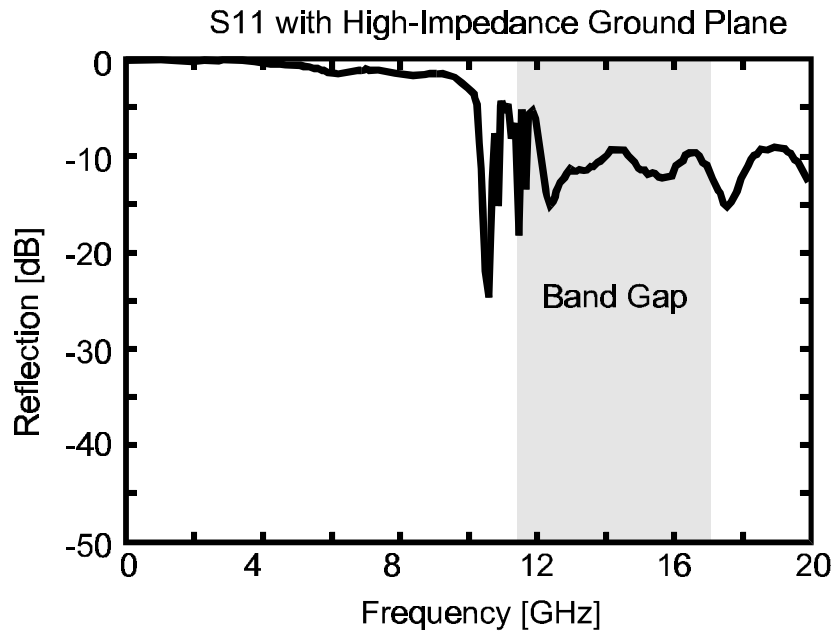


**Figure 9.3.4** Reflection loss of a horizontal wire on a high-impedance ground plane

A similar wire antenna on a high-impedance ground plane is shown in Figure 9.3.3. Within the band gap, which spans from 11 GHz to 17 GHz, this antenna has a much lower return loss, as shown in Figure 9.3.4. Below the TM band edge, the antenna performance is similar to the one on the metal ground plane. The surface impedance is low, and the image currents cancel the currents in the antenna.

Within the band gap however, the return loss is about -10 dB, indicating that only 10% of the power is being reflected back to the generator. In this range, the image currents are reversed, and they reinforce the antenna currents. Above the TE band edge, the return loss is also low because of coupling to TE surface waves. There is also strong coupling to TM waves near the TM band edge, where the density of states is very high.

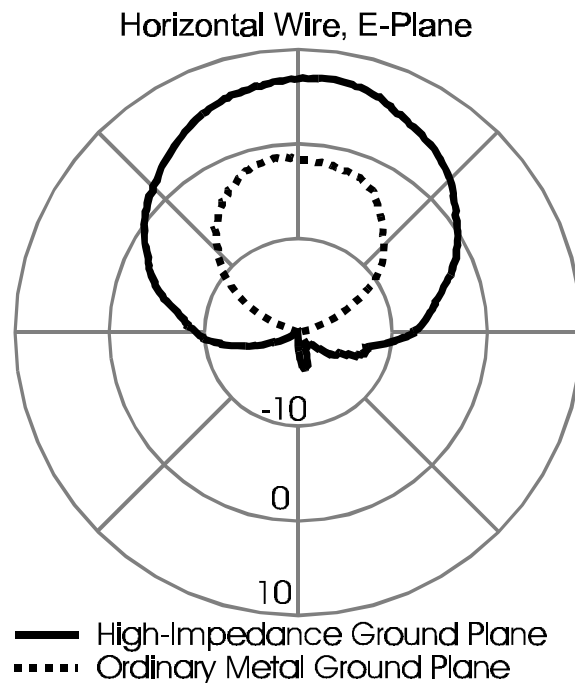


**Figure 9.3.5 E-Plane radiation pattern of two horizontal wire antennas**

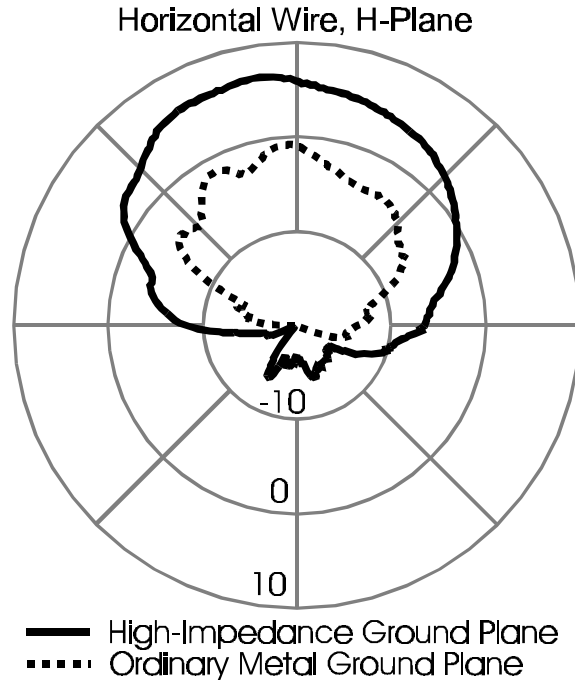


**Figure 9.3.6 H-plane radiation pattern of two horizontal wire antennas**

Although the antenna radiates over a broad band, it is only useful within the surface wave band gap, where it produces a smooth pattern. Outside the band gap, the pattern contains many lobes and nulls due to excitation of propagating surface waves.

The radiation pattern of both antennas is shown in Figure 9.3.5 and Figure 9.3.6. The dotted line is for the metal ground plane, and the solid line is for the high-impedance ground plane. The data in the radiation patterns supports the return loss data, in that the signal level is about 10 dB higher on the high-impedance ground plane. The data also contains an absolute calibration, referenced to an ideal isotropic radiator. The maximum gain of 7 dBi represents a typical value for an antenna on a high-impedance ground plane, regardless of the type of radiator used. Another typical feature of antennas on these high-

impedance ground planes is the rotationally symmetric nature of the radiation pattern, with both E- and H-planes displaying a characteristic apple-shape on a log-polar plot.

The horizontal wire antenna also performs well on high-impedance surfaces with three-layer construction, and produces a similar radiation pattern to that shown for the two-layer structure. The antenna radiates efficiently within the bandwidth of the ground plane, and the performance is best at the resonance frequency. For a smooth radiation pattern and an input impedance near  $50\Omega$ , the length of the wire should be between  $\lambda/3$  and  $\lambda/2$ . If the wire is too short, the input impedance is much higher than  $50\Omega$ . If it is longer than  $\lambda/2$ , an extra lobe appears in the radiation pattern.

It can sometimes be difficult to match the input impedance of the antenna to a  $50\Omega$  coaxial cable. This is often due to an unmatched capacitive component in the input impedance, and can be corrected by tuning the geometry of the horizontal wire, as shown in Figure 9.3.7. A small kink placed near the feed point can add a small amount of inductance, which is used to cancel the capacitive input reactance.

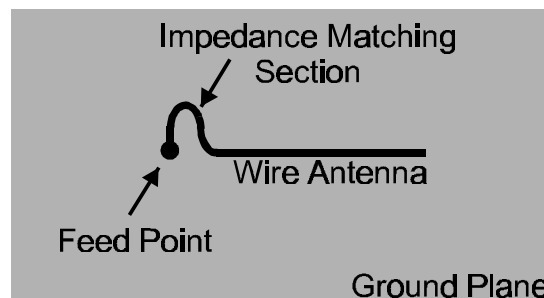


**Figure 9.3.7 A small kink placed near the feed point for impedance matching**

## 9.4 Circular Polarization

In some situations, circular polarization is desired. For example, satellite-to-earth communications are generally broadcast in circular polarization because it allows the receiver to have any orientation with respect to the transmitter. A simple way of generating nearly circular polarization is to use a circular wire, lying parallel to a high-impedance ground plane, as shown in Figure 9.4.1. The wire is fed at one end, and has a circumference of about one wavelength. The other end of the wire is usually left open, but similar results are produced if it is shorted to the ground.

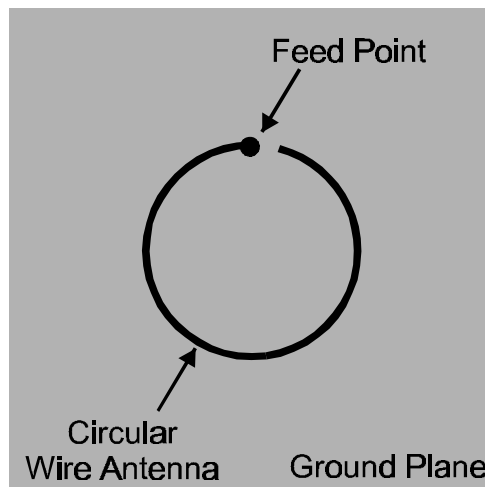


**Figure 9.4.1 A circular wire antenna on a high-impedance ground plane**

An antenna of this type produces a radiation pattern that is similar to that of the straight horizontal wire – a smooth, round pattern that is free from ripples or significant backward radiation. The polarization is nearly circular in the normal direction. However, as with most circular antennas, the polarization is generally elliptical at other angles. At the horizon, where the profile of the circle reduces to a straight wire, the polarization is linear.

The degree to which an antenna is circularly polarized can be determined by measuring the ratio of the power received by two antennas having opposite circular polarizations, which we will call the polarization ratio. The polarization ratio of this antenna in the normal direction has been measured to be 7.3 dB. In other words, the signal received by an antenna with the desired circular polarization is 7.3 dB higher than the signal received by an antenna with the opposite polarization. This simple circular wire is a crude form of the curl antenna, [47] which has been shown to produce nearly perfect circular polarization by careful tuning of the wire geometry.

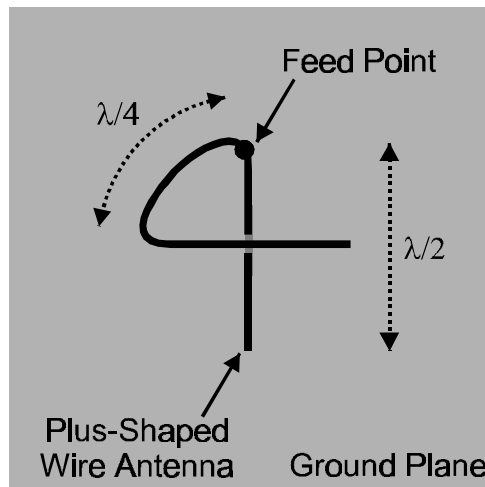


**Figure 9.4.2 A plus-shaped wire antenna**

Another way of producing circular polarization is to use a plus-shaped antenna such as the one shown in Figure 9.4.2. This antenna is based on the idea that a circularly polarized wave is a combination of two linearly polarized waves that are out of phase by one-quarter wavelength. The plus-shaped antenna functions as a pair of dipoles, fed in parallel, with one dipole having a one-quarter wavelength delay. The polarization ratio of this antenna has been measured to be 9.2 dB, somewhat better than the circular wire

antenna. The plus-shaped antenna could have an additional advantage when used in an array. For a given spacing, the inter-element coupling should be smaller for the plus-shaped antenna than for the circle-shaped antenna. This can be understood by considering that the plus-shaped antenna consists primarily of two orthogonal dipoles. E-plane coupling between each dipole is small because of the null along the dipole axis. H-plane coupling is also small because neighboring dipoles maintain a larger separation along that direction.

The polarization ratio of the plus-shaped antenna can be improved by considering the origin of each component of the polarization. The radiation of the two half-wave dipoles combine to produce circular polarization in the normal direction. However, the quarter-wavelength delay section also radiates, adding an additional linear component.

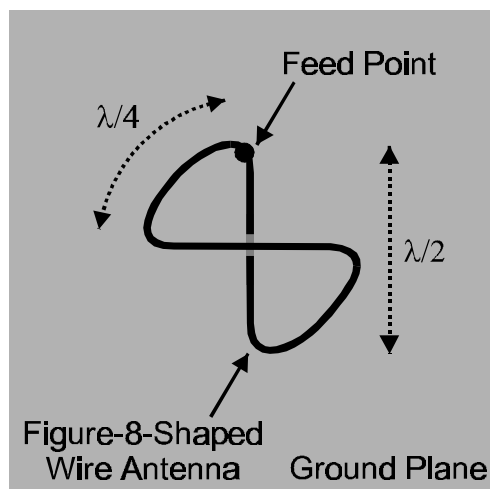


**Figure 9.4.3 A figure-8-shaped wire antenna**

An improvement is the more symmetrical, figure-8-shaped antenna shown in Figure 9.4.3. In this antenna, the radiation from both quarter-wavelength curved sections

cancel. The result is a measured polarization ratio of 11.8 dB, better than both the circular wire antenna, and the plus-shaped antenna.

## 9.5 Large and Small Antennas

Examples have been presented that illustrate the advantages of using a high-impedance ground plane for various types of antennas. The benefits arise from the reflection phase, which allows for low-profile antennas, and from the suppression of surface current propagation, which has been shown to produce improvements in the radiation pattern. A quantitative analysis of the degree of coupling between nearby antennas has a bearing on the design of large, multi-element arrays, as well as the minimum size ground plane that can be used for a single, compact radiator.

The coupling strength was determined by measuring the transmission between two antennas positioned near the high-impedance surface, and near a metal surface for comparison. For TM polarization, shown in Figure 9.5.1, the probe antennas were of the flared, parallel-plate waveguide type. They were moved across the surface, and the transmission between them was measured as a function of separation distance. For TE polarization, shown in Figure 9.5.2, wire antennas were aligned parallel to the surface. The data were taken at about 15 GHz, within the band gap of the high-impedance surface. Microwave absorbing foam was positioned several millimeters above the surface, in order to confine the measurement to the region just above the ground plane, and to eliminate interference from waves propagating through the surrounding space.

The results represent a combination of two factors: the coupling strength from the antennas to the surface determines the intersection with the vertical axis, while the

transmission across the surface is shown by the slope of each line. For TM polarization, shown in Figure 9.5.1, the coupling strength on the high-impedance surface is significantly reduced, and the signal decreases much more rapidly with distance than on the metal surface. However, for TE polarization, shown in Figure 9.5.2, the coupling strength on the high-impedance surface is greater than on the metal surface, and the signal decreases more slowly with distance. This can be understood by interpreting the graphs from the viewpoint of the surface as a boundary condition.

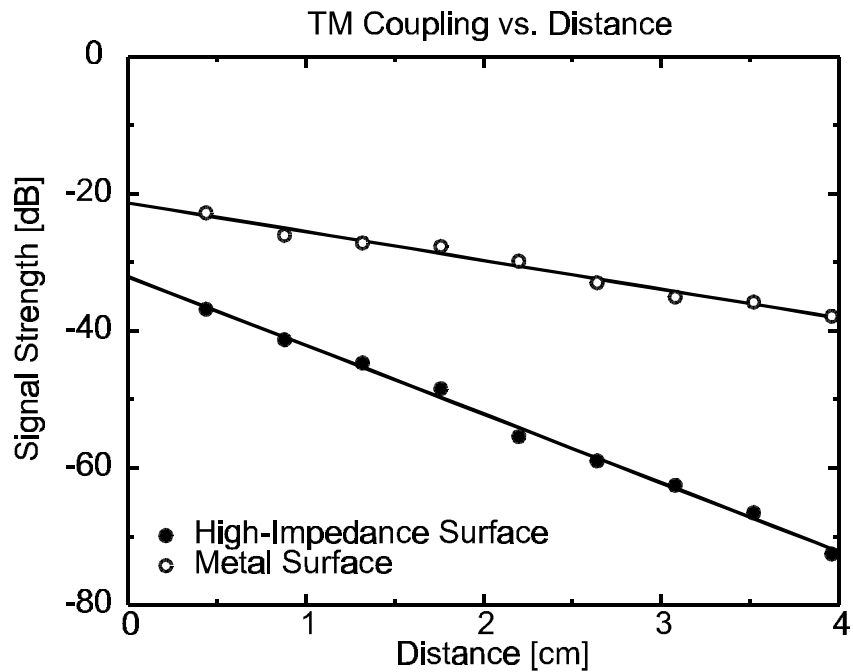


**Figure 9.5.1 Coupling between two antennas in TM configuration**

When an antenna is placed next to a flat metal surface, it generates plane waves, as well as currents in the surface. TM polarized waves and currents will readily be excited on a metal sheet, as the electric field is primarily perpendicular to the conductor.

The ensemble of fields and currents propagates unhindered by the metal, and radiates rather poorly.

On the high-impedance surface, the situation is reversed. This can be understood by recalling that the high-impedance surface functions as a kind of magnetic conductor. Just as a metal surface repels transverse electric fields, the high-impedance surface abhors transverse magnetic fields. Hence, TM transmission is very small, as is the coupling strength to a TM polarized antenna. In other words, if a surface current with TM polarization is generated on the high-impedance surface, it will rapidly radiate.

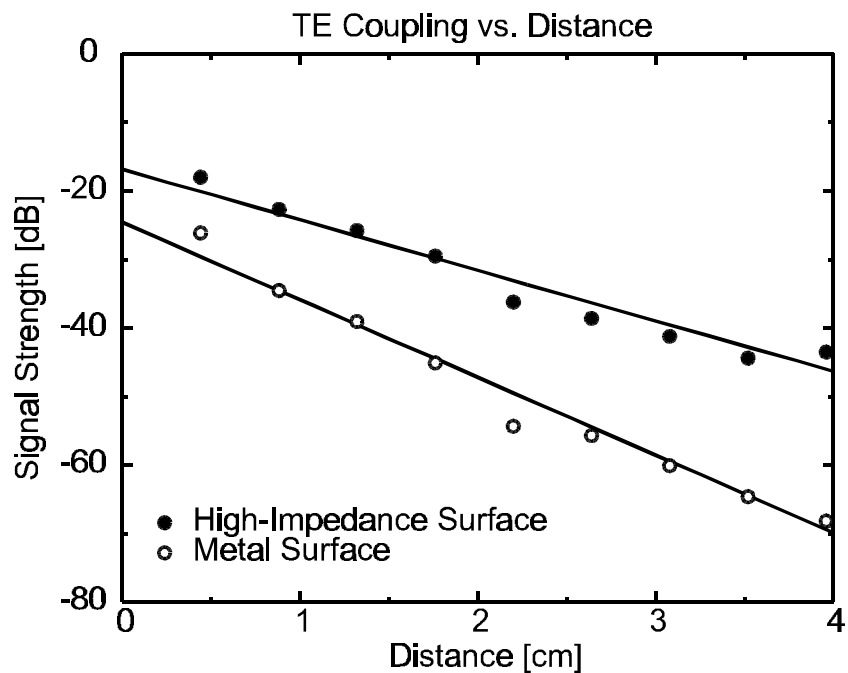


**Figure 9.5.2 Coupling between two antennas in TE configuration**

For TE polarized waves, the electric field is parallel to the surface. The image currents generated in a flat metal surface tend to cancel the nearby electromagnetic wave,

so TE waves are rapidly repelled. TE surface currents tend not to be excited on a flat metal sheet.

TE surface modes exist on the high-impedance surface throughout the band gap, but they consist of radiative, leaky waves. They are not bound to the surface, but they do not radiate as rapidly as they do on a conducting sheet. Due to the high impedance, the antenna is not shorted, and readily excites them. This is evident in the fact that the TE transmission is higher on the high-impedance surface than it is on the metal surface.

The measurements described above have an impact on the design of phased array antennas. [48] In phased arrays, in which the ground plane is very large, surface currents can form standing waves, and contribute to multipath interference. This can lead to blind angles – angles for which the antenna gain drops significantly. This effect can also be seen as ripples in the radiation pattern of a single antenna on a metal ground plane.

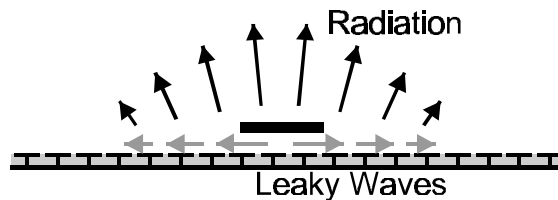


**Figure 9.5.3 Leaky TE waves radiate, and never reach the ground plane edge**

On a high-impedance ground plane, surface currents radiate efficiently, and never reach the edge. Even the leaky TE modes that exist within the band gap will radiate much of their power before reaching the edge of a large ground plane, as illustrated in Figure 9.5.3. This is apparent in both the attenuation measurements shown in this section, and the radiation patterns shown in previous sections. The fact that antennas on the high-impedance surface produce a smooth, symmetrical pattern in both the E- and H-planes is

evidence that both TE and TM surface current propagation is suppressed. Therefore, using a high-impedance ground plane for phased arrays should reduce blind angles.

Another problem with phased arrays is the presence of coupling between nearby elements, due to both surface waves and space waves. This coupling complicates steering of the beam, and degrades performance. According to the results of this section, TM coupling can be reduced by using a high-impedance surface in place of a metal ground plane. TE coupling could be worse on the high-impedance surface, so a good design might consist of stripes of high-impedance material, augmented by interleaving stripes of metal, such as the example shown in Figure 9.5.4.

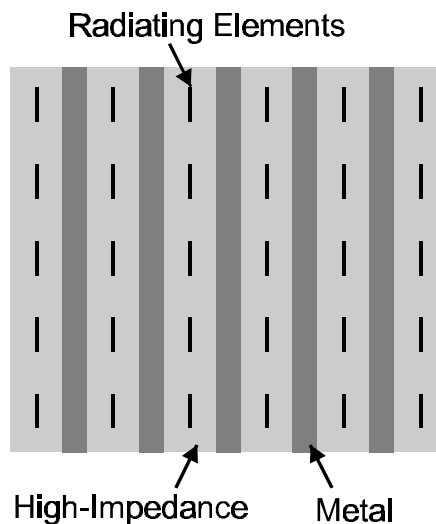


**Figure 9.5.4 Array design using stripes of metal and high-impedance material**

The results of this section also have an impact on the design of small antennas. The degree to which the signal is diminished with distance determines how much radiation will end up in the backward hemisphere for a given size ground plane. As the size is reduced, more power will spill over into the backward direction. In practice, if the

separation between the radiating element and the edge of a high-impedance ground plane is on the order of one-half wavelength, a front-to-back ratio of roughly 10 dB can easily be achieved. Using a larger ground plane, the backward power can be reduced even further.

For many applications, a compact design is required. However, if the ground plane is too small, its properties will have little impact on the antenna performance. This is because the reactive near field of the antenna wraps around to encircle the entire structure. For a small antenna, the reactive near field extends roughly  $\lambda/2\pi$ , or one-sixth of a wavelength in all directions, a distance designated by Wheeler as the “radiansphere”. [49, 50] Within this radius, the electromagnetic field is primarily reactive, rather than radiative. Thus, if the ground plane is smaller than about one-third wavelength across, the reactive near field of the antenna completely surrounds the ground plane, and there is little that can be done to improve the directivity.

The bandwidth of an antenna is also related to its size. In general, the fractional bandwidth of a small antenna is roughly equal to the volume of the smallest sphere that can fit around the antenna, divided by the volume of the radiansphere. This is a general truth about electrically small antennas, and can be derived several different ways. [51, 52, 53] For an antenna employing a high-impedance surface, the bandwidth of the ground plane usually limits the bandwidth of the antenna. Therefore, the antenna does not need to be any larger than what is necessary to match the bandwidth of the high-impedance surface. For example, to achieve a bandwidth of 10%, consistent with a typical three-layer structure, the antenna only needs to have a length of about  $\lambda/10$ . Thus, much

smaller designs should be possible than those discussed in this chapter. In one extreme, a single resonant element of the high-impedance surface could be modified to act as the antenna.

## **9.6 Portable Communications**

One important application of the high-impedance ground plane is in the area of portable communications. At present, the standard antenna geometry is a monopole, which is part of the handset and lies in close proximity to the user's head. It has been shown that with this configuration, roughly 50% of the radiated power is absorbed by the user. [54] The effect of the radiation on the user has not been evaluated conclusively, but the effect of the user on the antenna is significant. If this lost power could be reclaimed, the benefits for portable communication equipment could be an improvement in battery life, or a reduction in battery weight.

The power lost to absorption can be reduced by using a directional antenna. Directional antennas might appear impractical for portable communications. However, in a real environment, scattering from buildings and other objects tends to randomize the signal direction. For commercial products, cost is the most significant design factor, so the antenna must be inexpensive to produce, and simple to integrate into the handset hardware. Patch antennas are cheap and directional, but they have the disadvantage that they are easily detuned by nearby dielectric objects. Wire antennas are not as easily detuned, but they are only directional when combined with a reflector. If the reflector is a flat, metal sheet, it enforces a minimum thickness of one-quarter wavelength, which is unpractical. A good alternative is a high-impedance ground plane, with a horizontal wire

antenna mounted directly adjacent to the top surface. The frequency of operation is determined more by the surface than the wire, and since the resonance is controlled by the internal coupling between the individual elements, the structure is not easily detuned.

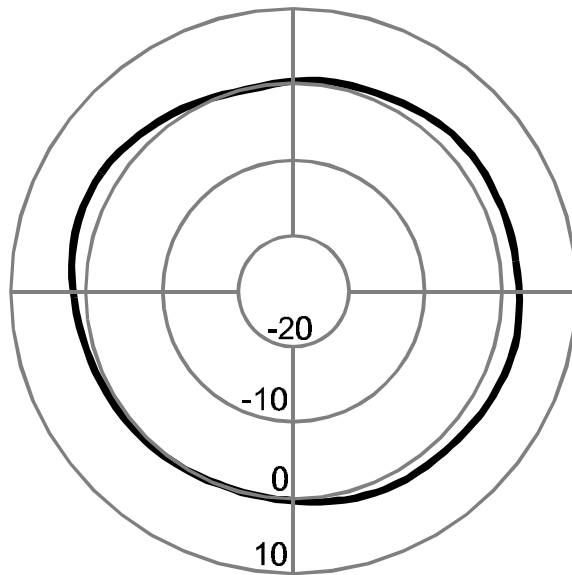


**Figure 9.6.1 Reference radiation pattern of a dipole antenna in free space**

Figure 9.6.1 shows the H-plane radiation pattern of a half-wave dipole antenna in free space, to be used as a reference. The frequency of the measurement is 2.3 GHz. The radial scale is dBi, decibels with respect to an isotropic radiator, and the dipole has the expected average gain value of around 2 dBi. The experiment shown in Figure 9.6.2 is designed to simulate a real communications environment. The presence of the user is modeled by a jar of water roughly the size of a human head. The dielectric constant of water is similar to most human tissues.

The plot shown in Figure 9.6.3 is the radiation pattern of the same dipole antenna placed near a jar of water. The radiation is blocked from propagating through the water, as indicated by the deep null in the direction of the jar. The overall signal level is also

reduced in all directions due to a combination of absorption, and modification of the antenna input impedance. The maximum gain is about 0dBi, in the direction away from the jar of water.

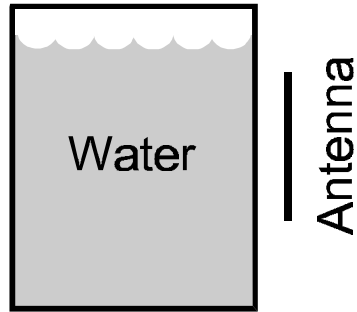


**Figure 9.6.2 Experiment to measure effects of the user in portable communications**

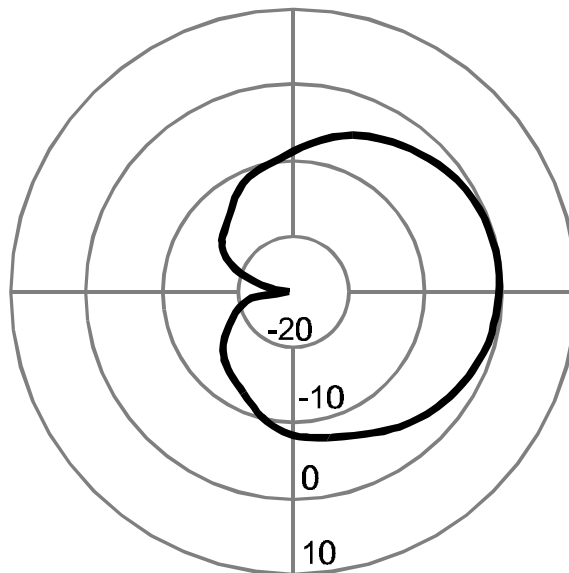


**Figure 9.6.3 Radiation pattern of a dipole antenna near a jar of water**

The radiation pattern shown in Figure 9.6.4 was produced by a wire antenna on a high-impedance ground plane. The jar of water was placed behind the ground plane, on the opposite side from the antenna. The antenna has a maximum gain of about 6dBi, in

the direction normal to the ground plane. The high-impedance surface acts as a shield between the radiating antenna and the absorbing water, blocking not only the direct radiation, but also the surface currents that would wrap around to the back side. The ground plane redirects the radiation that would otherwise be absorbed into the user, recovering it as useful power in the opposite direction. The combination of the antenna and the ground plane is compact and lightweight, allowing it to fit within the packaging of most portable communications equipment.

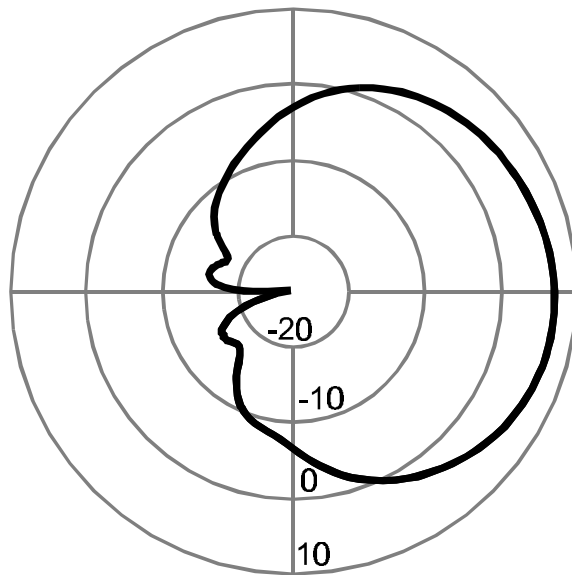


**Figure 9.6.4 Wire antenna on high-impedance ground plane, near jar of water**

## 10 Design

Using a few simple design rules, a high-impedance surface can be built according to predetermined frequency and bandwidth specifications. Numerous examples have been fabricated using printed circuit board technology, with resonance frequencies ranging from hundreds of megahertz to tens of gigahertz. These do not represent upper or lower limits however, and it should be possible to design high-impedance surfaces for any desired radio frequency. The primary limitation is on the bandwidth, which depends on the thickness of the structure with respect to the center wavelength.

### 10.1 Frequency and Bandwidth

In the effective medium model described in chapter 5, the structure is characterized by its surface impedance, which is equal to the impedance of an effective parallel LC circuit. According to the model, the properties of the high-impedance surface can be described entirely in terms of its sheet capacitance and sheet inductance, which are obtained from the geometry of the surface texture. This forms the basis for a set of simple design equations, which can accurately predict the properties of the textured surface.

For two-layer construction, in which the capacitors are defined by the fringing electric fields between pairs of co-planar metal plates, the value of each capacitor is given by the following equation, derived in section 5.1.

$$C = \frac{w(\epsilon_1 + \epsilon_2)}{\pi} \text{Cosh}^{-1} \left( \frac{a}{g} \right)$$

**Equation 10.1.1**

The dielectric constants of the circuit board material and the surrounding space are  $\epsilon_1$  and  $\epsilon_2$ . The center-to-center spacing of the vias is  $a$ , the gap between the plates is  $g$ , and the width of the capacitor is  $w$ . The dimensions are illustrated in Figure 10.1.1 for an example of a triangular lattice of hexagonal patches.

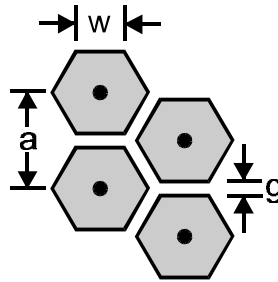


**Figure 10.1.1 Dimensions for calculating fringing-field capacitance**

Typical materials used for microwave printed circuit boards have dielectric constants ranging from 2 to 10. Using standard printed circuit fabrication techniques, the minimum gap width between adjacent metal regions is around 100 to 200 microns. For microwave structures, the lattice constant is typically several millimeters. Using variations of the geometry and materials given here, the achievable value for each capacitor can cover a broad range of roughly 0.01 to 1 picoFarad using two-layer construction.

With a three-layer structure, the capacitance can be much higher. The value of each capacitor is given by the following formula, in which  $\epsilon$  is the dielectric constant of the insulating material,  $A$  is the area of the capacitor plates, and  $d$  is their separation.

$$C = \frac{\epsilon A}{d}$$

**Equation 10.1.2**

As an example, a typical insulator is polyimide, which is commonly available for use in flexible printed circuits. With a dielectric constant of 4, a thickness of 50 microns, and a lattice constant of a few millimeters, values ranging from around 1 picoFarad to several tens of picoFarads or more are easily achievable.

The important parameter for the surface impedance is not the individual capacitance, but rather the sheet capacitance, in Farads-square. The difference can be understood by considering an arrangement of capacitors covering a square area. Long, thin capacitors provide more sheet capacitance than an equal number of short, wide capacitors. In other words, the sheet capacitance is higher if they are in parallel rather than in series. This is evident in the formula for the sheet capacitance derived in section 5.1, in which the length squared appears in place of the area.

$$C_s = \frac{\epsilon a^2}{d}$$

**Equation 10.1.3**

In the above equation,  $a$  is the length of the capacitors along the direction from one via to the next. In effect, the sheet capacitance is equal to the individual capacitance multiplied by the aspect ratio of each capacitor. If the capacitor plates do not cover the entire surface area, a more accurate formula is given below, also derived using the method of Section 5.1.

$$C_s = \frac{\epsilon(a \cdot a')}{d}$$

**Equation 10.1.4**

In the above equation,  $a$  is the separation between neighboring vias, which may not equal the lattice constant, and  $a'$  is the overlap distance, as shown in Figure 10.1.2. Obviously, this expression is only approximate, because the overlapping plates can take on various shapes.

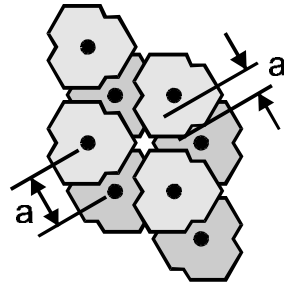


**Figure 10.1.2 Dimensions for calculating sheet capacitance**

The simplest method for calculating the sheet capacitance is to use the individual capacitance between adjacent lattice points, multiplied by a geometrical correction factor, which we will call  $F$ .

$$C_{\text{sheet}} = C_{\text{individual}} \times F$$

**Equation 10.1.5**

The correction factor can be calculated as the ratio of Equation 10.1.3 to Equation 10.1.2, for a structure in which the capacitors consume the entire surface area. This is also equal to the ratio of the length to the width, for each individual capacitor. The necessity of a geometrical factor is confirmed experimentally by the fact that structures having capacitors of equal value, but arranged in a different geometry, have different resonance frequencies. The correction factors are given in Table 10.1.1 for the square and

triangular lattices, as well as for hexagonal geometry, a version of the triangular lattice in which each unit cell is composed of two individual members.

Geometry	Correction Factor (F)
Square	1
Triangular	$\sqrt{3}$
Hexagonal	$\frac{1}{\sqrt{3}}$

**Table 10.1.1 Sheet capacitance correction factors for various geometries**

The sheet inductance is easier to calculate, since it depends only on the overall thickness, as derived in Section 5.1.

$$L_s = \mu t$$

**Equation 10.1.6**

In the above equation,  $\mu$  is the magnetic permeability of the circuit board material, and  $t$  is its thickness. For most materials,  $\mu$  is unity at microwave frequencies. If the structure is a few millimeters thick, the sheet inductance is several nanoHenrys/square. In the derivation of Equation 10.1.6 we assumed a solenoid of current, and neglected any direct contribution from the diameter of the vias. By using extremely thin vias, coils, or other special geometries, it may be possible to generate larger sheet inductance without the use of magnetic materials.

Once the sheet capacitance and sheet inductance are known, the resonance frequency and bandwidth are easily calculated from the following equations.

$$\omega_0 = \frac{1}{\sqrt{LC}}$$

**Equation 10.1.7**

$$\frac{\Delta\omega}{\omega_0} = \frac{\sqrt{L/C}}{\sqrt{\mu_0/\epsilon_0}}$$

**Equation 10.1.8**

Equation 10.1.7 is the LC resonance frequency, and Equation 10.1.8 is the bandwidth, derived in Section 5.5.  $\omega_0$  is the frequency where the reflection phase is zero, and where the surface behaves as a magnetic conductor. This is also the frequency where an antenna will perform best on such a ground plane. The bandwidth in Equation 10.1.8 corresponds roughly to the width of the surface wave band gap, or equally well, the frequency range over which the reflection phase falls between  $+\pi/2$  and  $-\pi/2$ . The bandwidth of the actual antenna might be smaller, depending on the geometry of the antenna, and the size and shape of the ground plane.

Clearly, any radio frequency can be obtained by adjusting the value of the sheet capacitance and sheet inductance. The goal is usually to make the thickness much less than the operating wavelength. Since the thickness is linked to the inductance, low frequencies are usually achieved by loading the structure with large capacitors. However, this reduces the bandwidth. Therefore, the primary trade-off in the design of a high-impedance surface is usually the thickness versus the bandwidth.

## 10.2 Geometry and Materials

From the explanation given in the previous section, the design of a high-impedance surface is a simple matter of determining what frequency and bandwidth are needed, and then calculating the required capacitance and inductance. The inductance depends only by the thickness of the circuit board, while the capacitance can be generated in several ways, two of which are described above. Using typical materials and dimensions, capacitors of less than about 1 picoFarad can be built using the two-layer technique, while larger capacitors generally require three layers. With a thickness of a few millimeters, two-layer structures can generally be employed above 5 or 10 GHz, while three-layer structures are usually required for lower frequencies.

The choice of materials is also related to the frequency of operation. For three-layer structures, the electric field is concentrated in the thin insulator between the capacitor plates, and the energy stored in the lower bulk region is primarily magnetic. Therefore, dielectric losses in this region are not significant, and a thermoset fiberglass laminate such as standard FR4 is an ideal material. In the thin insulator, the electric field is much higher, and a material with low dielectric loss should be used. Polyimide is a good choice, as it is commercially available for use in flexible printed circuits, and withstands conventional processing. In contrast to the three-layer structures, the fringing electric fields in the capacitors of a two-layer structure extend into the bulk, causing dielectric losses in that region to be significant. Since two-layer construction is usually used for high frequencies, where FR4 can be lossy, a teflon-based fiberglass laminate is often used instead.

In two dimensions, the two most obvious lattices are triangular, and square. In addition, there is hexagonal geometry, which is actually just a triangular lattice with two members per unit cell. Other, less symmetrical lattices are also possible. In fact, periodicity is not required, although it simplifies the design. The three geometries mentioned above are shown in Figure 10.2.1. One choice of unit cell is outlined in each, to illustrate the fact that the triangular and hexagonal structures are variations of the same lattice.

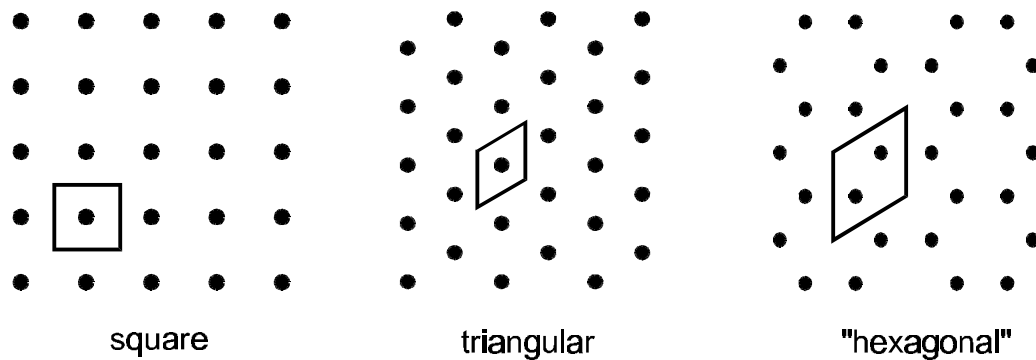


**Figure 10.2.1 Three common geometries used for 2-D periodic structures**

For two-layer construction, the dots in Figure 10.2.1 could be the positions of vertical metal vias. Each via connects to a metal patch on the top surface, and a continuous metal ground plane on the bottom surface. The configurations that have been studied consisted of simple shapes, such as a square lattice of squares, or a triangular lattice of hexagons. In some cases, a dielectric paste is used to fill the narrow slots between the patches, producing a slightly higher capacitance. It should also be possible to increase the capacitance using other methods, such as an interdigitated geometry.

More variety exists for three-layer construction, and several structures that have been studied are illustrated below. Figure 10.2.2 shows a three layer hexagonal structure.

The top layer is shown as outlines, while the second layer is shown as shaded regions. The third layer is the continuous metal ground plane, which is not shown. The vias are indicated by black circles in the centers of the patches.

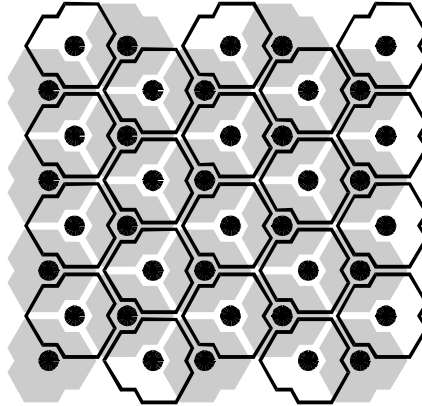


**Figure 10.2.2 Three-layer hexagonal structure**

In hexagonal geometry, each unit cell is made up of two individual members, represented here by one upper patch and one lower patch. Each individual layer appears as a triangular lattice, interlaced with the triangular lattice of the other layer. Each element is capacitively coupled to its three nearest neighbors on the other layer. This structure has the interesting feature that one subset of patches is completely hidden by the other, and half of the vias connect only to the upper surface, while the other half connect only to the hidden surface. If the vias are removed from one subset, the structure will still suppress surface waves. However, if the structure is to be used as an antenna ground plane, it may be desirable to retain as many vias as possible surrounding the antenna, for maximum surface wave suppression.

An alternate structure, in which none of the elements are completely hidden, is shown in Figure 10.2.3. This is a triangular lattice, in which each via connects to both the

upper and lower metal layers. Each element may be visualized as a flower with six petals, three on the upper layer, connected through a vertical via to three on the lower layer. In this geometry, each element is capacitively coupled to its six nearest neighbors. This structure has the advantage that the geometrical correction factor, described in Section 10.1, is three times higher than in the hexagonal structure discussed previously. Thus, if both structures have the same via spacing, they will have the same resonance frequency, even though the individual capacitors are three times smaller in the triangular lattice. Therefore, for the same resonance frequency, the triangular lattice can have a higher density of vias. This can be an advantage when designing small antennas, in which the ground plane may have a limited number of vias.

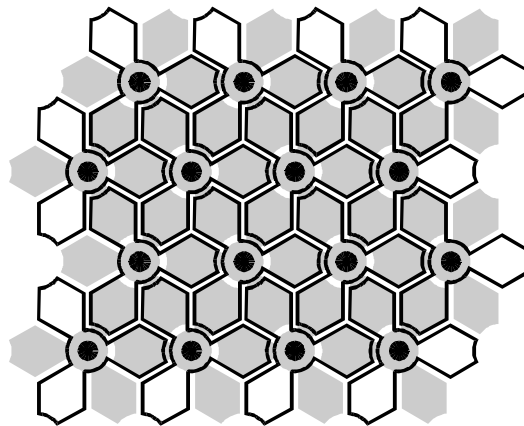


**Figure 10.2.3 Three-layer triangular structure**

Square structures have also been studied. In the example shown in Figure 10.2.4, one layer completely covers the other, as in the hexagonal structure described previously. For equal capacitor areas, the square and triangular structures have different resonance frequencies, serving as evidence for the necessity of the geometrical correction factor.

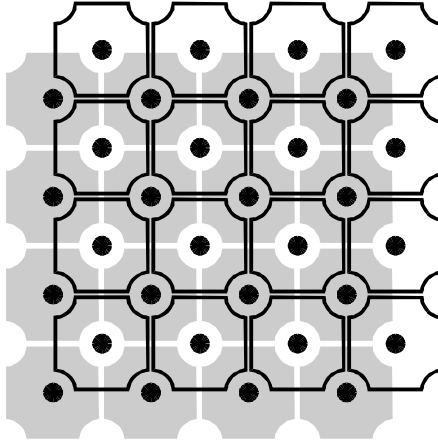


**Figure 10.2.4 Three-layer square structure with a hidden layer**

Two other configurations of the square geometry are also possible. In Figure 10.2.5, each element is exposed, as in the triangular design. The resonance frequency and bandwidth are the same as the previous square structure that has one layer completely hidden. It appears that having a hidden layer has no effect on the electromagnetic properties, and it is only the sheet capacitance and inductance that matter.

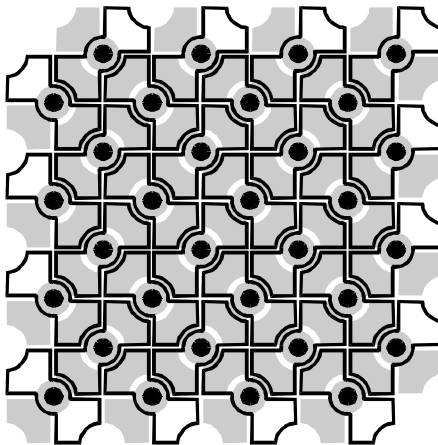


**Figure 10.2.5 Three-layer square structure with no hidden layer**

A less symmetrical structure is shown in Figure 10.2.6. In this case, half of each square is on the top layer, and half is on the bottom layer. This geometry had the same

frequency and bandwidth as the other two square structures. Furthermore, its surface wave properties appeared to be independent of direction.

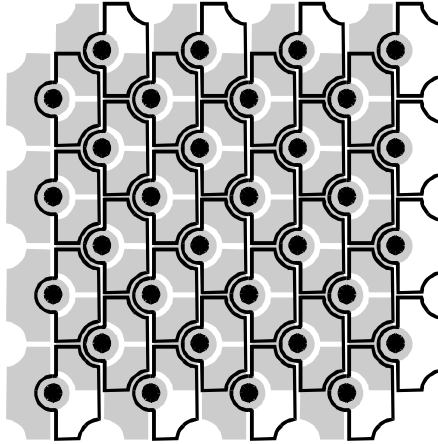


**Figure 10.2.6 Three-layer, lower-symmetry square structure**

### 10.3 Validation of the Model

Throughout this text, a model has been used in which the properties of a textured surface are described by an effective surface impedance. The impedance is equal to that of a parallel resonant LC circuit, made up of the sheet capacitance and the sheet inductance. The sheet capacitance is determined by the value of the individual capacitors, and a geometrical correction factor, while the sheet inductance depends on the thickness of the structure. The surface impedance derived in this way has been shown to predict the reflection phase, as well as the behavior of surface waves. The model was derived from simple ideas, but it has proven to be an accurate tool for analyzing and designing textured metal surfaces. A final check of the accuracy of the model is shown in the following graphs.

Figure 10.3.1 shows the measured resonance frequency plotted against the calculated resonance frequency, as determined by the effective medium model. The error bars represent the measured and calculated bandwidths of the surface wave band gap or the reflection phase, depending on the data available, for 23 different structures built during the course of this study. A dotted line is drawn with a slope of unity, and the proximity of the points to this line indicates the accuracy of the model in determining the resonance frequency. The degree to which the horizontal and vertical error bars have equal length indicates the accuracy of the model in determining the bandwidth.

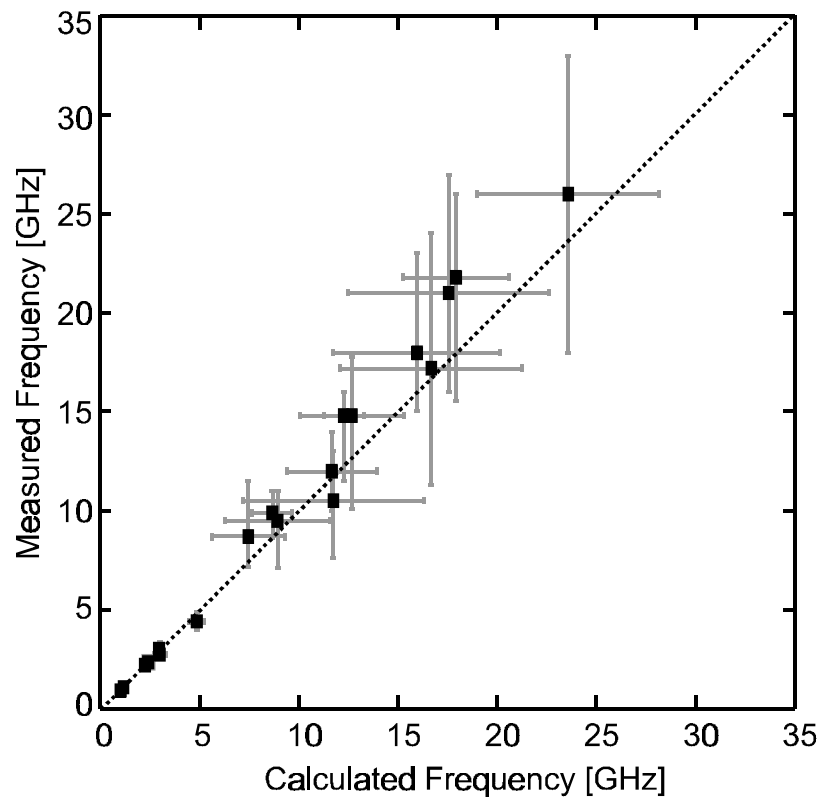


**Figure 10.3.1 Graph of measured frequency versus calculated frequency**

The graph represents data from structures having square, triangular, and hexagonal geometry, in both the two-layer and three-layer configurations. The calculated

values agree well with the measured data, considering the simplicity of the effective medium model. Inaccuracies are caused by the approximation used in calculating the capacitance, particularly for the two-layer design, and also the formula used for inductance, which admittedly neglects many effects, such as additional contributions from the vias. Furthermore, the use of a lumped parameter model is itself questionable for structures in which free-space wavelength approaches the lattice constant, which is true for the higher-frequency surfaces. The model is most valid for the low-frequency, three-layer structures. The data for these structures are plotted on an expanded scale in Figure 10.3.2.

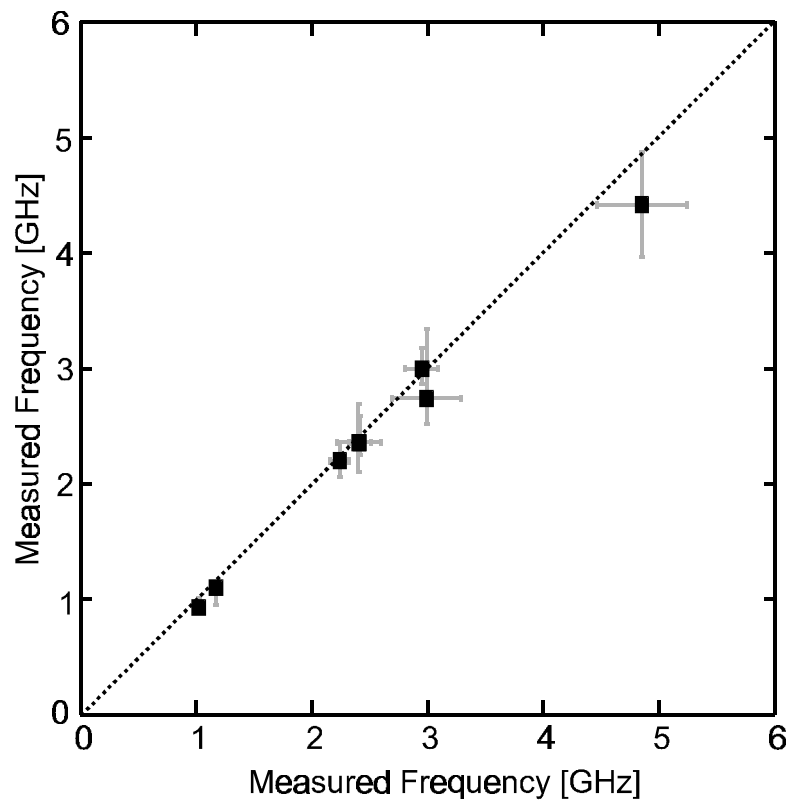


**Figure 10.3.2 Measured versus calculated frequencies for three-layer structures**

## 11 Conclusion

A new type of metallic electromagnetic structure has been presented that is characterized by having high surface impedance. It is made of continuous metal, and conducts DC currents, but it does not conduct AC currents within a forbidden frequency band. Instead, any currents that are induced in the surface radiate efficiently into surrounding space. This new surface also reflects electromagnetic waves with no phase reversal, behaving as a kind of magnetic conductor. The structure can be described using a lumped parameter circuit model, which accurately predicts many of its electromagnetic properties. This unique material is applicable to a variety of electromagnetic problems, including new kinds of low-profile antennas.

### 11.1 Summary

We have seen that while a conductive sheet is useful as a reflector, it also has several drawbacks such as permitting the propagation of surface waves, and a phase reversal for reflected plane waves. The presence of surface waves has been explored through analytical modeling and computational analysis. These surface waves have been identified as the normal AC currents that occur on any electrical conductor. Their relationship to optical plasmons, and to the skin depth of metals has also been illustrated.

It has been shown that texturing a metal surface can suppress surface currents. This was illustrated through two examples, a bumpy metal surface, and a corrugated slab. In the high-impedance surface, the corrugations are folded up into lumped elements, capacitors and inductors, and distributed in two dimensions.

The high-impedance structure is easily fabricated using printed circuit technology, and two different designs were presented. Using small probes, or specialized antennas, surface wave properties can be measured. It was shown that surface waves propagation is suppressed over a certain frequency range on the new textured surface. Within this same frequency range, plane waves are reflected with no phase reversal. By adjusting the geometry, the surface properties can be tuned to cover almost any radio frequency.

The high-impedance surface can be described using an effective medium model, in which it is parameterized according to its sheet capacitance and sheet inductance. This model can predict the reflection phase, the effects of material losses, and the surface wave dispersion. The model can also determine the bandwidth of an antenna placed near such a surface, and the behavior of leaky waves. The bandwidth is fundamentally limited by the thickness of the structure, with respect to the operating vacuum wavelength.

The effective medium model is confirmed by a more accurate, finite element model, in which detailed geometry is explicitly included. The finite element model illustrates the nature of the band gap, and other electromagnetic features, including higher bands, and leaky waves. The calculations also confirm the importance of the vertical conducting vias.

Various alternative structures are presented, and their relationship to the high-impedance surface is explored. These include frequency selective surfaces, and the grounded dielectric slab. The necessary role of the conducting vias is illustrated by contrast to other options.

The high-impedance surface is studied in the context of an antenna ground plane, and its benefits are illustrated in several examples. These include a vertical monopole, a patch antenna, and various horizontal wire antennas that can produce either linear or circular polarization. The applicability to phased arrays and the limitations of small antennas are also discussed.

Finally, the design of high-impedance surfaces is presented in terms of equations for frequency and bandwidth. Construction methods and materials issues are discussed, and several example designs are shown. Data from numerous structures are summarized to illustrate the validity of the effective medium model.

## **11.2 Future Research**

The invention of this new electromagnetic structure leaves many avenues for further research, some of which have already been mentioned. Since capacitive loading tends to limit the bandwidth, it is desirable to explore inductive loading. This could be done using coils, thin wires, or other possible techniques. Ideally, the inductance and capacitance would be used in equal ratio to the impedance of free space.

Several high-frequency features have appeared both in measurements and simulations, such as the existence of a second band gap, and higher-order bands. Studying the nature of these features, and their possible usefulness for electromagnetic devices can provide many opportunities for future research. With a deeper understanding of the interaction between textured surfaces and electromagnetic waves, one can anticipate designs that are even more imaginative.

Another area of future research involves the design of new kinds of antennas employing the high-impedance surface. Variations of the current topology could be explored, including graded structures to produce wider bandwidth, as well as tunable structures. Currently, antennas consist of wires or patches that use the surface as a ground plane. It has been shown that smaller designs should be possible, since it usually the ground plane that limits the bandwidth. In one possible embodiment, the surface itself could act as the antenna, with leaky surface waves producing the radiation.

## REFERENCES

- [1] D. Sievenpiper, E. Yablonovitch, U. S. provisional patent application, serial number 60/079953, filed on March 30, 1998
- [2] C. Balanis, Antenna Theory, Analysis, and Design, 2nd ed., John Wiley and Sons, New York (1997)
- [3] Ramo, Whinnery, Van Duzer, Fields and Waves in Communication Electronics, 2nd ed., John Wiley and Sons, New York (1984)
- [4] R. Collin, Field Theory of Guided Waves, 2nd ed., IEEE Press, New York (1991)
- [5] H. Raether, Surface Plasmons on Smooth and Rough Surfaces and on Gratings, Springer-Verlag, New York (1988)
- [6] N. Ashcroft, N. Mermin, Solid State Physics, Saunders College Publishing, Orlando (1976)
- [7] W. Barnes, T. Priest, S. Kitson, J. Sambles, "Photonic Surfaces for Surface-Plasmon Polaritons", *Phys. Rev. B* 54, 6227 (1996)
- [8] S. Kitson, W. Barnes, J. Sambles, "Full Photonic Band Gap for Surface Modes in the Visible", *Phys. Rev. Lett.* 77, 2670 (1996)
- [9] L. Brillouin, Wave Propagation in Periodic Structures; Electric Filters and Crystal Lattices, 2nd ed., Dover Publications, New York (1953)
- [10] A. Harvey, "Periodic and Guiding Structures at Microwave Frequencies", *IRE Trans.* 8, 30 (1959)
- [11] C. Elachi, "Waves in Active and Passive Periodic Structures: A Review", *Proc. IEEE* 64, 1666 (1976)
- [12] L. Brillouin, "Wave Guides for Slow Waves", *J. App. Phys.* 19, 1023 (1948)
- [13] W. Rotman, "A Study of Single-Surface Corrugated Guides", *Proc. IRE* 39, 952 (1951)
- [14] R. Elliot, "On the Theory of Corrugated Plane Surfaces", *IRE Trans. Ant. Prop.* 2, 71 (1954)
- [15] S. Lee, W. Jones, "Surface Waves on Two-Dimensional Corrugated Surfaces", *Radio Science* 6, 811 (1971)

- [16] Y.-L. Chen, Y. Lo, "Reactive Reflectors", IEE Proc. H 131, 263 (1984)
- [17] P.-S. Kildal, "Artificially Soft and Hard Surfaces in Electromagnetics", IEEE Trans. Ant. Prop. 38, 1537 (1990)
- [18] Z. Ying, P.-S. Kildal, A. Kishk, "Study of Different Realizations and Calculation Models for Soft Surfaces by Using a Vertical Monopole on a Soft Disk as a Test Bed", IEEE Trans. Ant. Prop. 44, 1474 (1996)
- [19] E. Yablonovitch, "Inhibited Spontaneous Emission in Solid-State Physics and Electronics", Phys. Rev. Lett. 58, 2059 (1987)
- [20] K.-M. Ho, C. Chan, C. Soukoulis, "Existence of a Photonic Gap in Periodic Dielectric Structures", Phys. Rev. Lett. 65, 3152 (1990)
- [21] C. Chan, K.-M. Ho, C. Soukoulis, "Photonic Band Gaps in Experimentally Realizable Periodic Dielectric Structures", Europhys. Lett. 16, 563 (1991)
- [22] S. Fan, P. Villeneuve, R. Meade, J. Joannopoulos, "Design of Three-Dimensional Photonic Crystals at Submicron Lengthscales, Appl. Phys. Lett. 65, 1466 (1994)
- [23] E. Ozbay, A. Abeyta, G. Tuttle, M. Tringides, R. Biswas, C. Chan, C. Soukoulis, K.-M. Ho, "Measurement of a Three-Dimensional Photonic Band Gap in a Crystal Structure Made of Dielectric Rods", Phys. Rev. B 50, 1945 (1994)
- [24] D. Smith, S. Schultz, N. Kroll, M. Sigalas, K.-M. Ho, C. Soukoulis, "Experimental and Theoretical Results for a Two-Dimensional Metal Photonic Band-Gap Cavity", Appl. Phys. Lett. 65, 645 (1994)
- [25] M. Sigalas, C. Chan, K.-M. Ho, C. Soukoulis, "Metallic Photonic Band-Gap Materials", Phys. Rev. B 52, 11744 (1995)
- [26] D. Sievenpiper, M. Sickmiller, E. Yablonovitch, "3D Wire Mesh Photonic Crystals", Phys. Rev. Lett. 76, 2480 (1996)
- [27] J. Pendry, A. Holden, W. Stewart, I. Youngs, "Extremely Low Frequency Plasmons in Metallic Mesostructures", Phys. Rev. Lett. 76, 4773 (1996)
- [28] V. Kuzmiak, A. Maradudin, F. Pincemin, "Photonic Band Structures of Two-Dimensional Systems Containing Metallic Components", Phys. Rev. B 50, 16835 (1994)
- [29] E. Brown, O. McMahan, "Large Electromagnetic Stop Bands in Metallodielectric Photonic Crystals", Appl. Phys. Lett. 67, 2138 (1995)

- [30] S. Fan, P. Villeneuve, J. Joannopoulos, “Large Omnidirectional Band Gaps in Metallodielectric Photonic Crystals”, *Phys. Rev. B* 54, 11245 (1996)
- [31] S. Gupta, G. Tuttle, K.-M. Ho, “Infrared Filters Using Metallic Photonic Band Gap Structures On Flexible Substrates”, *Appl. Phys. Lett.* 71, 2412 (1997)
- [32] D. Sievenpiper, E. Yablonovitch, J. Winn, S. Fan, P. Villeneuve, J. Joannopoulos, “3D Metallo-Dielectric Photonic Crystals with Strong Capacitive Coupling Between Metallic Islands”, *Phys. Rev. Lett.* 80, 2829 (1998)
- [33] G. Kurizki, J. Haus, eds., Photonic Band Structures, *Journal of Modern Optics* 41, special issue (1994)
- [34] J. Joannopoulos, R. Meade, J. Winn, Photonic Crystals: Molding the Flow of Light, Princeton University Press, Princeton (1995)
- [35] C. Soukoulis, ed., Photonic Band Gap Materials, Proceedings of the NATO ASI on Photonic Band Gap Materials, Elounda, Crete, Greece, June 18-30, 1995, Kluwer Academic Publishers, The Netherlands (1996)
- [36] R. Feynman, R. Leighton, M. Sands, The Feynman Lectures on Physics, vol. 2, Addison-Wesley, Reading (1964)
- [37] L. Zhang, to be published
- [38] S. Lee, G. Zarrillo, C. Law, “Simple Formulas for Transmission Through Periodic Metal Grids or Plates”, *IEE Trans. Ant. Prop.* 30, 904 (1982)
- [39] R. Ulrich, “Far Infrared Properties of Metallic Mesh and its Complimentary Structure”, *Infrared Phys.* 7, 37 (1976)
- [40] P. Yeh, Optical Waves in Layered Media, John Wiley and Sons, New York (1998)
- [41] E. Brown, C. Parker, E. Yablonovitch, “Radiation properties of a planar antenna on a photonic-crystal substrate”, *J. Opt. Soc. Am. B* 10, 404 (1993)
- [42] S. Cheng, R. Biswas, E. Ozbay, S. McCalmont, G. Tuttle, K.-M. Ho, “Optimized dipole antennas on photonic band gap crystals”, *Appl. Phys. Lett.* 67, 3399 (1995)
- [43] E. Brown, O. McMahan, “High zenithal directivity from a dipole antenna on a photonic crystal”, *Appl. Phys. Lett.* 68, 1300 (1996)

- [44] M. Kesler, J. Maloney, B. Shirley, G. Smith, "Antenna design with the use of photonic band-gap materials as all-dielectric planar reflectors", *Microwave and Optical Technol. Lett.* 11, 169 (1996)
- [45] M. Sigalas, R. Biswas, Q. Li, D. Crouch, W. Leung, R. Jacobs-Woodbury, B. Lough, S. Nielsen, S. McCalmont, G. Tuttle, K.-M. Ho, "Dipole antennas on photonic band-gap crystals: Experiment and simulation", *Microwave and Optical Technol. Lett.* 15, 153 (1997)
- [46] D. Pozar, "Microstrip Antennas", *Proc. IEEE* 80, 79 (1992)
- [47] H. Nakano, S. Okuzawa, K. Ohishi, H. Mimaki, J. Yamauchi, "A Curl Antenna" *IEEE Trans. Ant. Prop.* 41, 1570 (1993)
- [48] R. Mailloux, Phased Array Antenna Handbook, Artech House, Boston (1994)
- [49] H. Wheeler, "Fundamental Limitations of Small Antennas", *Proc. IRE* 35, 1479 (1947)
- [50] H. Wheeler, "The Radiansphere Around a Small Antenna", *Proc. IRE* 47, 1325 (1959)
- [51] L. Chu, "Physical Limitations of Omni-Directional Antennas", *J. Appl. Phys.* 19, 1163 (1948)
- [52] H. Wheeler, "Small Antennas", *IEEE Trans. Ant. Prop.* 23, 462 (1975)
- [53] J. McLean, "A Re-Examination of the Fundamental Limits on the Radiation Q of Electrically Small Antennas", *IEEE Trans. Ant. Prop.* 44, 672 (1996)
- [54] M. Jensen, Y. Rahmat-Samii, "EM Interaction of Handset Antennas and a Human in Personal Communications", *Proc. IEEE* 83, 7 (1995)